MSc. Thesis

Marine Technology

M.C. de Jong

An investigation into the possibilities
concerning Solid Oxide Fuel Cells in naval vessels

SDPO.20.034.m

TUDelft

Fuel Cells in Naval support vessels

Thesis to obtain a
Masters of Science Degree

by

Maarten Ch. de Jong

Delft University of Technology,
to be defended publicly on Wednesday October 14th, 2020 at 4:00 PM.

TUDelft Delft University of Technology

Preface

Concluding my years as a student at TU Delft, the Master of Science Thesis provides the opportunity to establish myself as an engineer. Defensie Materieel Organisatie (DMO), a part of the Netherlands Department of Defense, has kindly taken me on as a graduating Masters student and has granted me the opportunity to make use of the resources of the Royal Netherlands Navy. In this thesis, I attempt to create valuable knowledge to prove my prowess as an academic. Moreover, I hope this new information can be put to good use by DMO.

As a future marine engineer I feel the responsibility to help tackle the great challenges that lie ahead, and the energy transition embodies one of the defining challenges of our age. Carbon neutral sailing by the armed forces may be an elemental step in providing the shift to a more sustainable future. The final act of my Masters of Science studies in Marine technology, is to provide insight into one of the ways to take that step.

I would like to take this opportunity to thank the people that supported me along the way. First and foremost my family and friends, without whom I would have never made it this far. My family have had my back since before I can remember. Friends I have gained along the way. You have been amazing.

My gratitude also goes out to Peter de Vos and Klaas Visser for steering me in the right direction through their insights and on-point questions during our progress meetings. The resulting discussions were instrumental in uncovering the right direction for this investigation.

To my colleagues at DMO: Thank you for your warm welcome. You made me feel right at home, and I look forward to continue working with you on the future projects for the Royal Netherlands Navy.

Special thanks go out to Isaac Baredregt en Lindert van Biert. Isaac, thank you for your support, discussions and help during the the entire process. You were always available for questions or a quick review of my work. Lindert, Thank you for sharing your knowledge on Solid Oxide Fuel Cell systems. Thank you for the time you took to help me take some difficult hurdles.

M.C. de Jong
Scheveningen, september 2020

Defensie Materieel Organisatie
Ministerie van Defensie

TUDelft Delft University of Technology

Abstract

The Royal Netherlands Navy (RNLN) seeks to eliminate net green house gasses and other harmful-emissions. In this search, the operability of her vessels need to be secured. One of the options for eliminating net carbon emissions is Power to Liquid (PtL) conversion to Methanol. Fuel cells, and in particular Solid Oxide Fuel Cells (SOFCs) may be useful tools to power naval vessels efficiently and without the production of pollutants. The dynamic behaviour of these systems however is where a challenge is found.

Contrary to methane fuelled SOFCs, little research has been done on the behaviour of methanol fuelled SOFCs in the higher temperature range. It was decided that for this thesis the SOFC system would be pressurised to 20 bar to increase power density, a pre-reformer would be incorporated to improve dynamic behaviour, a Plate Heat Exchanger (PHE) would be used to re-integrate heat from the cathodic outflow to the cathodic inflow, and Anode Off Gas Re-Cycling (AOGRC) would be used to provide steam and heat to the pre-reformer.

A model was built that incorporates the following sub models: a pre-reformer that includes reaction kinetics, a dynamic SOFC stack model which incorporates heat losses normal to the cell orientation, and a PHE which includes its dynamic behaviours. These models are interconnected and controlled such, AOGRC is mimicked. These models were verified by checking energy- and mass-balances. The eventual chemical equilibrium of the (kinetics based) model of the pre-reformer was used to validate the pre-reformer model. The leading research by (Aguiar et al.) was used to validate the SOFC model. Typical thermal behaviours of PHEs were used to validate the PHE model.

Simulation results show that the pre-reformer could improve the system dynamics by providing a pre heated, hydrogen rich gas mixture to the SOFC. Running it at a temperature of higher than 530 K can pose danger due to more prominent exothermic, methane producing, reactions in the reactor vessel. Results from testing the SOFC show that the SOFC is best operated at an inflow temperature of around 800K for maximum efficiency (including outflow enthalpy). It shows that the SOFC is barely influenced by higher partial pressures of the reactants, and has slow load following characteristic, especially for low terminal current densities. The testing results for the PHE show that the this subsystem achieves higher heater effectiveness when more conductor plate area is used, but at the cost of dynamic response. It also shows that the PHE is the most important factor in the poor load following capabilities of the entire system. This is largly due to the limited convective heat coefficient. AOGRC has been shown to be an effective method to control the temperature of the pre-reformer, low AOGRC ratios make for large preventable energy losses. The interconnected methanol fuelled SOFC system simulation shows that external heating of the ingoing anode flow is detrimental to the efficiency of the system, but it could be instrumental in preventing thermal stresses on the Positive-Electrolyte-Negative (PEN) structure of the cell. Increasing the fuel and airflow excess is also detrimental to the system efficiency. These values are best kept at 1.1 due to uncertainty around for the models' accuracy for very low fuel- and air- flow excess. The settling time for the power output is in the order of several hundreds of seconds, and is largest for large sudden changes in power demands, and low terminal power demands.

It was concluded from these results that the here proposed system is not suitable to power a naval vessel of the Snellius class in a satisfying way. The investigation however, has produced valuable tools for future work. Recommendations for future work are to implement condenser/heat exchanger for the anode anode off gas, implement a burner to make use of the remaining chemical energy in the anode off gas and install a turbine to make use of potential energy in the outflowing gasses.

Nomenclature

Roman symbols

$\bar{b}$	Specific exergy	$[J/mol]$
$\bar{c}$	Molar heat capacity with constant pressure	$[J/(mol \cdot K)]$
$\bar{g}$	Molar Gibbs free energy	$[J/mol]$
$\bar{h}$	Molar enthalpy	$[J/mol]$
$\bar{s}$	Molar entropy	$[J/(mol \cdot K)]$
$\dot{m}$	Mass flow	$[kg/s]$
$\dot{Q}$	Heat flow	$[J/s]$
$\dot{q}$	Area specific heat flow	$[J/(s \cdot m^2)]$
A	Coefficient in natural logarithm form of the Tafel equation	$[V]$
A	Surface area	$[m^2]$
a	Chemical activity	$[-]$
a	Coefficient in base 10 logarithm form of the Tafel equation	$[V]$
B	Exergy	$[J]$
b	Plate width	$[m]$
C	Constant	dependent on constant
c	Heat capacity	$[J/(kg \cdot K)]$
E	Electro motive force	$[V]$
E_0	Electro motive force at Standard Temperature and Pressure (STP)	$[V]$
E_a	Activation energy	$[J/mol]$
E_a	Fluid strength	$[J/(K \cdot s)]$
E_{OCV}	Open cicuit voltage = Nernst voltage	$[V]$
F	Faraday's constant	$96458[C/mol]$
G	Gibbs free energy	$[J]$
g	Gravitational Constant	$9.81[m/s^2]$
H	Enthalpy	$[J]$
I	Electrical current	$[A]$
i	Electrical current density	$[A/m^2]$
K	Chemical (rate) constant	dependent on rate equation
k	Pre-exponential chemical rate constant	dependent on rate equation

L	Conductor plate length	$[m]$
M	Molar mass	$[kmol/kg]$
m	Mass	$[kg]$
N	Number of moles	$[mol]$
n	number of conductor plates, number of cells	$[-]$
P	power	$[W]$
p	(Partial) pressure	$[Pa]$
Q	Electrical charge	$[C]$
Q	Heat	$[J]$
Q	Reaction quotient	$[-]$
R	Electrical resistance	$[\Omega]$
R	Universal gas constant	$80314[J/(mol \cdot K)]$
r	Area specific electrical resistance	$[\omega \cdot m^2]$
r	reaction rate	$[mol/s]$
S	Entropy	$[J/K]$
T	Temperature	$[K]$
u	Velocity	$[m/s]$
V	Voltage	$[V]$
y	Molar fraction	$[-]$
Z		$[-]$
Z	Compression factor	$[-]$
z	number of moles of electrons exchanged per mole	$[-]$

Greek symbols

α	Convective heat transfer coefficient	$[W/(m^2 \cdot K)]$
β	Charge transfer coefficient	$[-]$
ϵ	Surface emissivity	$[-]$
η	Efficiency	$[-]$
γ	Fuel utilization ratio	$[-]$
λ	Flow excess ratio	$[-]$
λ	Thermal conductivity	$[J/(m \cdot s \cdot K)]$
μ	Inflow ratio	$[-]$
ρ	Mass density	$[kg/m^3]$
σ	Stephan Boltzmann constant	$5.670 \cdot 10^{-8}[W/(m^2 \cdot K^4)]$
τ	Thickness	$[m]$

ε	Effectiveness	$[-]$

Subscripts

0	initial, exchange (in exchange current density)
a	anode
act	activation
af	anode flow
c	cathode
c	cool
cf	cathode flow
$cross$	cross over: through electrolite
e	electrolyte
el	electrical
eq	equilibrium
f	forward
h	hot
in	at the inlet
l	limit $[\omega \cdot m^2]$
ohm	Ohmic
out	at the oulet
p	at constant pressure
p	at constant volume
r	reverse
rxn	for reaction
STP	at standart pressure and temperature
$trans$	transportation
w	wall

3D TF   three dimensional Thin Film

AC   Alternating Current

PEN   Positive-Electrolyte-Negative

AES   All Electric Ship

AMS   Afdeling Maritieme Systemen

AOG   Anode Off Gas

AOGCC   Anode Off Gas to Combustion Chamber

AOGRC   Anode Off Gas Re Cycling

BMS   Battery Management System

cf   cathodic flow

CH_3OH Methanol

CH_3OH **ICE**   Methanol Internal Combustion Engine

CH_4 Methane

CO   Carbon Monoxide

CO_2 Carbon Dioxide

COS   Carbonyl Sulfide

DC   Direct Current

DME   Di-Methyl Ether

DMO   Defensie Materieel Organisatie

EMF   Electro Motive Force

ER   external reforming

FC   Fuel Cell

GMM   green maritime methanol

GT   Gas Turbine

H_2 Hydrogen

HF   Hydrofluoric acid

HS   Hybrid System

H_2S Hydrogen sulfide

LHV   Lower Heating Value

Li-ion   Lithium-ion

ICE   Internal Combustion Engine

IMO   International Maritime Organization

IR   Internal Reforming

MCA   Multi-Criterion Analysis

MCFC   Molten Carbonate Fuel Cell

MCDO   Methanation of Carbon Di Oxide

MCMO   Methanation of Carbon Mono Oxide

MDO   Marine Diesel Oil

MDR   Methanol Decomposition Reaction

MLU   Mid Life Upgrade

MoD   Ministry of Defence

MSR   Methanol Steam Reforming

NH_3 Ammonia

NiMH   Nickel-Metal-Hydride

NO_x Nitrous Oxides

O^{2-} Oxide

OCV   Open Circuit Voltage

OES   Operationele Energie Strategie

PEL   Permissible Exposure Limit

PEMFC   Proton Exchange Membrane Fuel Cell

PEN   Positive electrode-Electrolyte-Negative electrode

PHE   Plate Heat Exchanger

PM   Particulate Matter

PR   Pressure Ratio

PtG   Power to Gas

PtH   Power to Hydrogen

PtL   Power to Liquid

RNLN   Royal Netherlands Navy

SM   Surge Margin

SOFC   Solid Oxide Fuel Cell

SOFC/GT-HS Solid Oxide Fuel Cell and Gas Turbine Hybrid System

SOFC/ICE-HS Solid Oxide Fuel Cell and Internal Combustion Engine Hybrid System

SO_x Sulphuric Oxides

STP   Standard Temperature and Pressure

THE   Tube Heat Exchanger

TPB   Three Phase Boundary

TRL   Technical Readiness Level

VFD   Variable Frequency Drive

VOCs   Volatile Organic Compounds

WGS   Water Gas Shift

WHS   Waste Heat System

Contents

1

Introduction

The current document contains the thesis to obtain the degree of Master of Science. It addresses question if it is feasible to equip a naval vessel with a SOFC-based power unit with the current state of technology. This question is a significant one, as the shift away from fossil driven diesel engines is a priority the world over.

Navies around the world realize that climate change is increasingly leading to natural disasters and conflicts. As a result, the armed forces are being called upon more often. Therefore it should be on their agenda to look at the root of the problem, partially caused by the impact of military deployment itself. Regulations by International Maritime Organization (IMO), but also social responsibility dictates that an effort be made to limit the emissions of green house gasses and pollutants from maritime vessels.

Moreover, from the standpoint of the Ministry of Defence (MoD) it is of great importance to keep the armed forces as agile as possible, as was stated in the Operationele Energie Strategie (OES). Reduced dependency on (fossil) fuels will be of mayor importance, as this opens the door to modular fuel production.

Opportunities to implement new cutting edge systems have arisen in the Royal Netherlands Navy (RNLN). They present a great opportunity to take a step away from the use of polluting power sources and dependability on fossil fuels.

This chapter describes the motivation behind this research and the process of this investigation.

1.1. Motivation

The motivation for investigating this particular subject has multiple facets. Firstly there is the need and wish for the Netherlands government to heed or improve on the set *climate goals*. Secondly, a reliability in efficiency & effectiveness of military apparel was identified by the MoD. *Increasing operational reach, safety and security* (section 1.1.2) will be of great importance to the development of a successful naval vessel. Finally, the timing for implementing new technologies in naval vessels is very suitable, as some vessels will be replaced or upgraded. In light of these points of interest, there are some serious challenges ahead for the RNLN and Defensie Materieel Organisatie (DMO), if the aim is to satisfy all these wishes.

1.1.1. Climate goals

Since the invention of the steam engine, transportation of goods of any kind has relied, at least in some part, on the combustion of fossil fuels. Nowadays indications are that our extended use of fossil fuels may well damage the delicate ecosystem we live in. As a part of the Netherlands government, the MoD and RNLN carry the obligation to lead the way in protecting the environment that sustains us on this planet. The use of new technologies may well aid in reaching emission-less operation of the military.

Reducing carbon emissions

The Netherlands government takes its social responsibility and takes on a leading role in the shift away from fossil fuels. The MoD have decided that dependency on fossil fuels for all military operations has to be -compared to the use of fossil fuels in 2010- reduced by 20% by 2030 and reduced by 70% in 2050. Little wonder that non-diesel fuels, and in particular methanol, have gained a lot of interest by DMO. Though not inherently carbon-less, the emissions of new technologies will be lower than the emissions of diesel engines. The renewable,synthetic manufacturing of these alternative fuels may well be key to carbon neutral sailing. This subject does not reside within the scope of this project, but the means to efficiently and cleanly convert these fuels into usable power, most certainly *do*.

Reducing other emissions

In extension to the stricter Carbon Dioxide (CO_2)- goals, social accountability as well as IMO regulations demand that harmful emissions like Sulphuric Oxides (SO_x), Nitrous Oxides (NO_x), Volatile Organic Compounds (VOCs) and Particulate Matter (PM) be reduced. Here, fuel cells demand attention. Fuel Cells do not have moving parts (prevents the forming of PM), can operate without sub optimal combustion(prevents the forming of VOCs), and lack extremely high temperatures (prevents the forming of NO_x). Furthermore, viable fuels do not contain Sulphur. These characteristics virtually guarantee the elimination of the production of these emissions.

1.1.2. Increasing operational reach, safety & security

Obviously, for the RNLN, operational reach, safety & security of personnel and vessels, is of paramount importance. The successful completion of it's missions as well of preservation of sailors lives highly depend on these factors. [1]

Increasing operational reach

An important point of interest for many NATO-affiliated defenses is increasing the efficiency and/or self-sustainability of military apparel. Recent missions in Iraq and Afghanistan have shown that low fuel efficiencies of military apparel in combination with long supply lines could impede operability [38]. The wishes of the MoD are that the efficiency, effectiveness and resilience of the Defense forces will be enhanced by reducing the dependency on sources of fossil fuel in the vicinity. Implementation of new power technologies may lead to weapon systems that can operate for longer time spans with an extended reach and with more agility. Efficiency of power converters will be of great importance to provide as much usable energy from the energy carrier as possible.

To conclude: being (partially) fuel-independent will have a positive effect on:

- vulnerability of fuel supply lines

- required planning-, transport- and maintenance-capacity

- therefore: Speed and agility of units and operations

safety & security

Above mentioned goals are to be pursued whilst guaranteeing similar or better safety for personnel, redundancy in perilous situations, and maximized reliability in all conditions. These requirements are of paramount importance. The modular characteristics of power units [2] may assist in generating redundancy for weapons systems. However, the measure in which power units are modular, has to be investigated as they may require intricate auxiliary systems that enable proper functionality.

---

[1]However, it must be noted that for the type of vessel for which the design is made, this point is less critical as they presently have an exorbitant operational reach compared to their purposes, due to a late design change.
[2]From here on, the term 'power unit' is used to describe the entire system that delivers all electrical power onboard of the vessel

1.1.3. Opportunity
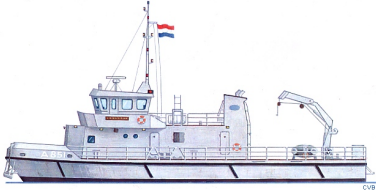
The third reason why an investigation is neccesary, is that there is great opportunity at the present moment to implement change in technologies. One of the very promising new technologies that are looked into as of now are Fuel Cells. Section 2.1 will take a closer look at fuel cell technology A particularly promising technology within the fuels cell family are SOFCs. These types high temperature of fuel cells are capable of reaching high electric efficiencies without the production of harmful emissions.

Opportunities are plentiful as developments in fuel cell technology succeed each other rapidly. More importantly, numerous vessels of the RNLN are due for either replacement or upgrades. This opens up the possibilities to remain a leader in adaptation to promising new technologies.

In the following years the RNLN has numerous upgrades and new-builds planned. A brief overview of the alterations to the fleet is provided in table 1.1. The table shows the ship classes that may be assimilated into a new class of modular ships called 'family'. For the investigation at hand, this is a very exiting development.

Because of the 'family's' modular nature, these ships can be equipped for a number of tasks. The consequences of this decision is that the functions of the here mentioned ship classes will be covered by the same ship class, though with a modular setup. This decision means that this new family of ships will all have the same hull and power unit [8]. The result is that a successful power unit may be used for multiple ship types within the family.

Table 1.1: Overview of vessels to be upgraded or replaced in the foreseeable future

Type (Dutch)	Class	Action	visual
Diving support vessels (haven duikvaartuigen)	Cerberus class	Mid Life Upgrade/ family	
Multi-purpose logistics support vessels (ondersteuningsvaartuigen)	Pelikaan class	family	
Hydrographic Survey vessels (Hydrografich opnamevaartuig)	Snellius class	family	
Submarine support vessel (torpedowerkschip)	Mercuur class	family	

Type (Dutch)	Class	Action	visual
Education vessel (opleidingsvaartuig)	Van Kinsbergen	replacement/ family	

The design is based on the layout of the hydrographical survey vessels. These hydrographical survey vessels are the most recent vessels to come into service. Therefore they are the most representative vessels to obtain reference for the new ship class family. These ships will be delivered with an fully electric propulsion and distribution system, which may be fuelled with Methanol (CH_3OH)-Internal Combustion Engine (ICE) [8]. This means that, even for the vessels for which this possible technological innovation will be too late, both the electrical system and the methanol containment- and supply-system are already present. This opens up possibilities for implementation of SOFC-based power units to be implemented during a Mid Life Upgrade (MLU).

Moreover, at DMO, the project green maritime methanol (GMM) has been initiated with other stakeholders in the maritime sector. This project is set to investigate the possibilities into a renewable methanol infrastructure for the maritime sector and the RNLN in particular. It seems therefore that the RNLN is invested in Methanol as a means to fuel their fleet.

1.2. Problem identification

As briefly mentioned in the section 1.1.3, there has been some interest in implementing Fuel Cells as main power unit on board naval ships. Of these fuel Cells SOFCs gather most of the attention. SOFCs have the ability to run with very high electrical efficiency, and may do so while running on non-hydrogen fuels. This is possible because SOFCs are able to internally reform certain fuels. This averts the need highly pure H_2. This presents a clear advantage compared to Proton Exchange Membrane Fuel Cell (PEMFC) systems for which readily available, pure hydrogen needs to be presented at the anode. The need to carry hydrogen aboard and the need for the highly sophisticated reformers that produce the very pure hydrogen is thus avoided.

SOFC technology is promising, but a problem is found in the notoriously bad performance of SOFCs in dynamically loaded conditions. This is of great concern, considering current and past developments that "(the) traditional ratio between the steady ship electrical service load and electrical high power loads, will demand fast deliverable high power reserves"[17]. The challenge will be to adequately supply for rapidly varying power demands.

The interest in methanol of as a renewable energy carrier in naval vessels sparks a question: Can methanol be used in combination with SOFC technology to power a naval vessel? This becomes the question that this thesis attempts to answer.

A literature study has been conducted to create a better understanding the knowledge that is needed to make sailing on methanol by means of an SOFC a reality. For this thesis it was identified that the literature is so far lacking knowledge on the use of CH_3OH in SOFCs. Little has been done on this subject, and most of it focuses on medium temperature fuel cells ([26], [4], [29]). As power densities of these machines are low, these may be less suited for use in naval vessels. All works on methanol driven SOFCs concern direct-methanol([34], [25], [40]), meaning that there is no external reforming process present. *All* of these works focus on the chemistry or electro-chemisty on either or both of the electrodes. Therefor this thesis focuses on a methanol fuelled SOFC of: pre-reformer, SOFC, AOGRC and heat exchanger. It asks what the ideal operating conditions of such a system are, if these conditions are obtainable and what the the dynamic behaviour of such a system would be like.

1.3. Thesis statement

In order to find the best design for an SOFC based power unit, this thesis aims to answer the following research question:

Main research question

"What are the (dynamic) power output limitations of a methanol fuelled Solid Oxide Fuel Cell (SOFC) system, and would it be able to adequately provide power for a naval vessel similar to the Snellius class?"

Sub-questions

To adequately answer this question, the system and its constituents are studied more in depth. This is done by answering several sub questions:

- What would a methanol fuelled SOFC system look like?

- Which of the components: SOFC, pre-reformer and PHE and which characteristics of these components will be limiting for the system, in the dynamic sense?

- In what way can the performance of the SOFC and other system components be expected to change as a result reforming process in which methanation is present?

- Will the use of AOGRC as the exclusive means of heating be able to maintain the desired pre-reformer temperature, and how much of the Anode Off Gas (AOG) will be left in this case?

- What will the power outputs and the efficiency of the system be for stable operation?

- What will the transient behaviour of the system be?

- Would the output, efficiency and transient behaviour suffice to adequately power a naval vessel similar to the Snellius class?

1.4. Report outline

Chapter 2 "Literature Study" will provide background information concerning fuel cells and SOFCs in particular, methanol reforming, methanation reactions and Heat exchangers. More importantly, it exposes the areas where the information is lacking, considering the the design and operation of fuel cell based power systems. Chapter 3 "Design decisions" deals with early stage design decisions. These will further narrow the scope of the investigation and define the SOFC based power system that will be investigated. Chapter 4 "Modeling the System" shows the models for the the components to be studied. The model will be integrated and written in Simulink. Chapter 5 deals with the verification of the models and sensitivity analysis. This is done for the individual components. Chapter 6 shows the behaviour of all the components in standalone operation and behaviour of the connected system. Chapters 7.1 and 7.2 provide answers to the research questions and recommendations for future work respectively.

2

Literature Study

In terms of climate goals and pollution, methanol Fuel Cell Electric is the most viable solution to supply operability for naval vessels in the future. This is according to an investigation by the renowned research center MARIN. This solution has great potential when the investment price goes down and the systems power density increases significantly [21].

In this chapter the working principles and governing equations fuel cells -and specifically SOFCs- will be discussed to create a basis from which the investigation into the viability of a methanol fuelled SOFC system can be evaluated. Also auxliliary systems will be studied:

- Fuel reforming. This process may protect the SOFC from undergoing severe thermal stresses, which limit the load-following behaviour of the cell. It also provides a way to re-integrate some of the heat generated in the cell via AOGRC.

- Heat exchangers, essential for recuperation of useful heat in the system which would otherwise go to waste.

The aim of this chapter is to collect the major components that will constitute the system and study them in order to understand their characteristics, so they can be modelled in later stages. The knowledge gaps are identified, so the creation of new information can be precise.

2.1. Fuel Cells

The working concept of all fuel cells is similar to the concept as shown in figure 2.1. The fuel cell consists out of 4 main components.

- The anode, where fuel is presented and split in to ions and electrons. Exhaust products are formed here from ions, presented fuels and electrons.

- The cathode, where the oxidizer is presented and split into ions. Exhaust products can be formed here from ions and electrons

- Electrolyte, a sort of barrier between the anode and the cathode, that allows certain ions to pass through, but inhibits electrons to pass through

- An electrical conductor connecting the anode to the cathode, allowing electrons to flow from the anode to the cathode

The kind of ions, fuels, anodes, cathodes and electron inhibiting barriers(electrolytes) differ for every kind of fuel cell, but the main concept remains the same[7].
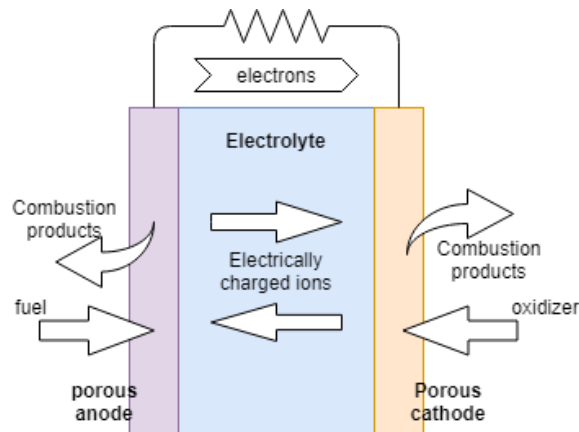
Figure 2.1: Generic working principle of all fuel cells.

Note that for the electro-chemical reaction at either the anode or the cathode to take place, three 'phases' are required at a single point. The points where this is the case are called the Three Phase Boundary (TPB). For the speed of the reaction the area of the 3-phase barrier is very important as it is near-proportional (except for minor deviations) to the reaction speed. The three phases are:

- The electrode (anode or cathode), to accept or deliver the electrons.

- The electrolyte, to accept or deliver the ions

- The gas containing the fuel, oxidizer or gas that will accept the combustion products.

2.1.1. Solid Oxide Fuel Cells

The SOFC, being a fuel cell, operates on the same general principle as explained in section 2.1. However, there are some peculiarities that make it different from the more widely used PEMFC. Notably:

- The operating temperature is high 650 °C - 1100°C.

- The role of protons as charge carrier through the electrolyte is instead fulfilled by Oxide (O^{2-}) in SOFCs. These ions are formed at the cathode which travel to the anode through the electrolyte.

- Due to the high operating temperatures no catalysts are required to enable the reaction. Also internal reforming of fuels is possible at these temperatures.

- Carbon monoxide could be used as a fuel as O^{2-}-ions and electrons are presented at the anode. $CO + O^{2-} + 2e^- \rightarrow CO_2$. (though in reality all CO is consumed in the water gas shift reaction as shown in section 2.2.

The the working principle of the SOFC is given visually in figure 2.2.

For the governing equations for the fuel cell behaviour, electro chemistry and losses, the reader is referred to the appendix B.1.

2.1.2. Knowledge Gap

The areas where the literature is lacking for this technology are identified to be The behaviour of high temperature fuel cells that are fuelled with methanol. Not to say that there is no work available of methanol use in solid oxide fuel cells. Yet, these works ([26], [4], [29]) concern the fuel cell behaviour at lower temperatures in cases where a pre-reformer is not present. This information is crucial if the goal is to predict what the behaviour of the methanol fuelled SOFC system will be.

Figure 2.2: Generic working principle of Solid Oxide Fuel Cells

2.2. Fuel reforming

SOFCs are able to electro-chemically combust non-Hydrogen fuels at the anode. Oxygen atom are provided by the electrolye an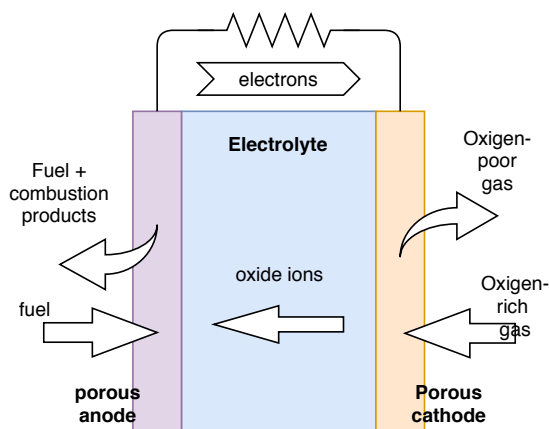d the high temperatures enable reforming without catalysts. However, certain species at the anode can still influence the reaction at the anode in an undesirable way. Conventional wisdom advises against high concentration of carbon based fuels at the anode. These can be oxidized at lower concentrations, but higher concentration could still lead to carbon poisoning of the electrode, which will severely inhibit the speed of the reactions, shortening the life span of the cell. This however, is contested by those who say that, especially CO, is perfectly combustible, especially in the presence of oxygen holding compounds. [7] [3], to prevent methanation (see section 2.2.1.

In the reforming of methanol, several reactions can occur either internally, which is called Internal Reforming (IR) or externally , which is called external reforming (ER). These reactions are Methanol Steam Reforming (MSR), MDR, Water Gas Shift (WGS). However, two reactions which are also known to occur under certain circumstances are MCMO and MCDO. In order to better enable the electro-chemical reactions at the anode of the SOFC[1], a pre-reformer is installed to reform the fuel. This pre-reformer is fairly simple in the case of the SOFC. Indeed, the pre-reformer is often just a reaction vessel that combines the flow of the fuel and steam at a temperature that enables MSR ($CH_3OH+H_2O \leftrightharpoons CO_2+3H_2$) but also MDR ($CH_3OH \leftrightharpoons CO+3H_2$). Often times this happens in the presence of a catalyst. The second reaction is more endothermic than the first and can largely be prevented by the presence of enough water. The water that does not react in the pre-reformer flows through to the anode. In the reactor, the presence of water will also enable WGS $CO + H_2 \leftrightharpoons CO_2 + H2$ to occur.

The most important reason to use an external reformer in an system that includes a high temperature fuel cell, is the endothermic nature of the process taking place in the reactor. This can be shown by using the old assumption that MSR the superposition of MDR and WGS. In that case it ca be shown that as long as methanol reacts at a higher rate than that it is formed, the overall process will be endothermic[2]. The result of this phenomenon is that the surroundings will be cooled from this process; especially when the reaction rates are high. IR would have these reactions take place at the anode at high temperatures. It is to be expected that high reaction rates at these temperatures will create large temperature gradients within the cell and the stack. This could severely limit the life of the cell or even crack it.

It remains unclear what the overall equilibrium and the kinetics of all the reactions in the reforming process will be. In any case it will be of great influence on the oxidation reactions of the fuel cell. In modeling the pre-reformer (see section 4.2), the hope is to shed light on this phenomenon.

---

[1] For low temperature fuel cells, notably PEMFCs the allowable concentration of CO is extremely low. The pre-reformers that are required to provide a pure supply of Hydrogen (H_2) are highly complicated machines. This is not the case for pre-reformers of high temperature fuel cells.

[2] The attentive reader will have noticed that the methanation reactions are conveniently left out of this reasoning. Running the pre-reformer model will have to show if this can be validated. However, [27] notes that the use of copper based catalysts as most reformers do, completely prevents these reactions from occurring.

1	MSR	$CH_3OH + H_2O \rightleftarrows CO_2 + 3H_2$	$\Delta H = +49.7 kJ/mol$ STP
2	MDR	$CH_3OH \rightleftarrows 2H_2 + CO$	$\Delta H = +90.7 kJ/mol$ STP
3	WGS	$CO + H_2O \rightleftarrows CO_2 + H_2$	$\Delta H = -41.2 kJ/mol$ STP
4	MCMO	$CO + 3H_2 \leftrightharpoons CH_4 + H_2O$	$\Delta H = -206 kJ/mol$ STP
5	MCDO	$CO_2 + 4H_2 \leftrightharpoons CH_4 + 2H_2O$	$\Delta H = -164 kJ/mol$ STP

Table 2.1: Five reactions that are known to occur when reforming methanol

2.2.1. A word on the methanation reactions

During the search for useful information it came to light, that two other reactions than MSR, MDR and WGS might be happening during methanol reforming. This came to light after conversation with Lindert van Biert, who was at that time writing his PhD thesis on a fuel cell system that uses an Methane (CH_4) fed SOFC in combination with an ICE to power a ship. In the reforming of methane it was noticed that the reaction rates of both the methanation reactions (denoted in the table below) were, at lower temperatures, unfavourable to create large quantities of H_2, due to the endothermic nature of the production of hydrogen by means of these reactions:

| 1 | methanation of CO | $CO + 3H_2 \leftrightharpoons CH_4 + H_2O$ | $\Delta H = -206 kJ/mol$ STP |
| 2 | methanation of CO_2 | $CO_2 + 4H_2 \leftrightharpoons CH_4 + 2H_2O$ | $\Delta H = -165 kJ/mol$ STP |

It was noted that these reactions with their fast kinetics could well interfere with the process of methanol reforming. For instance, it can be seen that methane production is highly exothermic. Therefore the conditions under which the reforming of the fuel will take place can also be severely influenced by the presence of these reactions. The decision has therefore been made to research this subject more deeply. In order to do so, extra research questions were composed.

- "What will the effect of the of the presence of methanation reactions be on the process of the reforming of methanol?"

- "In what way can the performance of the SOFC and other system components be expected to change as a result of the changed reforming process?"

2.2.2. Knowledge gap

Whereas the literature is abundant on reforming methanol to a hydrogen-rich gas under the influence of heat, pressure and the presence of steam; the behaviour of the system under our particular circumstances remains unknown. Literature mainly focuses on the reforming of methanol before PEMFCs, for which it is imperative that *all* CH_3OH is converted CO_2 and H_2 exclusively, and no CO exists in the presented flow of fuel. These systems are exceedingly complex and mostly superfluous, as the SOFC is perfectly able to use CO as a fuel.

Chemical processes and their kinetics that take place under the influence of very specific catalyst remain beyond the scope of this this investigation. However, the kinetics of these reactions will have to be investigated very thoroughly if a SOFC based power unit is to be equipped with a pre-reformer. For the details on this recommendation, the reader is redirected to section 7.2.6.

In particular the influence of the methanation reactions that could take place will have to be studied and documented, as a lot of heat could be produced is these reactions are taking place at a high rate. These reactions would also implicate that the there will be a presence of methane (CH_4) at the anode of which the effects will have to be studied in the literature.

2.3. Heat Exchangers

From [10] it is gathered that in many cases, the dynamic response of SOFC systems may be limited by the dynamic behaviour of heat exchangers. These components are of frequent occurrence in high temperature systems and notably in SOFC systems. These reasons grant justification into studying these components in more detail, and modeling them and their dynamic behaviour.

3

Design decisions

This chapter explains the early-stage design decision which create a defined design space, to limit the extent of the investigation. This will enable better focus on the configurations within the design space, thereby ensuring thorough investigation. This chapter describes what design decisions have been made before the modelling was commenced.

The challenge in investigating if a methanol fuelled SOFC system for a naval vessel, is very much a systems engineering one. That means to say that the success of a system is not solely dependent upon the the performance of a single component. Rather, the success this system is the result of the performance of all components *and* of the interaction between all these components. This is kept in mind for all the design decisions that are to be made.

Also note that the effectiveness is determined, dependent of the task the system has to perform. For naval ships, effective systems will be very diverse and mostly vastly different from other, non-naval vessels. Redundancy, safety and agility will be more important naval ship. Fuel efficiency and cost, although important factors will be less of a priority for a naval ship than for a commercial vessels. These considerations are kept in mind for all design decisions that are made.

In order to design an effective system, the criteria must be set on which to judge if the system is successful. These criteria have been identified to be:

- Operational safety

- Operational reaction time

- Operational reach

- CO_2 emissions

- Polluting emissions

As safety is a boundary condition and the lack of polluting emissions is vitually guarenteeed in a methanol fuelled SOFC system, the success of the system will largely depend on the measure in which the the power unit will be able to deliver the required power demand within a agreeable amount of time. Of course, the cost will also play a role, but this thesis focuses on the feasibility of an SOFC based power unit.

3.1. Pre-reformer

Reformers (in the current document referred to as "pre-reformer", to distinct from the reforming that takes place in the SOFC itself) are not always necessary for an SOFC to operate on non-H_2 fuels. As [36] shows, certain non-H_2 fuels can be reformed or oxidized at the anode of the SOFC.

A pre-reformer is integrated in the system for several reasons:

- Prevent large temperature gradients along the length of the cell because of the endothermic reforming reactions

- Exert a certain amount of control of the properties of the inflow to the SOFC.

    - Create a buffer of readily available fuel, which can be sent to the SOFC, so settle time of the system can be reduced
    - Heat the mixture to an elevated temperature compared to the methanol and steam inflow

It should be clear that the decision for an external pre-reformer from is a result of the priorities in properties of the system. It is well known that Internal Reforming has the potential to enable higher system efficiencies [36]. However, robustness of the system will, in naval vessels, be of a higher priority.

3.2. Pressurised vs. atmospheric systems

Different configurations can be divided into 2 main groups: Presurrized and atmospheric systems. The pressurised system might be more susceptible to damages due to mechanical stresses within the fuel cell. However, pressurised operation enables a higher power density of the fuel cell, and it has been shown that the electrical efficiency of such a system is better than that of a comparable atmospheric system [36]. These notions lead to using the pressurised methanol fuelled SOFC system for this investigation.

3.2.1. Decision for a pressurised system

In stable operation, it has been proven that the pressurised systems yield better total efficiencies and less irreversibilities[5] [36] [18]. More importantly for the current investigation; The power density of a pressurised system can be significantly increased as compared to the atmospheric system. The main advantage of a fuel cell with a higher power density is twofold

- Capital expenses can be reduced, as the fuel cell is the most expensive part of the system. If the possibility is to be maintained that a system is implemented on a naval ship, the cost will be a factor. This will be even more true for implementation by commercial parties further down the road.

- Since methanol lacks the energy density of conventional fuels, the power density of the entire system will be of great importance. A power system with high power density is desired when a sufficient operational reach is to be achieved.

3.3. Heat recovery

Heat recovery is vital in creating an efficient methanol fuelled SOFC system. Use can be made of the high temperature heat flows to pre-heat the system components, and enable chemical processes in the pre-reformer. SOFC's are known to operate most efficiently and responsively at high temperatures. In fact, manufacturers will often claim that the the cell should be operated at the highest temperature that the material in the cell will allow[36][1]. Favourable characteristics of the high temperature fuel cells are:

- Low activation losses due to lower activation energy at higher temperatures

- Lower ohmic losses due to higher diffusion rates of ions through the electrolyte

- Lower susceptibility for anode poisoning from carbon monoxide

---

[1]Section 6.3.2 will elaborate on the truth of this claim. The results for this thesis suggest that there is an optimal operating temperature, which varies for varying current densities. This optimal operating temperature is, admittedly, high.
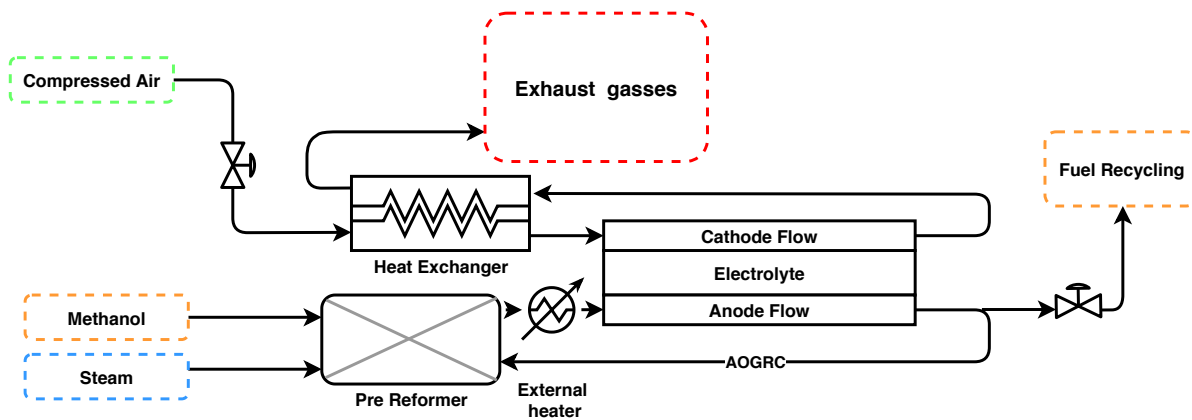
Figure 3.1: Shows the places in the methanol fuelled SOFC system where PHE and AOGRC are to be implemented.

The system's agility in load-following is largely dependent on heat recovery, due to the varying properties of the fuel cell, as a function of temperature. For instance, [22] proposes a strategy of power management in which the temperature of the SOFC is kept constant for a certain power demand range.

3.3.1. Means of heat recovery

Heat can be recovered by making use of heat exchangers, and re-incorporating massflows.

Heat exchangers offer a route for heat flows whilst keeping the mass flow separate. Their dynamic behaviour is to be studied. This is needed because it is known from [2], that the thermal inertia in the heat exchangers is a significant contributor to the load-following inertia of the hybrid systems of fuel cell and combustion engines. This claim makes it imperative that this component is modeled such, that the dynamic behaviour can be tested (this is done in sections 4.4 and 6.4).

Re-integration of mass flows offers a responsive way to to heat up the pre-reformer, whilst making use of the steam present in the AOG.

3.3.2. Decision for PHE and AOGRC as a means of heat re-integration

The decision was made to implement a PHE, in counterflow configuration, between the incoming and outgoing flows of the cathode. This is done because:

- A lot of heat is available in the the exhaust gasses of the cathodic flow

- The SOFC's preferred operation temperature is very high (see section 6.3.2)

- PHEs are considerably compacter than Tube Heat Exchanger (THE)s, and yet can withstand pressures up to 30 Bar if there is limited pressure difference between the flows

- Counterflow enables far more effective operation of a heat exchanger than parallel flow

In many instances of SOFC based power units, a pre-reformer is used, for reasons discussed in section 3.1. In many cases AOGRC is used to provide heat, steam and a measure of control over the pre-reformer. The decision has therefor been made to implement AOGRC in the methanol fuelled SOFC system.

The PHE and AOGRC are implemented in the methanol fuelled SOFC system as is depicted in figure 3.1

3.4. control strategy

The means to control the power output of the system, is decided upon in this section. Reviewing figure 3.1, six parameters are identified that can be directly controlled.

1. The magnitude of the flow of compressed air tot he cathode (Compression to 20 Bar will adia-batically increase the temperature of the gas to 710 K, which for this thesis is viewed as a given. compressor losses however, will be included in the system efficiency in section 6.8)

2. The magnitude of the flow of superheated methanol gas to the pre-reformer(The inflow temperature is determined to be 445K, slightly over the condensation temperature at 20 Bar)

3. The flow ratio of superheated steam(-to methanol) into the pre-reformer(The inflow temperature of the steam is determined to be 485K, slightly over the condensation temperature at 20 Bar)

4. The flow rate from the pre-reformer to the anode flow

5. The heat flow from the external heater to the incoming anode flow

6. The ratio of AOG that is re cycled to the pre-reformer (AOGRC ratio)

Note that density i , is not amongst them. The current density is dependent on the complex electrical resistance of the system that is linked up to, as well as changes in cell voltage. This relation is reciprocal as voltage, resistance, temperature, heat production and current density all impact each other. The premises of this thesis however, is that the current density can be perfectly controlled via the electrical switchboard of the naval vessel.

3.4.1. Decision on controlled parameters

1. Compressed air flow:

   To be a constant ratio to the current density. It must be ensured that this ratio is high enough, so there is enough oxygen present to enable electrochemical combustion at a reasonable cell voltage. The ratio must be low enough to prevent excessive cooling of the cell

2. Super heated methanol gas flow:

   To be controlled by a controller that is connected to the pressure in the pre-reformer. This is done to ensure that there will always be enough reformed fuel available to provide for the pre-reformer outflow rate (see bullet point 4)

3. Super heated steam flow ratio $\left(\mu_{steam} = \frac{\dot{N}_{steam}}{\dot{N}_{CH_3OH}} \right)$:

   Decided to be the controlled parameter. Varying this parameter will be done in an attempt to find the the most effective operation of the system. This was decided upon because of the great influence the presence of steam has on the effectiveness of the pre reformer.

4. Pre-reformer outflow rate:

   To be a constant ratio to the current density. It must be ensured that this ratio is high enough, so there is enough fuel present to enable electrochemical combustion at a reasonable cell voltage. The ratio must be low enough to prevent excessive cooling of the cell

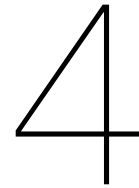5. Heat flow to the anode flow:

   Decided to be the controlled parameter. Varying this parameter will be done in an attempt to find the the most effective operation of the system. This was decided upon because of the great dependency of the SOFC behaviour on the cell temperature

4

Modeling the system

In order create a comprehensive model for the simulation of the behaviour of a methanol fuelled SOFC system, the entire system will be divided into subsystems, which will be integrated such, that the final model represents the entire system. The computer program which is used to to model and simulate is Simulink®and an extension thereof, Simscape™.

4.1. Simulation in Simulink® & Simscape™

The company Mathworks® offers several platforms for modelling all kinds of systems. Particularly suited for dynamic modelling are the Matlab based Simulink format and its extension, Simscape. These programs provide a visual way of building the models for the subsystems and connecting them. For the methanol fuelled SOFC system, the subsystems operate in different physical domains (electrical, thermal, electro-chemical, chemical) and are therefore different from each other. The agility and compatibility of the models in the Simulink format is a great advantage when the systems that need to be integrated have vastly different properties.

4.1.1. Simulink®

Simulink takes one or multiple signals that can be imported, defined, or otherwise generated and shows it as an arrow in the environment. This signal is called a "Simulink signal". "Blocks" are defined in the Simulink library that can be used to convert such a signal to mimic certain events in the system. These blocks can represent mathematical operators, logical operators, discrete operators, transfer functions and so on. Together, intricate systems can be modelled that will remain compatible with other systems that are modelled in Simulink .

The graphical nature of the Simulink environment and the user interface makes the program suited for the programming of multi-domain dynamical systems and system controls by means of feedback loops.

4.1.2. Simscape™

Simscape is an extension on the Simulink library which offers blocks that represent system components rather than mathematical conversions. This offers a big advantage when modelling complex physical systems. When these components operate in the same physical domain, connections represent actual physical connections. Within these domains two variables are defined; Through and Across, for which the Kirchhoff laws are enforced. These connections are called conserving ports and will require both a "through" and "across" variable from the component. An overview of several through- and across-variables is given in table 4.1.

These component blocks have equations specific to these components built in. The current model uses only thermal components. These are well suited to model the temperatures and heat flows in the cells

Domain	Through	Across
	(for every node)	(for a closed loop)
	$\sum_{i=1}^{n} T_i = 0$	$\sum_{j=1}^{m} A_j = 0$
electrical	current I	voltage V
mechanical (translational)	Force F	Velocity u
mechanical (rotational)	Torque T	Rotational velocity ω
gas	volume flow $\dot{V}$ / Heat flow $\dot{Q}$	pressure p / temperature T
thermal	heat flow $\dot{Q}$	temperature T
magnetic	magnetic flux	magnetomotive force F_m

Table 4.1: Several Through- and Across variables for their corresponding domains

at the extremes of a SOFC stack, in a detailed way (see sections 4.3.3 and 6.7).

4.2. pre-reformer model

In order to fully understand the behaviour of the pre-reformer,a model is built so tests can be run. the building of the model is done with the folowing questions in mind.

- What is the effect of the presence of methanation reactions on the process of MSR?

- At what temperature and pressure should the pre-reformer be operated?

- What should the dimensions of a pre-reformer be, and how do the dimensions influence the transient behaviour of the outflow?

The pre-reformer model mimics the the chemical reactions and half-reactions that take place simultaneously in the reactor vessel. The reaction kinetics are modelled so that the transient behaviour of the pre-reformer and its effects on the power system can be studied. The model takes into account the partial pressures, temperatures, reaction kinetics, and reaction enthalpies.

4.2.1. Model assumptions

The pre-reformer reactor is modelled with the chemical reactions that occur there as the leading processes. A model is always a simplification of reality, ant this one is no exception. Assumptions have to be made to enable modelling, keep calculation time in check and create a comprehensible model. These assumptions are the following:

1. Ideal gas law is valid (see section A.3.2).

2. Kinetics of all the forward and reverse reactions are adequately described by the Arrhenius equation.

3. Gasses move through the system at low speeds, so dynamic pressure effects can be neglected.

4. Gas flows to, and from the reactor are considered to be isentropic.

5. A slender tubular reaction vessel is proposed so particles have ample time to react and mix.

6. Only five reactions take place, of which the third one is the sum of the first two. The reactions are listed in table 2.1 in chapter 2.

7. The flow of heat through the insulated wall of the reactor vessel is non-significantAs a result, only the following heat flows will occur:

- AOGRC
- Methanol flow in
- Steam flow in
- Flow to the anode
- Heat flows from and to the reactions

8. There will be no leaking of any species of either reactants or products

9. Gasses inside the reactor will be homogeneously mixed in the largest part of the reactor

   - the mixture of the outflow will be representative for the the mixture inside the reactor
   - all reactions can take place at the same time
   - all reaction rates are dependent on the partial pressures of the reactants the temperatures.[1] This assumption will have to be tested.

A model for the pre-reformer should be centered around the reactions that take place inside that reformer. These reactions and their kinetics depend on a variety of circumstances inside the reactor vessel. The forward and reverse reaction rates (r_f, r_r)depend on:

- Reaction-rate constants(K_f, K_r).
- Stoichiometric coefficients of the reactions.
- Partial pressures or concentrations (dependent on the information source that is used) of the reactants.
- The presence of catalytic materials in the reactor.

The reactions that will be modelled in Simulink are given in table 2.1 in chapter 2.

4.2.2. Model setup
With these assumptions in mind, the model is set up in the following way

1. - Simulink will take the initial partial pressures by multiplying initial pressure by the molar fractions of the gasses. (1st step: an initial temperature and pressure are used.)
    - Simulink will take the temperature (assumed to be the same everywhere).

2. Simulink calculates reaction rates

   - calculates rate constants from relations found in the literature
   - calculates reaction rates

3. - Simulink calculates the produced and reacted fractions of species
    - Simulink calculates the produced heat from the reactions

4. Simulink calculates the new molar fractions (Inflow, outflow, reactions)

5. Simulink calculates new heat capacity of the gas mixture

6. Simulink calculates the new temperature and pressure. This concludes the first time step. A new iteration is started from step 2 with the values gathered from the current step.

This process is reproduced in a flowchart that is depicted in figure 4.1.

---

[1]In reality, a great deal depends on the material and internal construction of the reactor. However, the influence of different catalysts on the reaction in the reactor is beyond the scope of this investigation. For details of this subject, the reader is referred to the recommendations (section 7.2.6)
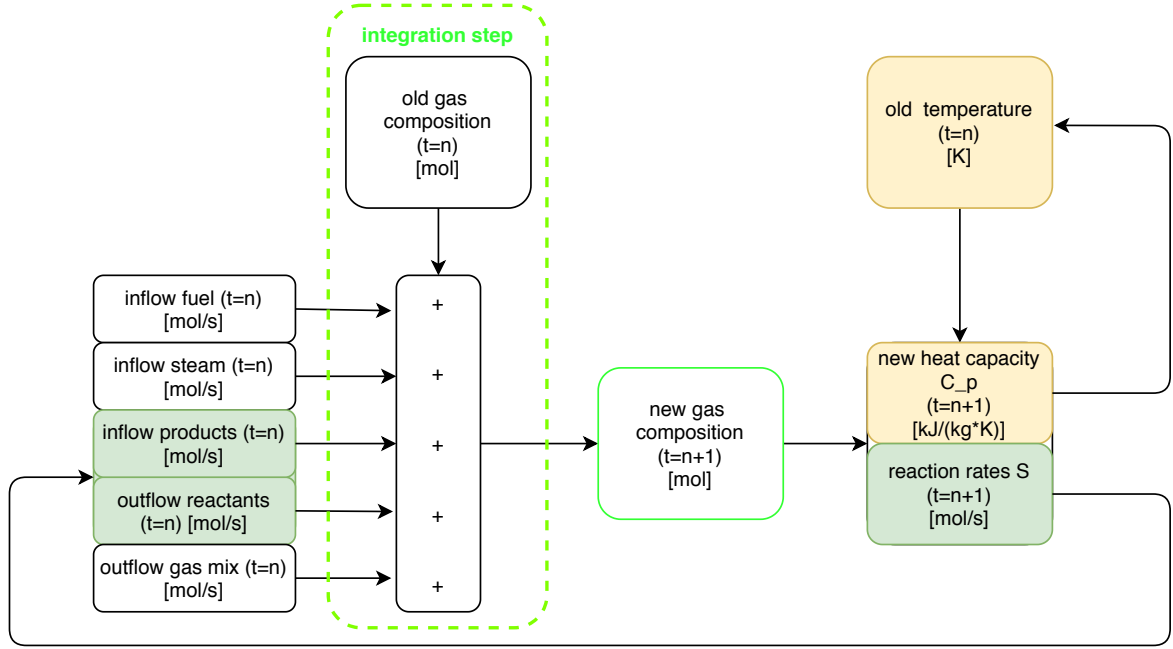
Figure 4.1: A schematic representation of the iterative process that is used inside the Simulink model of the pre-reformer. Moments in time are attached for every calculation. The arrows that circle round depict the data that is used for the next time step.

4.2.3. Molar quantities- and temperature- calculation

The molar quantity of all the species present in the pre-reformer are calculated in equation

$$N(t) = N(0) + \int_0^t \left(\sum_{reactions} \cdot \dot{N}_x(t) + \sum_{out} \cdot \dot{N}_i(t) + \sum_{out} \cdot \dot{N}_i(t) \right) dt \qquad (4.1)$$

where

$$i \in \{CH_3OH,\ H_2,\ H_2O,\ CO,\ CO_2,\ CH_4\}$$

$$\sum \dot{N}_i(t) = \dot{N}_{i,MSR}(t) + \dot{N}_{i,WGS}(t) + \dot{N}_{i,MDR}(t) + \dot{N}_{i,MCMO}(t) + \dot{N}_{MCDO}(t) \qquad (4.2)$$

The temperature of the reactor and its contents is calculated in equation 4.3

$$T(t) = T(0) + \int_0^t \left(\frac{\Sigma \dot{Q}}{\Sigma(N_x(t) \cdot c_{p,x}(T)) + C_{reactor}} \right) dt \qquad (4.3)$$

where

$$\sum \dot{Q} = \dot{Q}_{in} + \dot{Q}_{out} + \dot{Q}_{MSR} + \dot{Q}_{WGS} + \dot{Q}_{MDR} + \dot{Q}_{MCMO} + \dot{Q}_{MCDO} \qquad (4.4)$$

$$\dot{Q}_{in} = \dot{N}_{steam} \cdot \bar{h}_{H_2O}(T_{steam}) + \dot{N}_{fuel} \cdot \bar{h}_{CH_3OH}(T_{fuel}) + \sum (\dot{N}_{AOG} \cdot \bar{h}_x(T_{AOG})) \qquad (4.5)$$

$$\dot{Q}_{out} = \sum (T_{x,out} \cdot \bar{h}_x(T_{out})) \qquad (4.6)$$

The means of implementation in Simulink is given in the appendix C in figures C.1, C.2 and C.3 for equations 4.1 (for CH_3OH), 4.4 and 4.3 respectively.

4.2.4. reaction rates

Although the equilibrium constant of a great number of reactions has been experimentally determined, finding the reaction rates in the pre-reformer is far from trivial. First of all, even if all reactions that

occur except the ones listed in table 4.3 (copied from table 2.1 for convenience) are disregarded as non influential, at any given time, ten reactions are taking place.

In reality however, reactions like the ones in table 4.3 do not occur as such. These reactions are the superposition of numerous elementary reactions. This is especially true when catalysts are used to create a more favourable yield or faster kinetics. The list of elementary reactions of the Water Gas Shift is given in table 4.2, as an example. In this list the letter S is used to signify a site where molecules and other species can attach to the catalyst. The $\cdot S$ signifies that site is attached to the species that is written before it.
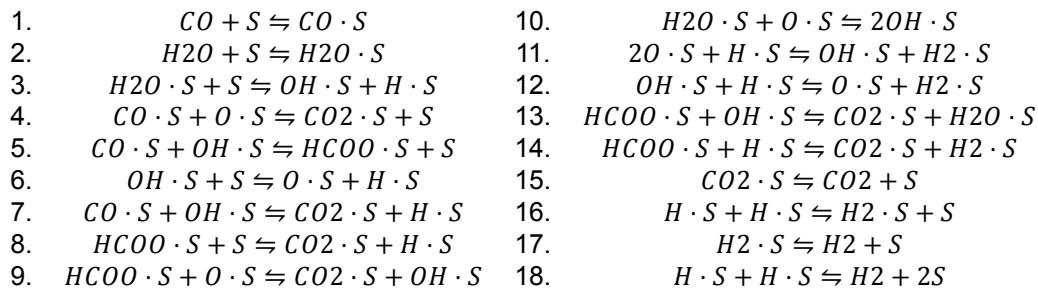
1.	$CO + S \leftrightarrows CO \cdot S$	10.	$H2O \cdot S + O \cdot S \leftrightarrows 2OH \cdot S$
2.	$H2O + S \leftrightarrows H2O \cdot S$	11.	$2O \cdot S + H \cdot S \leftrightarrows OH \cdot S + H2 \cdot S$
3.	$H2O \cdot S + S \leftrightarrows OH \cdot S + H \cdot S$	12.	$OH \cdot S + H \cdot S \leftrightarrows O \cdot S + H2 \cdot S$
4.	$CO \cdot S + O \cdot S \leftrightarrows CO2 \cdot S + S$	13.	$HCOO \cdot S + OH \cdot S \leftrightarrows CO2 \cdot S + H2O \cdot S$
5.	$CO \cdot S + OH \cdot S \leftrightarrows HCOO \cdot S + S$	14.	$HCOO \cdot S + H \cdot S \leftrightarrows CO2 \cdot S + H2 \cdot S$
6.	$OH \cdot S + S \leftrightarrows O \cdot S + H \cdot S$	15.	$CO2 \cdot S \leftrightarrows CO2 + S$
7.	$CO \cdot S + OH \cdot S \leftrightarrows CO2 \cdot S + H \cdot S$	16.	$H \cdot S + H \cdot S \leftrightarrows H2 \cdot S + S$
8.	$HCOO \cdot S + S \leftrightarrows CO2 \cdot S + H \cdot S$	17.	$H2 \cdot S \leftrightarrows H2 + S$
9.	$HCOO \cdot S + O \cdot S \leftrightarrows CO2 \cdot S + OH \cdot S$	18.	$H \cdot S + H \cdot S \leftrightarrows H2 + 2S$

Table 4.2: Constituents of the WGS-reaction ($CO + H_2O \leftrightarrows CO_2 + H_2$) over a nickel catalyst. S denotes a position in the catalyst surface.

The takeaway from this, is that it is near impossible to find the reaction rates (r_f, r_r) and the constants (K_f, K_r, K_{eq})in an analytical way. All these terms are influenced by pressure, temperature, the sort of catalyst, and the ratios of reactants. The constants, therefore, are far from constant.

Secondly, with only the equilibrium constant there can be no calculation of the actual reaction rates. The equilibrium constant, K_{eq}, is merely a means to calculate the fractions of reactants and products at the final state. This is not very useful in a dynamic process, where it could well be that equilibrium is never fully reached [2].The reaction rates are calculated as indicated in equation 4.7, where, the subscript f indicates the forward reaction and the subscript r indicates the reverse reaction of the fictional equilibrium $aA + bB \leftrightarrows cC + dD$.

$$r_f = K_f \cdot [A]^m \cdot [B]^n \qquad r_r = K_r \cdot [C]^p \cdot [D]^q \tag{4.7}$$

In equation 4.7, the exponents m, n, p & q are not necessarily the same as the stoichiometric constants of the overall reactions. Therein the calculation of the rate constants differs from the calculation of the equilibrium constants(see equation 4.8). Reaction rates are limited by the rate of the slowest elementary step. The exponents m, n, p and q reflect this rate limiting step or a combination of rate limiting steps. In the case of MCMO and MCDO for example, the forward rates are determined by more intricate relations, dependent on the catalyst applied(see sections 4.2.7 and 4.2.8).

$$K_{eq} = \frac{[A]^a \cdot [B]^b}{[C]^c \cdot [D]^d} \tag{4.8}$$

It is important to note that even though K_{eq}, K_f & K_r are constants, they are hardly constant as they are dependent on temperature. This dependency has to be integrated in the model. The temperature dependent K_{eq} was gathered from [39], which is a review of many findings and measurements. This work summarizes all these works into a single temperature dependent expression for the K_{eq} for the three equilibria present in the pre-reformer. Figure 4.2 shows the relations found in a graphical frame. The found expressions for K_{eq} are:

for MSR

$$\ln(K_{eq}) = 7.333 \cdot T^{-1} - 24.8 \quad \Rightarrow \quad K_{eq} = \exp\left(7.333 \cdot T^{-1}\right) \cdot \exp\left(-24.8\right) \tag{4.9}$$

---

[2]in evaluating the model it becomes clear that for a reformer of 2 m^3 at a pressure of p= $2 \cdot 10^6$ and temperature of around 500 K, the reactor will have the characteristics of a an equilibriumreactor for steady operation. This is further elaborated upon in section 6.2.2

forward MSR	$CH_3OH + H_2O \rightarrow CO_2 + 3H_2$
reverse MSR	$CO_2 + 3H_2 \rightarrow CH_3OH + H_2O$
forward MDR	$CH_3OH \rightarrow CO + 2H_2$
reverse MDR	$CO + H_2 \rightarrow CH_3OH + H_2O$
forward WGS	$CO + H_2O \rightarrow CO_2 + H_2$
reverse WGS	$CO_2 + H_2 \rightarrow CO + H_2O$
forward MCMO	$CO + 3H_2 \leftrightharpoons CH_4 + H_2O$
reverse MCMO	$CH_4 + H_2O \leftrightharpoons CO + 3H_2$
forward MCDO	$CO_2 + 4H_2 \leftrightharpoons CH_4 + 2H_2O$
forward MCDO	$CH_4 + 2H_2O \leftrightharpoons CO_2 + 4H_2$

Table 4.3: Ten reactions of consequence that take place in the pre-reformer reactor simultaneously.

for MDR

$$\ln(K_{eq}) = 11.6 \cdot T^{-1} - 30.6 \quad \Rightarrow \quad K_{eq} = \exp(11.6 \cdot T^{-1}) \cdot \exp(-30.6) \tag{4.10}$$

for WGS

$$\ln(K_{eq}) = -4.6 \cdot T^{-1} + 4.235 \quad \Rightarrow \quad K_{eq} = \exp(-4.6 \cdot T^{-1}) \cdot \exp(4.235) \tag{4.11}$$

This relation is implemented in the Simulink®pre-reformer model as is shown in figure C.5. The relation is shown for MSR. For MDR and WGS the graph are the same, with different constants, as can be found in equations 4.10 and 4.11 respectively.

The overall production of CO in the pre-reformer will be well within the limits of what a SOFC can handle if the molar inflow ratio of steam over CH_3OH will be kept around 1 [27].

[27] also provided a framework for the reactions that will be modelled to take place in the pre-reformer. This research shows that that of the reactions MSR, MDR and WGS, all take place within the context of methanol steam reformating. Before, it was believed that the direct form of the MSR did not exist in itself, but was merely the superposition of MDR and WGS as shown in table 4.4

MDR	$CH_3OH \rightleftarrows 2H_2 + CO$	$\Delta H = +90.7kJ/mol$ STP	
WGS	$CO + H_2O \rightleftarrows CO_2 + H_2$	$\Delta H = -41.2kJ/mol$ STP	+
MSR	$CH_3OH + H_2O \rightleftarrows CO_2 + 3H_2$	$\Delta H = +49.7kJ/mol$ STP	

Table 4.4: Studying this table, it becomes obvious how people came to suspect that MSR is the superposition of MDR and WGS.

It is important to notice that the partial pressures and their ratios have a profound influence on the the kinetics of the reactions, yet, the overall pressure has no strong connection to either K_{eq}, K_f or K_r (This is according to hard-sphere collision theory of gas-phase reactions[13]).

Overall pressure is calculated by using the ideal gas law, which is assumed to be heeded. This assumption is substantiated in the section A.3.2.

$$p = Z \cdot \frac{n \cdot R \cdot T}{V}$$

partial pressures are then calculated by equation 4.12, where 1 till 5 represent the 6 different species present in the reactor.

$$p_j = p \cdot \frac{\sum n_i}{n_j} \quad \text{where} \quad i, j \in \{CH_3OH, H_2, H_2O, CO, CO_2, CH_4\} \tag{4.12}$$

4.2.5. Reaction parameters

It has to be noted that different parameters for the the reactions involved were retrieved. These parameters can differ from investigation to investigation and must therefore be seen more as an indication for what is actually happening, rather than a 'set in stone' physical law. This is also exactly the caution
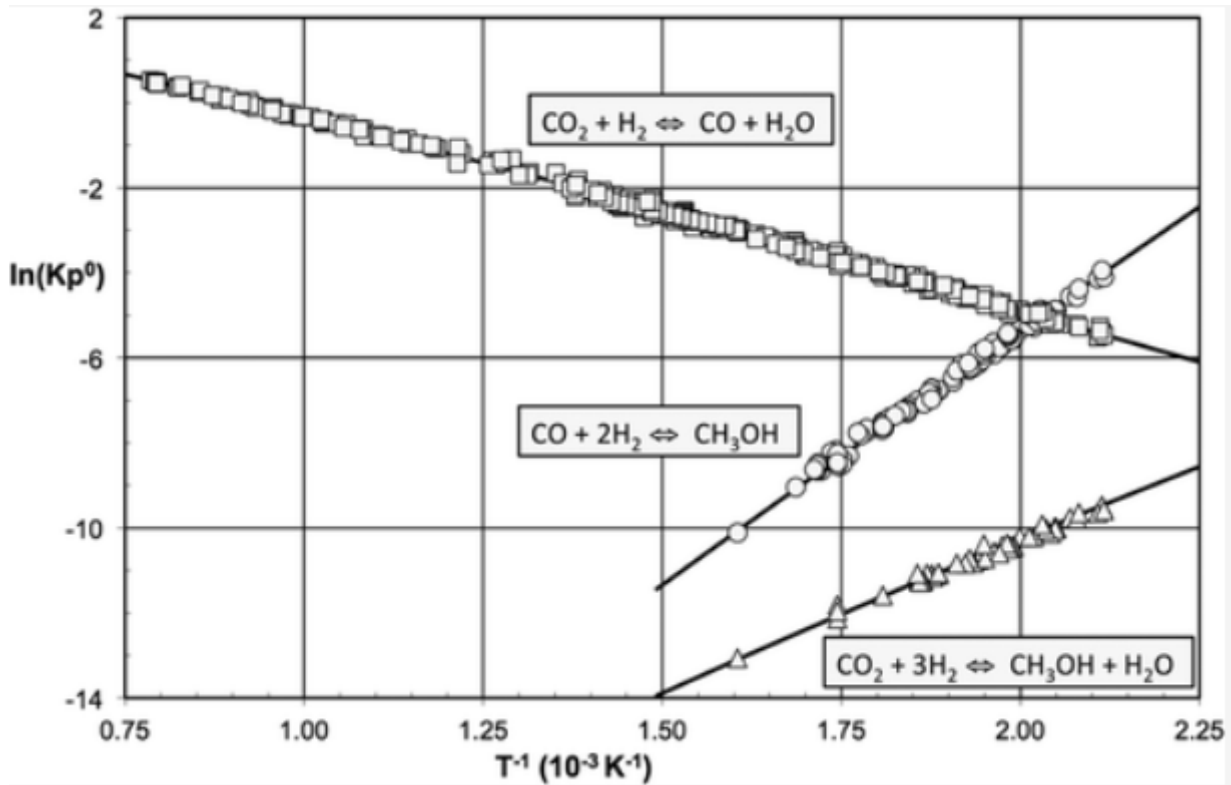
Figure 4.2: the relations found between temperature and K_{eq} for MSR, MDR and WGS according to [39]

that should be taken by using the Arrhenius equation on reactions that are not elementary(this was explained at the beginning of section 4.2.4).

Substantial differences can be found between the use of different catalysts. Most notably, according to [27], using a copper based catalyst will prevent the methanation reactions from happening altogether. The implications of this notion will very likely be severe. If we were to add to this that copper based catalysts tend to have more more favourable properties to enhance the yield of the pre-reformer, it could be argued that a decision for a copper based catalyst is the most likely. Parameters for the Arrhenius equation for the forward rate constant of the MSR reaction are found in [31].

In general the rate equations for a reaction:

$$a \cdot A + b \cdot B \rightleftharpoons c \cdot C + \cdot D \tag{4.13}$$

will be built up in the following manner

$$r_f = K_f [A]^a [B]^b \quad \text{where} \quad K_f = K_{A,f} \cdot EXP\left(\frac{-E_{a,f}}{R \cdot T}\right) \tag{4.14}$$

for the forward rate, and

$$r_r = K_r [C]^c [D]^d \quad \text{where} \quad K_r = K_{A,r} \cdot EXP\left(\frac{-E_{a,r}}{R \cdot T}\right) \tag{4.15}$$

for the reverse rate. This yields that in equilibrium:

$$K_f [A]^a [B]^b = K_r [C]^c [D]^d \quad \rightarrow \quad K_{eq} = \frac{[C]^c [D]^d}{[A]^a [B]^b} = \frac{K_f}{K_r} \tag{4.16}$$

If the rate equations differ from this format it will be stated.

Parameter	Value	Unit of measure	Source
WGS			
$K_{eq,wgs}$	$EXP\left(4.467 \cdot 10^3 \cdot T^{-1}\right) \cdot EXP\left(-4.10\right)$	[-]	[39]
$K_{A,r}$	$4.0 \cdot 10^8$	$[m^3 mol^{-1} s^{-1}]$	[31]
$E_{a,r}$	$1.0 \cdot 10^5$	$[J \cdot mol^{-1} K^{-1}]$	[31]
MDR			
$K_{eq,MDR}$	$EXP(-11.6 \cdot 10^3 \cdot T^{-1}) \cdot EXP(30.6)$	$[-]$	[39]
$E_{a,f}$	$362 \cdot 10^3$	$[J/mol]$	[11]
$K_{A,f}$	$2.12 \cdot 10^{13} \cdot \left(\frac{T}{298.15}\right)^{1.22}$	$[mol \cdot m^6 J^{-2} s^{-1}]$	[11]
MSR			
$K_{eq,MSR}$	$EXP(-7.333 \cdot 10^3 \cdot T^{-1}) \cdot EXP(24.8)$	$[-]$	[39]
$E_{a,f}$	$7.0 \cdot 10^4$	$[J \cdot mol^{-1} \cdot s^{-1}]$	[31]
$K_{A,f}$	$8.0 \cdot 10^8$	$[s^{-1}]$	[31]
r_f [3]	$K_{A,f} EXP\left(\frac{-E_{a,f}}{R \cdot T}\right) \cdot [CH_3OH]^{0.6}[H_2O]^{0.4}$	$[mol \cdot m^{-3} s^{-1}]$	[31]
MCMO			
$K_{eq,MCMO}$	$EXP\left(\frac{-206 \cdot 10^3}{8.314 \cdot T}\right)$	[-]	[12]
$E_{a,f}$	$2.58 \cdot 10^4$	$[J \cdot mol^{-1} \cdot k^{-1}]$	[19]
$K_{A,f}$	$8.55 \cdot 10^6$	$[mol^{0.29} \cdot s^{-1} \cdot m^{-1.74}$	[19]
r_f [4]	$K_{A,f} \cdot EXP\left(\frac{-E_{a,f}}{R \cdot T}\right) \cdot [CH_3OH]^{0.6}[H_2O]^{0.4}$	$[mol \cdot s^{-1}]$	[19]
MCDO			
$K_{eq,MCDO}$	$EXP\left(\frac{-165 \cdot 10^3}{8.314 \cdot T}\right)$	[-]	[12]
E_A	$4.54 \cdot 10^4$	J/mol	[19]
$K_{A,f}$	27.78	$mol^{-1} s^{-1}$	[19]

Table 4.5: The collected values for the parameters involved with determining the rates of the reactions taking place in the pre-reformer
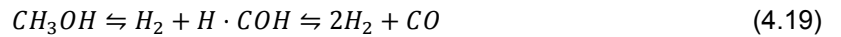
parameters for the Arrhenius equation for the forward rate constant of the MSR reaction are found in.

$$E_{a,f} = 7.9 \cdot 10^4 [J/mol] \tag{4.17}$$

$$K_{A,f} = 3.246 \cdot 10^5 [mol \cdot m^6 J^{-2} s^{-1}] \tag{4.18}$$

4.2.6. kinetics of MDR

It has long since been known that the decomposition of methanol is a 2-stage reaction where formaldehyde is formed in the process [11]:

$$CH_3OH \leftrightharpoons H_2 + H \cdot COH \leftrightharpoons 2H_2 + CO \tag{4.19}$$

In this process $CH_3OH \leftrightharpoons H_2 + H \cdot COH$ is the rate-limiting step. According to [11] the rate of this step in the reaction is

$$r_f = 2.12 \cdot 10^{13} \left(\frac{T}{298}\right)^{1.22} EXP\left(\frac{-362 \cdot 10^3}{RT}\right) \tag{4.20}$$

4.2.7. Kinetics of MCMO

According to [33], the most reliable model for the the forward rate of the methanation reaction of Carbon Monoxide, in the temperature range [T= 453.15K, T= 675.15K] in the pressure range [p=20 bar, p= 30bar] is given by the relation:

$$r_f = -\frac{k \cdot K_C \cdot K_H^2 \cdot p_{CO}^{0.5} \cdot p_{H_2}}{(1 + K_C \cdot p_{CO}^{0.5} + K_H \cdot p_{H_2}^{0.5})^3} \tag{4.21}$$

where the constants k, K_C, K_H (reaction rate constant, absorption rate constant of C in catalyst, absorption rate constant of H in catalyst,) are determined with the Arrhenius equation

$$k = k^0 EXP\left(\frac{-E_a}{RT}\right) \qquad K_i = K_i^0 EXP\left(\frac{-\Delta \bar{h}_i}{RT}\right)$$

, where i represents either H or C.

k^0	$4.8/3.6 \cdot 10^9$	$[mol/(kg_{cat} \cdot s)]$
E_a	103000	$[J/mol]$
K_C^0	$5.8 \cdot 10^{-4}$	$bar^{0.5}$
$\Delta \bar{h}_C$	-42000	$[J/mol]$
K_H^0	$1.6 \cdot 10^{-2}$	$bar^{0.5}$
$\Delta \bar{h}_H$	-16000	$[J/mol]$

Implementation in Simulink of this equation is shown in appendix C in figure C.6

4.2.8. Kinetics of MCDO

According to [15], the most reliable model for the the forward rate of the methanation reaction of Carbon Monoxide, in the temperature range [T= 453.15K, T= 675.15K] in the pressure range [p=20 bar, p= 30bar] is given by the relation:

$$r_f = -\frac{k_a \cdot p_{CO_2}^{0.5} \cdot p_{H_2}^{0.5}}{\left(1 + k_b \left(\frac{p_{CO_2}}{p_{H_2}}\right)^{0.5} + k_c \cdot p_{CO_2}^{0.5} \cdot p_{H_2}^{0.5} + k_d \cdot p_{H_2O}\right)^2} \tag{4.22}$$

where the constants k_a, k_b, k_c, k_d are determined with the Arrhenius equation

$$k_a = A \cdot EXP\left(\frac{-E_a}{RT}\right) \qquad k_i = k_i^0 \cdot EXP\left(\frac{-\Delta \bar{h}_i}{RT}\right) \quad \text{where} \quad i \in \{b,c,d\} \tag{4.23}$$

.From evaluating this relation it can be gathered that at higher temperatures, the rate becomes insensitive to changes in partial pressures of carbon dioxide and hydrogen[15].

A	2652	$[mol/(g_{cat} \cdot s)]$
E_a	85400	$[J/mol]$
k_b^0	0.055	$[-]$
$\Delta \bar{h}_b$	-9200	$[J/mol]$
k_c^0	0.0251	$[bar^{-1}]$
$\Delta \bar{h}_c$	-8100	$[J/mol]$
k_d^0	0.0958	$[bar^{-1}]$
$\Delta \bar{h}_d$	-1140	$[J/mol]$

Implementation in Simulink of this equation is shown in appendix C in figure C.7. Note that even though the the relation that describes the forward rate of the carbon dioxide methanation reaction has shed its similarity to the numerator of the equilibrium equation (4.8), the overall assumption that the equilibrium constant describes the the ratio between the forward and reverse rate of a certain reaction is maintained.

4.3. Solid Oxide Fuel Cell model

In order to fully understand the behaviour of the SOFC, model results are generated. These are generated with the following questions in mind.

- What are the preferred operating conditions of the SOFC?

- What power outputs and efficiency can be expected in these conditions and in non-optimal conditions?

- What are the load-following characteristics of the reformed methanol fuelled SOFC?

- Does the position of a cell within the stack have an impact on its behaviour?

4.3.1. Model assumptions

In the process of creating dynamic models, certain assumptions have been made. These assumptions were made to simplify reality as to be able to obtain a working model. These assumptions have to be validated. They have been validated during the course of building the model and writing the report. The findings of the validation processes are compiled in this chapter.

- Laminar flow in channels. Fully developed fluid dynamics. This was assumed in notable works by ([1],[37])

- Gasses move through the system at low speeds, dynamic pressure differences can be neglected> this has been checked in appendix A.3.1

- Oxide ions travel perpendicular to flow channels

- Low temperature gradient perpendicular tot the flow direction within Positive electrode-Electrolyte-Negative electrode (PEN)-structure, neglected.This was assumed in notable works by ([1],[37])

- Gasses behave like ideal gasses in the SOFC. This has been checked in appendix A.3.2

- H_2, CO, CH_3OH and CH_4 show fast reaction kinetics so their electrochemical oxidation reactions occur at a rate that is proportional to their presence.This might be a crude assumption, as it is known that CO is mostly reacted in the Water Gas Shift before it reaches the TPB. It is however, a conservative assumption because the reaction kinetics of Hydrogen are faster than that of other species.

- Thermal conductivity as well as isobaric heat capacity is considered constant throughout the channels. For the temperature range at which the SOFC is operated this is close to reality.

- The SOFC stack is an insulated unit. Heat flows the edges of the individual cells is far out weighed by the heat flow perpendicular to the plate structure. Therefore, for single cell calculations, only cell-to-cell and cell-to-endplate-to-environment heat flows are considered. The results as shown in section 6.7 re-affirm this assumption.

- Clear fluids are assumed. Therefor, radiation heat exchange will only take place from solid to solid. Convective heat flows exist between solids and fluids.

- Gas flows to and from the gas channels are considered to be isentropic.

4.3.2. Further reforming of the anode gasses

I has to be kept in mind that, even though the reforming of methanol has mainly been performed in the pre-reformer, a shift in the composition of the gas mixture could well take place in the fuel channel. This is to be expected, because the conditions in the fuel channel of the SOFC will be vastly different from the conditions in the pre-reformer. From the pre-reformer model it is known that equilibrium constants and kinetics of reactions- and half- reactions are highly dependent on the temperature. Section 7.2.1 elaborates on this problem.

4.3.3. Model setup

The model that will describe the behaviour of the Solid oxide fuel cell is depicted in figure 4.3. This figure shows the mathematical flow that is maintained to calculate the different properties of the gasses, components and electrical currents in a single fuel cell. As is clear from the diagram, there are multiple connections between the different domains. Temperature has an influence on the Nernst voltage as well as the on the irreversible voltage drops within the cell. The partial pressures influence the Nernst voltage and the heat capacity of the system. the electrical current and voltage drops influence the temperature within the cell. The flow is as follows:
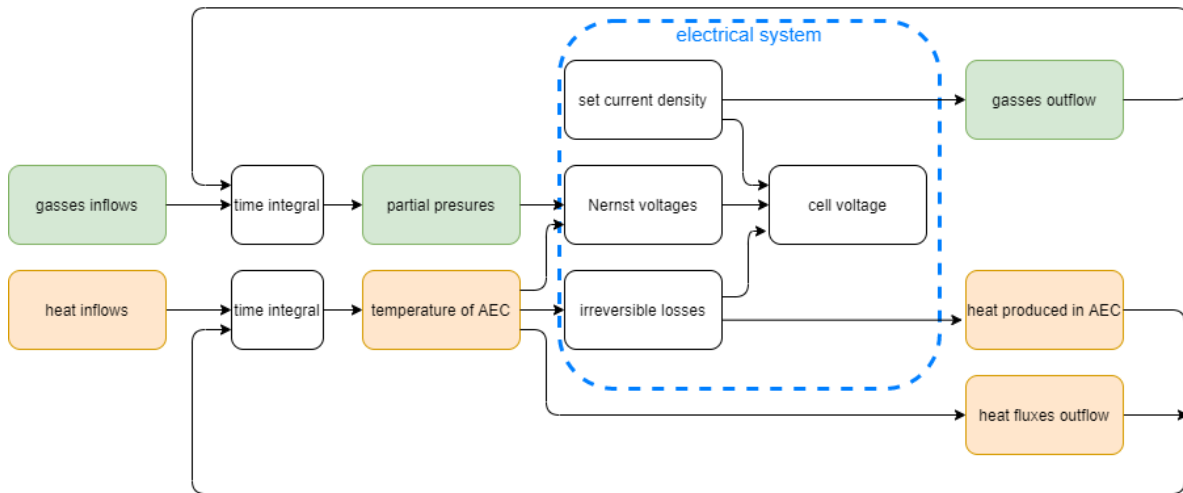
Figure 4.3: Block diagram for the dynamic SOFC model

1. The model takes the temperature and partial pressures of the previous time step

2. The Nernst voltage and the irreversible losses are calculated for these circumstances for the given current density.

3. • Heat production due to the irreversible losses is calculated and integrated as shown in figure (4.6).

   • Employment and production of gas species are calculated.

4. • The sum of the heat production is integrated over time and delivers new heat content of the system of the system.

   • The change in gas composition is calculated from which also c_p can be obtained.

5. The new pressures and temperature are calculated and a new iteration commences.

The model of a single cell is divided into main four sections. These are chosen such that heat flows, heat sinks, heat sources and mass flows can be defined in the model in a comprehensive way. This means that sinks and sources are located within the defined sections, and that flows are situated between different sections to prevent disambiguity within the model. The sections of a single cell and the heat flows between them are depicted in figure. 4.4.

Temperature behaviour of cells at end of stack

For the radiative- and convective- heat flows, Simscape provides "components" that determine the heat flows between cell components and mass flows within the cell.

Radiative heat flow, $\dot{Q}_{rad}$, is determined by the Stefan-Boltzmann law:

$$\dot{Q}_{1,2}^{rad} = \frac{\sigma \cdot \epsilon_1 \cdot \epsilon_2 \cdot A_{cell}(T_1^4 - T_2^4)}{\epsilon_1 + \epsilon_2 - \epsilon_1 \cdot \epsilon_2} \tag{4.24}$$

Where 1 and 2 represent solid surfaces in within the cell opposite to each other.

Convective heat flow, $\dot{Q}^{conv}$, between surfaces and mass flows, is determined by

$$\dot{Q}_{1,2}^{conv} = \alpha_2 \cdot A_{cell} \cdot (T_1 - T_2) \tag{4.25}$$

where 1 represents a solid cell component and 2 represents a mass flow through the gas channels.

Figure 4.5 shows the illustrations that represent the radiative- and convective heat blocks in Simscape.
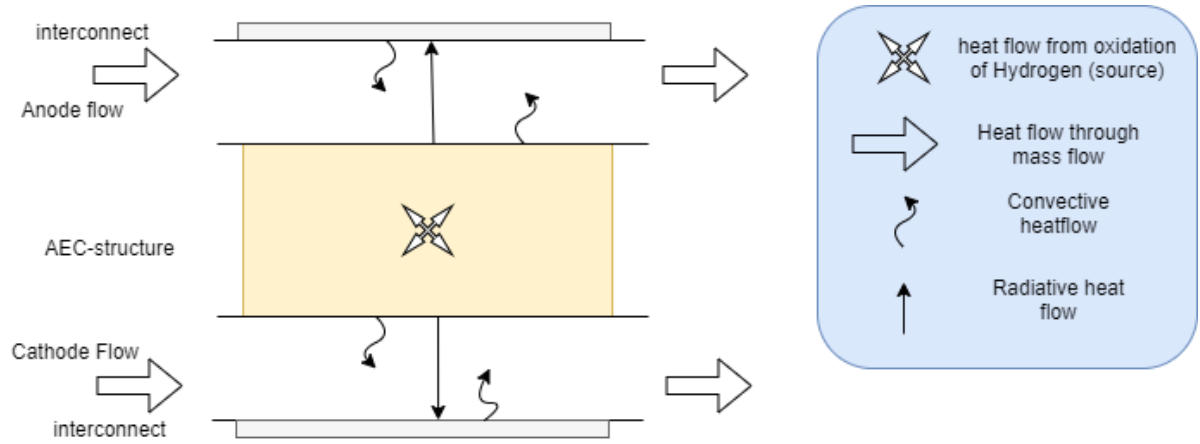
Figure 4.4: An overview of the configuration of a single cell and the different heat flows between them.

Figure 4.5: Simscape "components" that calculate radiative- (left) and convective- heat flow between defined cell elements.

For the complete assessment of the heat flows within a single cell, this only leaves the heat that is convected in and out of the gas channels. These flows are calculated:

$$\dot{Q}_{af} = \sum_{i} \dot{N}_i \cdot \bar{h}_i - \sum_{out,af} \dot{N}_i \cdot \bar{h}_i \tag{4.26}$$

$$\dot{Q}_{cf} = \sum_{in,cf} \dot{m}_j \cdot \bar{h}_j - \sum_{out,cf} \dot{m}_j \cdot \bar{h}_j \tag{4.27}$$

4.3.4. Molar inflows and outflows of the fuel- and oxidizer channels

Inflows at the fuel channel are taken directly from the from the pre-reformer model, as they will be the same as the outflow of that model. Inflow of the air channel is a ratio to the in flow of the fuel channel.

$$\sum_{in,cf} \dot{N}_j = \lambda \cdot \sum_{in,af} \dot{N}_i \tag{4.28}$$

Particle flows along the flow direction of the channels change as a function of the generated current. The changes in the particle composition of the anode flows are defined by:

$$\dot{N}_{N_2,out} = \dot{N}_{N_2,in} \tag{4.29}$$

$$\dot{N}_{O_2,out} = \dot{N}_{O_2,in} - \frac{1}{2} \cdot \dot{N}_{H_2,reacted} - \frac{1}{2} \cdot \dot{N}_{CO,reacted} - \frac{3}{2} \cdot \dot{N}_{CH_3OH,reacted} - \cdot\dot{N}_{CH_4,reacted} \tag{4.30}$$

$$\dot{N}_{H_2,out} = (1 - \gamma) \cdot \dot{N}_{H_2,in} \tag{4.31}$$

$$\dot{N}_{CO,out} = (1 - \gamma) \cdot \dot{N}_{CO,in} \tag{4.32}$$

$$\dot{N}_{CH_3OH,out} = (1 - \gamma) \cdot \dot{N}_{CH_3OH,in} \tag{4.33}$$

$$\dot{N}_{CH_4,out} = (1 - \gamma) \cdot \dot{N}_{CH_4,in} \tag{4.34}$$

For the cathode flow:

$$\dot{N}_{H_2O,out} = \dot{N}_{H_2O,in} + \dot{N}_{H_2,reacted} + 2 \cdot \dot{N}_{CH_3OH,reacted} + 2 - \dot{N}_{CH_4,reacted} \tag{4.35}$$

$$\dot{N}_{CO_2,out} = \dot{N}_{CO_2,in} + \dot{N}_{CO,reacted} + \dot{N}_{CH_3OH,reacted} + \dot{N}_{CH_4,reacted} \tag{4.36}$$
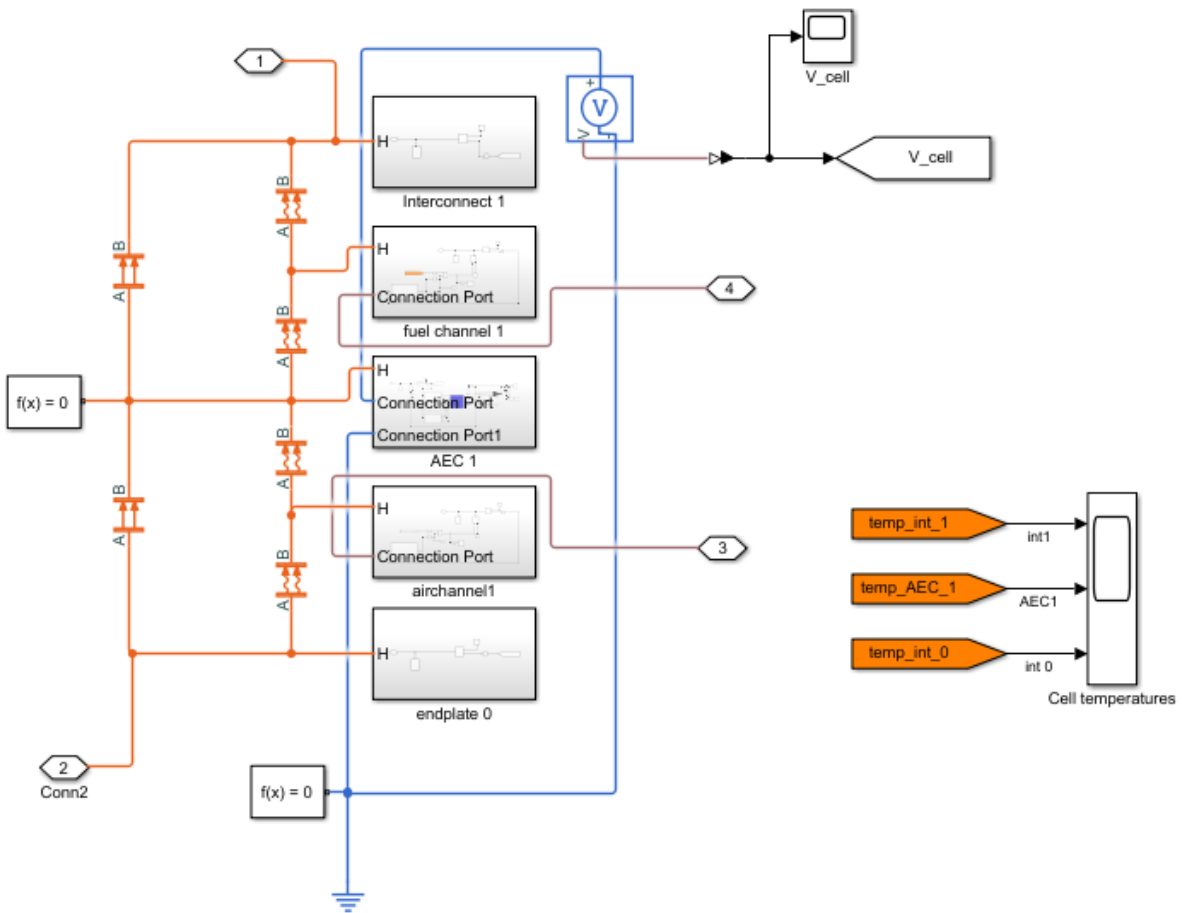
Figure 4.6: Model for the heat integration built in Simscape. This model calculates the temperatures and heat flows for a single cell. The model mimics figure 4.4 although the heat flows caused by mass inflow and outflow are covered in figure C.9. The model covers radiative- and convective heat flows between components that each have their own thermal mass
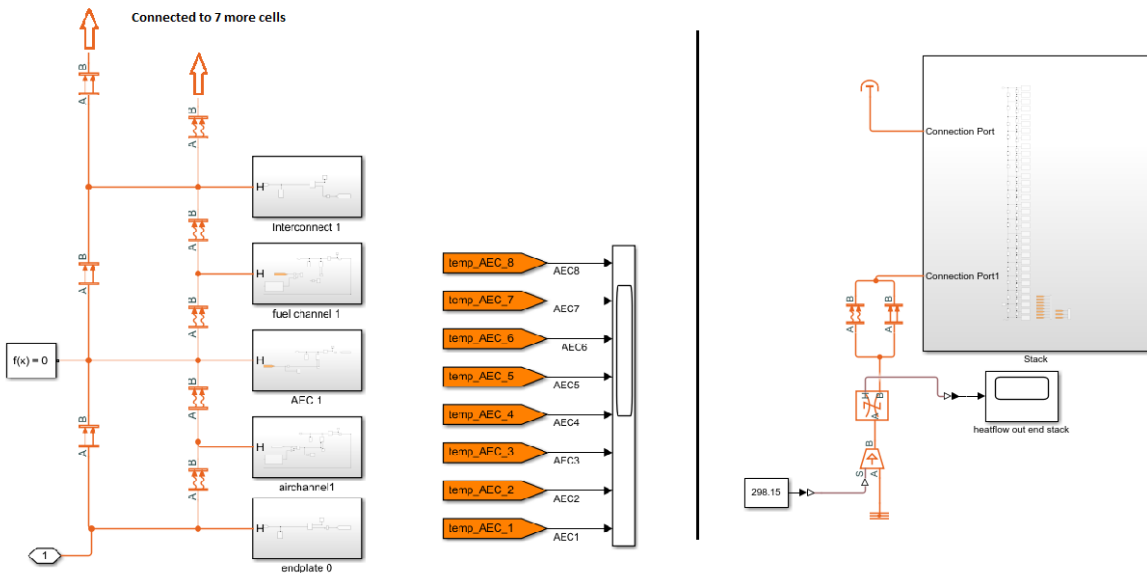

Figure 4.7: Thermal model of the cells at the end of the stack. the top is totally insulated , simulating the behaviour of a cell distanced from the end of the stack. The bottom has a connection to the environment, simulating the end of the stack. Heatflow to the environment is simulated by the circuit depicted on the right side of the figure

Here , the fuel utilisation factor γ is used. It is defined as:

$$\gamma = \frac{\sum_{used} \dot{N}_i}{\sum_{in} \dot{N}_i} = \frac{i \cdot A_{cell}}{zF \cdot \sum_{in} \dot{N}_i} \tag{4.37}$$

Implementation of the calculations of the outflows in Simulink is shown in figures C.13, C.16, C.18 and C.20 of the appendix C, where calculations of $\dot{N}_{i,af,in}$, $\dot{N}_{i,af,out}$, $\dot{N}_{i,cf,in}$, and $\dot{N}_{i,cf,out}$ are shown respectively.

The outflow of the air channel is different from the inflow of the fuel channel an can be characterised by:

$$\dot{N}_{O_2,out} = \dot{N}_{O_2,in} - \frac{1}{2F} \cdot I_{cell} \tag{4.38}$$

$$= \dot{N}_{O_2,in} - 1/2\,\dot{N}_{H_2,used} - 1/2\,\dot{N}_{CO,used} - 3/2\,\dot{N}_{CH_3OH,used} - 4/2\,\dot{N}_{CH_4,used} \tag{4.39}$$

$$\dot{N}_{N_2,out} = \dot{N}_{N_2,in} \tag{4.40}$$

The assumption that all reactants at the anode undergo such fast reaction kinetics that all reactants are consumed in the same ratios, is a bit crude. However, this is mainly an issue for lower operating temperatures, as the utilisation of methane could be overestimated because of kinetic impairment. The effect on the calculated voltages and molar flow of different species will be limited. As tests with the pre-reformer model have shown, the reforming at high temperatures will result in small molar fractions of methane, methanol and carbon monooxide at the anode. Furthermore, the voltages that can be reached by the electro-chemical oxidation of the different available fuels do not differ all that much. A resulting combined voltage will be minimally impacted by a lower actual utilisation ratio of CH_4 than calculated.

4.3.5. SOFC outflow delay

To adequately capture the dynamic behaviour of the methanol fuelled SOFC system, it is of importance to accurately describe the delay of flows through the separate components. For the pre-reformer and the PHE however, this effect is an inherent part of the respective models.

The pre-reformer features

- Kinetics of the reactions

- Outflow in equilibrium state due to scale of the component

- Pressure-regulated outflow

The PHE features

- Dynamic flow changes

- Varying heatfluxes

This means that the outflow of the pre-reformer (magnitude and composition) and the PHE (magnitude and temperature) are delayed, compared to their inflows.

For the SOFC this effect is not naturally embedded in the model. Therefore, some means of capturing the delay of the outflow compared to the inflow must be implemented.

Considering the volume per unit time $\dot{V}$, a change in the inflow will be instantaneously adopted by the outflow of the SOFC channels. This assumption was made because the velocities in the SOFC system are well below the speed of sound. Consequently, pressure changes can be considered to be instantaneous.[5]

---

[5]This will also be the case for the gasses in the pipes that connect the the components. In these pipes, the difference in gas compositions in inflows and outflows is neglected as well, as these are in the order of 0.2s

Contrarily, the composition of of the gasses changes over a larger timescale.

The change in flow velocity of the flow through a flow channel can be computed from combining the ideal gas law with the assumption that flow through the channels is laminar and homogeneous.

The mean flow velocities ids used for both channels to estimate the the delay is gas composition between the in- and out- let of the channels.

$$\bar{u}_{af} \approx \frac{u_{af,in} + u_{af,out}}{2} \tag{4.41}$$

$$\bar{u}_{cf} \approx \frac{u_{cf,in} + u_{cf,out}}{2} \tag{4.42}$$

where

$$u = \frac{\dot{V}}{A_{channel}} = \frac{\sum \dot{N} \cdot RT}{p \cdot A_{cell}} \tag{4.43}$$

The delay in gas composition $\Delta t_{af} = l/\bar{u}_{af}$ or $\Delta t_{cf} = l/\bar{u}_{cf}$ is implemented by using a "Transport delay block" in Simulink for both channnels

4.3.6. Nernst voltage

Since the Nernst voltage is a function of temperature as well as pressure and partial pressures, the calculation of the Nernst voltage must be part of the dynamic system. The Nernst voltage is calculated in equations 4.44 and 4.45. The implementation in Simulink of these relations is shown in figures C.10 and C.11(for the oxidation of Hydrogen).

$$E = E^0 + \frac{RT}{zF} \ln Q \tag{4.44}$$

Where Q represents the reaction quotient:

$$Q = \frac{a_J^j * a_K^k}{a_M^m} = \frac{p_{H_2} \cdot p_{O_2}^{1/2}}{p_{H_2O}} \cdot p^{1/2} \tag{4.45}$$

$$E_{OCV} = \frac{\sum_i \left(E_{OCV,i} \cdot z_i \cdot [i] \right)}{\sum_i \left(z_i \cdot [i] \right)} \tag{4.46}$$

where

$$E_{OCV,i} = \frac{\Delta \bar{g}_f}{z_i \cdot F} \quad \text{and} \quad i \in \{ H_2, CO, CH_3OH, CH_4 \}$$

Implementation of equation 4.46 in Simulink is shown in figure C.10 in appendix C.

However, by using the model for the pre-reformer it can be be verified that at the operational temperature of the fuel cell at the PEN, all the methanol will have been reformed.

An estimation of the mean values of the partial pressures of the species is made in equation 4.47. It should be noted that the there is uncertainty concerning the the parial pressures along the cell length. For lower fuel utilisation ratios the partial pressures along the anode are a function of the reaction kinetics. For higher fuel utilisation ratios, the partial pressures will be subject to chemical equilibrium.

For the mean partial pressure of species i equation 4.47is considered a fair estimate, keeping in mind the marginal impact on the Nernst Voltage of slight changes in pressure:

$$\bar{p}_{i, l} \approx \frac{1}{3} \cdot \left(p_{i, in} + 2 \cdot p_{i, out} \right) = \cdot \frac{\dot{N}_{i, in} + 2 \cdot \dot{N}_{i, out}}{\dot{N}_{i, in}} \cdot p_{i, in} \tag{4.47}$$

This is assuming there is exponential decay of concentrations along the anode. In other words: this approximation only holds when all the electrochemical reactions are fast so that all these reactions are in equilibrium over the length of the electrodes. It is more conservative than assuming that the kinetics are limiting for the change in partial pressures.

A problem with this approach is that , at very high fuel utilisation ratios, the partial pressures of the reaction could be over estimated.

4.3.7. activation- and crossover losses

The activation overpotential is given in equations 4.48, 4.49 and 4.49.

$$\Delta V_{act} = \Delta V_{act,a} + \Delta V_{act,c} \tag{4.48}$$

$$\Delta V_{act,a} = sinh^{-1}\left(\frac{i}{2 \cdot i_{a,0}}\right) \tag{4.49}$$

$$\Delta V_{act,c} = sinh^{-1}\left(\frac{i}{2 \cdot i_{c,0}}\right) \tag{4.50}$$

Current exchange density is, in fact, the the current that exchanges at the surface of the electrodes in the condition that the cell produces zero net current.This means that the reactions at the electrodes are in equilibrium. I.e: the reaction rate forward is the same as the reverse reaction rate, which are not zero. It can be seen that exchange current density is :

$$i_0 = \frac{r_f}{z \cdot F} = \frac{r_r}{z \cdot F} \tag{4.51}$$

By extrapolation and by making use of the ideal gas law, the expressions for the current exchange density at the anode and the cathode becomes:

$$i_{0,a} = \frac{RT_{PEN}}{zF} \cdot A_a \cdot EXP\left(\frac{-E_{a,a}}{RT_{PEN}}\right) \tag{4.52}$$

$$i_{0,c} = \frac{RT_{PEN}}{zF} \cdot A_c \cdot EXP\left(\frac{-E_{a,c}}{RT_{PEN}}\right) \tag{4.53}$$

Note that by adopting these equations it is implicated that the rate determining reactions at the electrodes are of the 1st order.

The electrochemistry at the surfaces of the electrodes is very intricate and is not confined to 1 reaction per electrode. Just as is the case for the reactions that happen in the reformer, many reactions that are a part of the main reaction take place at the same time. The result is that finding Arrhenius parameters for to determine the current exchange density is cumbersome. The following parameters were found in [32],and were used:

Electrode property	Symbol	Value	Unit
Anodic pre-exponetial constant	A_a $6.54 \cdot 10^{11}$	Ω^{-1}/m^2	
Cathodic pre-exponetial constant	A_c $2.35 \cdot 10^{11}$	Ω^{-1}/m^2	
Activation energy anode	$E_{a,a}$ $140 \cdot 10^3$	J/mol	
Activation energy cathodet	$E_{a,c}$ $137 \cdot 10^3$	J/mol	

4.3.8. Concentration losses

The modelling of the voltage drop that occurs as a result of the so called concentration losses, is done by using an empirical formula shown in equation 4.54. It is the result of the concentration of reactants near the electrodes. Since diffusion is the only mechanism that transports the reactants to the 3-phase points in the electrodes the speed of this process is limiting for the current density of the cell.

$$\Delta V_{conc} = m \cdot EXP(n \cdot i) \quad \text{where} \quad m = 3 \cdot 10^{-5} \quad \text{and} \quad n = 8 \cdot 10^{-3} \tag{4.54}$$

These parameters are widely in use in the fuel cell community according to [7]. These parameter do not vary significantly, as these losses occur as a result of the limiting diffusion rate, and are therefore not influenced by the fuel cell configuration.

Implementation of these losses in the Simulink model is simple and shown in figure C.12
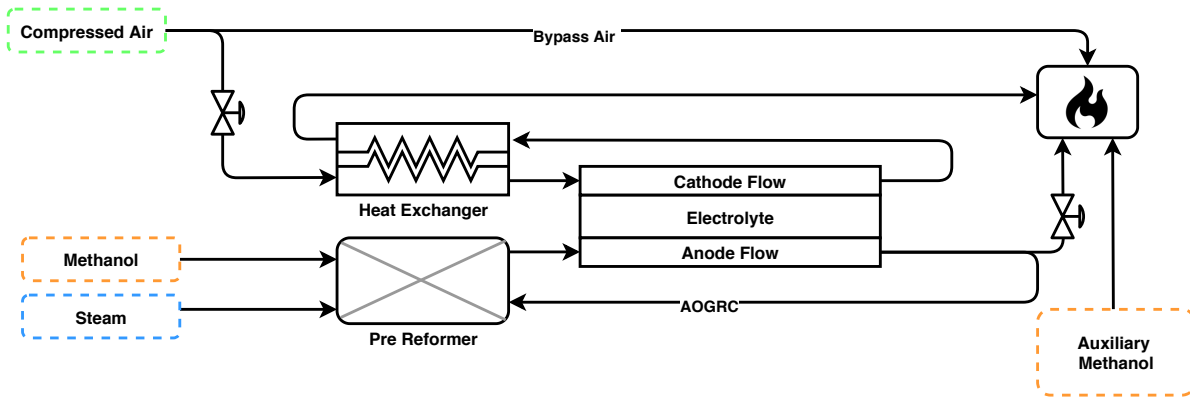
Figure 4.8: Configuration of the heat exchanger which is used to pre heat the cathode flow. In order to control the temperature of the Anode-Electrolyte-cathode structure, the the magnitude of the cathodic flow is controlled by a control valve.

4.3.9. Ohmic resistance losses

The Ohmic resistance losses amount to the resistances of the anode, cathode and the electrolyte, which can be seen as a series connection. Therefore

$$R_{ohm} = R_{ohm,a} + R_{ohm,e} + R_{ohm,c} \tag{4.55}$$

$$R_{ohm} = \frac{1}{A_{cell}} \cdot (r_{ohm,a} \cdot \tau_a + r_{ohm,e} \cdot \tau_e + r_{ohm,c} \cdot \tau_c) \tag{4.56}$$

Of these, the anodic- and cathodic- resistance are the resistance of electrons through a metal. The Ohmic resistance of the electrolyte is the resistance of ion traveling through the electrolyte. This value will be far greater and temperature-dependent.

quantity	symbol	value	unit of measure
Cell area	A_{cell}	0.04	$[m^2]$
Anode thickness	τ_a	$500 \cdot 10^{-6}$	$[m]$
Cathode thickness	τ_c	$200 \cdot 10^{-6}$	$[m]$
Electrolyte thickness	τ_e	$50 \cdot 10^{-6}$	$[m]$
specific resistance anode	$r_{ohm,a}$	$2.0 \cdot 10^6$	$[\Omega m^{-1}]$
specific resistance cathode	$r_{ohm,e}$	$3.34 \cdot 10^4 EXP\left(\frac{-10.3 \cdot 10^3}{T_{PEN}}\right)$	$[\Omega m^{-1}]$
specific resistance electrolyte	$r_{ohm,c}$	$2.1 \cdot 10^5$	$[\Omega m^{-1}]$

Table 4.6: parameters used to calculate the Ohmic resistance of the modelled cell.

4.4. Plate Heat Exchanger model

From [2], it becomes clear that in many instances, the heat exchangers play a significant role in the dynamic behaviour of hybrid fuel cell systems. Their inertia and sluggishness is even considered to be the greatest contributor to the overall slow reactions in hybrid systems of SOFCs and combustion engines. The same may be the case for the current system, but a literature search delivered no answers. Writing the model for the heat exchanger is done to enable precise definition of a control strategy for the temperature of the fuel cell.

This creates the need for a detailed model for a heat exchanger, as it will play an important role in the heat integration of the system. Similar to the way that the AOG is used to control the temperature of the pre-reformer, the heated outflow of the cathode can be used to preheat the air that flows to the cathode of the SOFC. Controlling the magnitude of the cathodic flow can than be used to control the temperature of the Anode-Electrolyte-Cathode structure of the SOFC. An overview of the methanol fuelled SOFC system, with the position of the heat exchanger is shown in figure 4.8.

It was decided to implement the same calculation for temperature as was done in the pre-reformer model(equation 4.3). This Decision was made because this method has been proven to be a reliable and accurate method to calculate the change in temperature in volumes of gas where the conditions and composition are variable.

Calculations were made according to the governing relations as shown in [9]. These assume that the transfer of heat will always be perpendicular to the the flow direction of the fluids. This assumption is made because the temperature gradient perpendicular to the flow direction is far greater than the temperature gradient parallel to the flow direction. Figure 4.9 shows the the heat flows and the magnitude of those heat flows through one plate. If it is assumed that the number of plates is large, the boundary effects at the extremes of the stack will not have great effect on the overall behaviour of the PHE

The the total heat flow from the hot flow to the cool flow is evaluated over the length of the heat exchanger:

$$\dot{Q} = b \cdot n \cdot \int_0^L \dot{q}(x) \, dx \tag{4.57}$$

In equation 4.62, $\dot{q}(x)$ is found.

$$T_h(x) - T_{h,w}(x) = \frac{\dot{q}(x)}{\alpha} \tag{4.58}$$

$$T_{h,w}(x) - T_{c,w}(x) = \frac{\dot{q}(x) \cdot \tau}{\lambda} \tag{4.59}$$

$$T_c(x) - T_{c,w}(x) = \frac{\dot{q}(x)}{\alpha} \tag{4.60}$$

$$\therefore \quad \dot{q}(x) = \frac{T_h(x) - T_c(x)}{(\frac{2}{\alpha} + \frac{\tau}{\lambda})} \tag{4.61}$$

$$\tag{4.62}$$

Using equation 4.63, the relation shown in 4.63 is found.

$$T_h(x) - T_c(x) = e^{-C_1 \frac{Z}{F} \cdot x} = C_2 \cdot e^{\frac{Z \cdot x}{F}} \tag{4.63}$$

Where combined fluid strength F is defined as

$$F = (\frac{1}{F_h} + \frac{1}{F_c})^{-1} = (\frac{1}{\dot{m}_h \cdot c_{p,h}} + \frac{1}{\dot{m}_c \cdot c_{p,c}})^{-1} \tag{4.64}$$

And heat admittance Z is defined as

$$Z = (\frac{1}{Z_h} + \frac{1}{Z_w} + \frac{1}{Z_c})^{-1} = (\frac{1}{\alpha_h \cdot A_{w,h}} + \frac{\tau}{\lambda_w \cdot A_w} + \frac{1}{\alpha_c \cdot A_{w,c}})^{-1} \tag{4.65}$$

Where, because of the configuration as a PHE

$$A_{w,h} = A_w = A_{w,c} = A$$

The complete term for $\dot{q}(x)$ then becomes

$$\dot{q}(x) = \frac{C_2 \cdot e^{-\frac{Z}{F} \cdot x}}{(\frac{2}{\alpha} + \frac{\tau}{\lambda})} \tag{4.66}$$

In these relations, the C_2 becomes the temperature difference between the two flows on the side of the PHE that is defined as x=0. Fluid strength of the hot flow, F_h, is defined to be negative, as the mass flows in the negative x-direction. This means that $C_2 = T_h(0) - T_c(0) = T_{h,out} - T_{c,in}$

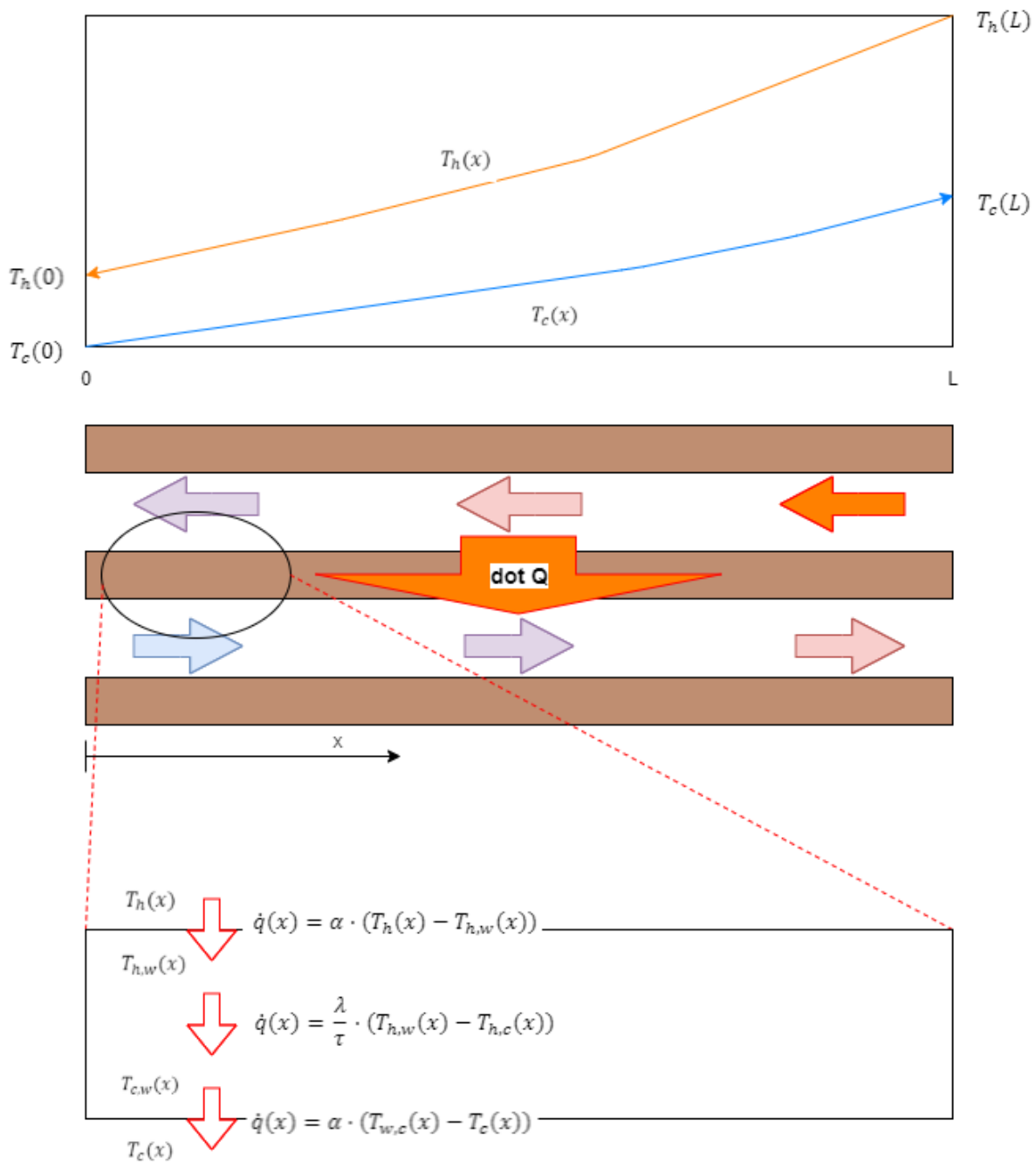The total heat transfer from the hot flow to the cold flow becomes

Figure 4.9: Shows the heat flows and mass flows in the PHE. For the heat flows, the magnitude of the convection and conduction of heat per unit area is given. From these equations, the term for the total heat flow to the cold fluid $\dot{Q}$ is gained.

$$\dot{Q} = A_w \cdot \int_0^L \dot{q}(x)dx = A \cdot \frac{F}{Z} \cdot \frac{(T_{h,out} - T_{c,in})}{(\frac{2}{\alpha} + \frac{\tau}{\lambda})} \cdot \left(1 - e^{-\frac{Z}{F} \cdot L}\right) \tag{4.67}$$

The calculated transferred heat is integrated in the gas volumes of the the flow channels of the PHE. Calculations of the resulting outflow temperatures is done much in the same way as with the pre-reformer model.

$$N_i(t) = N_i(0) + \int_0^t \left(\sum_{in} \dot{N}_i(t) - \sum_{out} \dot{N}_i(t)\right) dt \tag{4.68}$$

where

$$i \in \{N_2, O_2\}$$

The temperature of the outflow is calculated in equation 4.69

$$T(t) = T(0) + \int_0^t \left(\frac{\Sigma \dot{Q}}{\Sigma(N_i(t) \cdot c_{p,i}(T)) + C_{PHE}}\right) dt \tag{4.69}$$

The heat capacity of the metal walls of the exchanger are incorporated in the calculation in their entirety , which is an overstatement of the inertia in the system. This should be a close approximation of reality. If it is assumed that the temperature off the wall is the mean of the temperature of the hot flow and the temperature of the cold flow (this can be done because the fluid strengths of both blows nearly have the same magnitude), than the entire structure should change in temperature as much as either of the gas flows.

$$\sum \dot{Q} = \dot{Q}_{in} + \dot{Q}_{out} + \dot{Q}_{PHE} \tag{4.70}$$

$$\dot{Q}_{in} = \sum (T_{in} \cdot \bar{h}_x(T_{in})) \tag{4.71}$$

$$\dot{Q}_{out} = \sum (T_{out} \cdot \bar{h}_x(T_{out})) \tag{4.72}$$

5

Model -verification & -validation

This chapter focuses on the verification and validation of the separate models. Once the separate models are verified an validated, they should provide a thrust-worthy model for the entire system. That is, if care is taken in connecting the models

First the models will be verified by means of checking the mass balance of the entire system, and checking the energy balances of the separate subsystems.

Validation against literature proves more challenging, especially for the pre reformer. Still, ways will be shown to prove the merit of the separate models.

5.1. Verfication

5.1.1. Mass balance

Even though molar quantities change under the influence of chemical reactions in the SOFC and the pre-reformer, the mass flow into the system must equal the mass flow the out of the system. Comparing these mass flows is therefore a useful tool to evaluate if the models were built without faults.

In-going mass flows are identified to be:

- The airflow into the cathode flow

- The methanol flow into the pre-reformer

- The Steam flow into the pre-reformer

The outgoing mass flows are identified to be:

- The cathodic outflow

- The anodic outflow $(= (1 - \mu_{AOGRC}) \cdot \dot{m}_{AOG})$

One other way to test the mass balance is to split up the molecules and count per species of atom. The results for both methods are given in table 5.1. The very minor deviations of the mass balance are due to the multitude of transfers that occur in the model and their associated inaccuracies. Therefore it is it is decided that the mass balance is in order.

5.1.2. Energy balance

For the energy balance, the same goes as for the mass balance. Evaluating the energy balance has the extra advantage that it uncovers faults in the stack power generation as well.

	$i = 2000\ [A/m^2]$	$i = 4000\ [A/m^2]$	$i = 6000\ [A/m^2]$
$\frac{\sum_{in} \dot{m} - \sum_{out} \dot{m}}{\sum_{in} \dot{m}}\ [-]$	$7 \cdot 10^{-5}$	$7 \cdot 10^{-5}$	$6 \cdot 10^{-5}$
$\frac{\sum_{in} \dot{N}_H - \sum_{out} \dot{N}_H}{\sum_{in} \dot{N}_H}\ [mol/s]$	0	0	0
$\frac{\sum_{in} \dot{N}_C - \sum_{out} \dot{N}_C}{\sum_{in} \dot{N}_C}\ [mol/s]$	$1 \cdot 10^{-6}$	$1 \cdot 10^{-6}$	$1 \cdot 10^{-6}$
$\frac{\sum_{in} \dot{N}_O - \sum_{out} \dot{N}_O}{\sum_{in} \dot{N}_O}\ [mol/s]$	$2.5 \cdot 10^{-5}$	$1.5 \cdot 10^{-5}$	$1.0 \cdot 10^{-5}$
$\frac{\sum_{in} \dot{N}_N - \sum_{out} \dot{N}_N}{\sum_{in} \dot{N}_N}\ [mol/s]$	0	0	0

Table 5.1: Shows the deviation from the mass balance of the model.

Pre-reformer

The pre-reformer operates at a stable temperature. Therefore the energy balance is:

$$\sum_{in} \left(\bar{h}_{in,i}(T_{in,i}) \cdot \dot{N}_{in,i} \right) + \sum_{out} \left(\bar{h}_{out,i}(T_{out}) \cdot \dot{N}_{out,i} \right) = \sum_{reactions} \left(\Delta \bar{h}_j \cdot (r_f - r_r)_j \right) \tag{5.1}$$

where

$$i \in \{CH_3OH,\ H_2,\ H_2O,\ CO,\ CO_2,\ CH_4,\ O_2,\ N_2 \}$$
$$j \in \{ MSR,\ MDR,\ WGS,\ MCMO,\ MCDO \}$$

This was tested for $i = 2000\ [A/m^2]$, $i = 4000\ [A/m^2]$ and $i = 6000\ [A/m^2]$, and the relative deviations are shown in table 5.2

	$i = 2000\ [A/m^2]$	$i = 4000\ [A/m^2]$	$i = 6000\ [A/m^2]$
$\frac{\sum H_{in} - \sum H_{out} - \sum \Delta H_{rxn}}{\lvert \sum H_{in} \rvert + \lvert \sum H_{out} \rvert + \lvert \sum \Delta H_{rxn} \rvert}\ [-]$	$0.0 \cdot 10^{-3}$	$0.0 \cdot 10^{-3}$	$0.0 \cdot 10^{-3}$

Table 5.2: Relative deviation from energy balance of the pre-reformer. The results are so close to zero that the noise on the signal makes the actual deviation insignificant.

SOFC

In stable operation the temperature of the cell will be stable. The energy balance than becomes:

$$\sum_{in} \left(\bar{h}_{in,i} \cdot \dot{N}_{in,i} \right) - \sum_{out} \left(\bar{h}_{out,i} \cdot \dot{N}_{out,i} \right) = P_{stack} \tag{5.2}$$

where
$$i \in \{CH_3OH,\ H_2,\ H_2O,\ CO,\ CO_2,\ CH_4,\ O_2,\ N_2 \} \tag{5.3}$$

Table 5.3 shows the relative deviation from this balance. The balance was evaluated at $i = 2000\ [A/m^2]$, $i = 4000\ [A/m^2]$ and $i = 6000\ [A/m^2]$.

	$i = 2000\ [A/m^2]$	$i = 4000\ [A/m^2]$	$i = 6000\ [A/m^2]$
$\sum H_{in} - \sum H_{out} - P\ [J/s]$	0	0	0

Table 5.3: Relative deviation from energy balance of SOFC

It can be seen from table 5.3, that the deviation from the energy balance is exactly zero. This is due to the way the model is built. The model takes the conditions at 2/3 times the length of the cell and calculates the open circuit voltage from the Gibbs energy difference of the reactions, the pressures and the temperature. The difference between the enthalpy change and Gibbs energy change ($\sum_{rxn} \Delta H - \sum_{rxn} \Delta G$) is added to the heat flow into the PEN-structure. It represents the reversible heat of the combined reactions.

PHE

The efficiency of the PHE is modelled to be 98% , meaning that the energy balance for the PHE is given by equation 5.4. This is assuming that the pressure in the hot and cold flows stays more ore less the same, and that there will be no phase shifts of the fluids.

$$\sum_{out} \left(\dot{N}_{h,i} \cdot \bar{h}_{h,i} \right) + \sum_{out} \left(\dot{N}_{c,i} \cdot \bar{h}_{c,i} \right) = (1 - \eta_{PHE}) \cdot \left(\sum_{in} \left(\dot{N}_{in,i} \cdot \bar{h}_{in,i} \right) + \sum_{in} \left(\dot{N}_{c,i} \cdot \bar{h}_{c,i} \right) \right) \quad (5.4)$$

Deviation from this energy balance is given in table 5.4

	$i = 2000 \ [A/m^2]$	$i = 4000 \ [A/m^2]$	$i = 6000 \ [A/m^2]$
$\frac{(i-\eta_{PHE}) \cdot \sum_{in} \Delta H - \sum_{out} \Delta H}{\dot{Q}} \ [-]$	$4.4 \cdot 10^{-3}$	$1.9 \cdot 10^{-3}$	$1.3 \cdot 10^{-3}$

Table 5.4: Relative deviation from energy balance of SOFC

Here too, the energy balance deviates slightly from what it is supposed to be. Slight inaccuracies in the enthalpy (enthalpy is calculated from a lookup table)calculations seem to account for this deviation.

For either SOFC, pre-reformer as well as PHE, it is decided that the energy balance is in order.

5.2. Validation

5.2.1. Pre-reformer

Verification of the model of the pre-reformer presented a challenge. A lot of literature has been publishes concerning the production of methanol from syngas as this process is of interest to those who pursue the fabrication of methanol and its numerous derived products. However, on the reforming of methanol, the information is scarce, due to the lack of need for the process before recent times.

Nevertheless, some tactics have been applied to enable at least some degree of verification and validation of this model. In order to better judge the performance of the model it has been decoupled fromthe rest of the dmodel of the methanol fuelled SOFC system..

Approach

Initially, it was suggested to use other software to verify the pre-reformer model by comparing results. Finding suitable software packages proved to be a dead end.

Validation would have to be done in another manner. The method that was used makes use of the fact that the subsystem is modelled as a balance reactor. I.e. the outflow composition is the same as composition of the entire rector vessel. This means that when conditions are kept stable in the reactor, the molar fractions of the species present should settle on values that comply with the equilibrium constants for a certain reaction at certain temperature. This is easily tested for each of the reaction equilibrium described in the model, by disconnecting the other reactions, and and evaluating the molar fractions at several temperatures. The results are shown in table 5.5.

Because of the way that the reactions MSR, MDR and WGS are modelled in the pre-reformer model, the calculated K_{eq} ought to be nearly exactly the same as the ones used in the calculations (see equations 4.14, 4.15 and 4.16). For MDR however, the Hydrogen fraction at low temperatures becomes so small that the sum of the forward and reverse rate oscillates ever so slightly. The effect is that the found $K_{eq} = \frac{[CO] \cdot [H_2]^2}{[CH_3OH]}$ deviates somewhat from the K_{eq} found from [39]. The effect of this is marginal as the kinetics of this reaction at lower temperatures are slow compared to the kinetics of the other reactions present ($-5 \cdot 10^{-9} mol/s \leq r_{f,MDR} + r_{r,MDR} \leq 5 \cdot 10^{-9} mol/s$) .

For MCMO and MCDO however, the equilibrium constant is not used in the calculation of the rates. Table 5.5 shows that there is a deviation from the equilibrium constants that are taken from the van 'T Hoff equation. The Values differ, but not severely. This grants confidence that the model is quite accurate. Accurate enough for the purposes of this thesis.

T [K]	400	500	600	700	800
MSR	943.9	$31.26 \cdot 10^3$	$32.23 \cdot 10^4$	$17.07 \cdot 10^5$	$59.57 \cdot 10^5$
MSR	943.9	$31.12 \cdot 10^3$	$32.24 \cdot 10^4$	$17.07 \cdot 10^5$	$59.55 \cdot 10^5$
MDR	2.58	582.4	$20.23 \cdot 10^3$	$24.27 \cdot 10^4$	$15.09 \cdot 10^5$
MDR	0.654	230.4	$11.50 \cdot 10^3$	$18.77 \cdot 10^4$	$15.25 \cdot 10^5$
WGS	1173	125.7	28.36	9.79	4.41
WGS	1053	125.9	28.34	9.79	4.32
MCMO	$1.444 \cdot 10^{13}$	$24.33 \cdot 10^6$	3105	4.46	$33.64 \cdot 10^{-3}$
MCMO	$1.40 \cdot 10^{15}$	$1.38 \cdot 10^{09}$	$1.30 \cdot 10^{05}$	$1.40 \cdot 10^{02}$	$8.00 \cdot 10^{-1}$
MCDO	$3.74 \cdot 10^{14}$	$4.14 \cdot 10^9$	$7.25 \cdot 10^5$	1388	10.45
MCDO	$6.75 \cdot 10^{14}$	$1.15 \cdot 10^{10}$	$2.89 \cdot 10^6$	7576	73.95

Table 5.5: Shows the values for K_{eq} for the modelled reactions for different temperatures. The rows preceded by black reaction abbreviations show the values of K_{eq} from literature. The rows preceded by blue reaction abbreviations show the values of K_{eq} from the partial pressures and concentrations found as model outputs.

Just like for the calculation of the equilibrium constant for MCMO, the calculation of the Methanation reaction of Carbon Dioxide (MCDO) is done by making use of the Van 't Hoff equation:

$$K_{eq} = EXP\left(\frac{-\Delta \bar{g}_f}{RT}\right) \quad (5.5)$$

A depiction of the implementation of this equation in the simulink model is given in the appendix C in figure C.4

An interesting behaviour of the pre-reformer was found in generating results. It was found that from a certain temperature (535K to 550K) onward, the methanation reactions kinetics become faster compared to the other reactions. The result is that the exothermic methanation reactions heat up the the reactor, forcing the dominance of the methanation reactions even further. The results could be a runaway reaction that endangers the reactor. This is an effect one would expect to be described in literature, if the model is accurate. This effect has indeed been discussed in literature and is called a 'major concern' in the business of methane production from synthetic gas [24], [23], [14].

Another behaviour that catches the eye is the fact that all methanol seems to disappear in the reactor, for temperatures over 420K. Finding confirmation of this behaviour would contribute to the merit of the pre-reformer model. This effect has indeed been described in the literature. [30] notes:" the production of methanol in the reverse reactions can be practically excluded.".Similar claims are stated in [11] (for reverse MDR) and [20].

5.2.2. Heat Exchanger

Since the model for the PHE was built from the the equations that are given in [9], a logical step in in the verification of the model is to check if the special cases that are named in this work concur with model output of these special cases. One such a case that should generate eye-catching results is the case where the fluid strengths F_h and F_c are opposite and have the same magnitude. Since the combined fluid strength is given by equation 5.6, the temperature difference over the length of the heat exchanger will be constant. $\Delta T(x) = C_2 \cdot e^{-\frac{Z}{F}x} = C_2$.

The way to show this effect is by realising that $\Delta T(x) = C_2 = \Delta T(0) = \Delta T(L)$, and that integration of a constant is just a multiplication. Therefore, $\dot{Q} = C_3 \cdot L$ should have a linear relation with the plate length, if the fluid strength of the fluids are equal and opposite. This can be tested, and the results are shown in figure 5.1.

$$F = (F_h^{-1} + F_c^{-1})^{-1} \quad (5.6)$$

It can be seen from figure 5.1 that the model's behaviour very closely mimics the expected behaviour. The likeness to the line that is plotted as a comparison becomes better as the combined fluid strength approaches infinity.
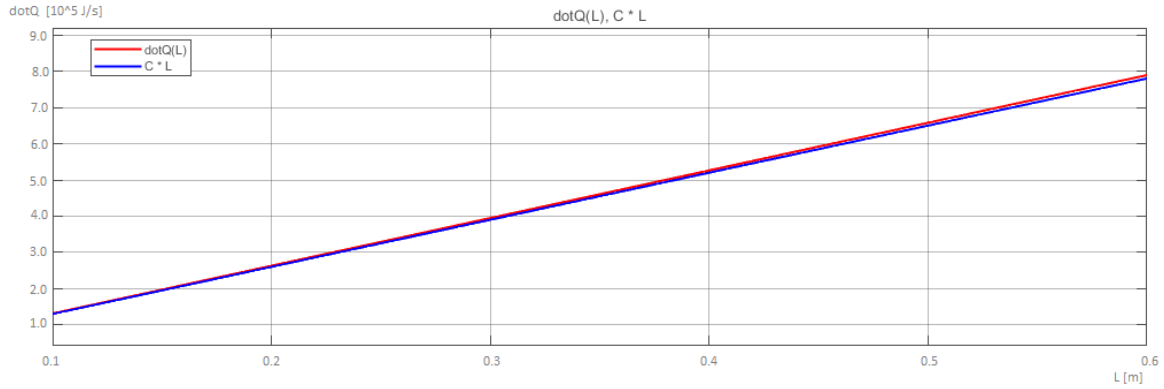
Figure 5.1: Heat transfer as a function of heat exchanger length. As a comparison, a constant factor of the plate length is plotted.

$$\varepsilon_{heater}^{CF} = \frac{\frac{F}{F_c} \cdot \left[1 - e^{-\frac{Z}{F}}\right]}{e^{\frac{Z}{F}} + \frac{F}{F_c} \cdot \left[1 - e^{-\frac{Z}{F}}\right]} = \frac{1 - e^{-\frac{Z}{F}}}{1 + \left(\frac{F_c}{F} - 1\right) \cdot e^{-\frac{Z}{F}}} \tag{5.7}$$

$$\varepsilon_{heater}^{CF} = \frac{\Delta T_c}{\Delta T_{max}} \tag{5.8}$$

Yet another way to verify the PHE model is to use the relations given in [9]. Equation 5.7 shows an expression for the effectiveness of the heater of a heat exchanger according to [9]. It was verified that calculations for heater effectiveness from the model by the definition 5.8 produce the exact same results.

5.2.3. SOFC

For the validation of the SOFC model, use was made of the results as published by [1]. As far as could be determined, this was one of the few studies of relevance for which detailed test result data were published. The model by [1] is an often referenced benchmark in SOFC literature.

However, this paper concerns a methane fuelled SOFC instead of a methanol fuelled SOFC system. This issue was dealt with through the versatility of the here described SOFC model. The current model was isolated from the rest of the system, so it allows for calculations that include the oxidation of Hydrogen, Carbon Monooxide, Methanol and Methane, in every defined ratio. Also, (partial) pressures, inflow temperatures and inflow magnitudes can be easily defined. In this capacity, the current model was tested and the results were compared to that of the 1-dimensional model presented in [1]. Note that - although it is by no means a one-dimensional model - the current model includes a correction for the concentration gradient over the length of the electrodes.

electro-chemical model

First, the electro-chemical behaviour of the cell was evaluated. [1] shares the cell voltage and and its constituents in figure 5.2 for a pressure distribution as given in figure 5.3. The fact that the model presented by [1] is 1-dimensional, is circumvented by taking the the values at a dimensionless axial position of $L^* = 0.3$. This is done because the evaluation of the cell performance in [1]is done for those values over the length of the cell.

The inputs, results of [1] and the results of the here developed model are given in table 5.6

It is clear from these results that the here developed model generates results very similar to the results a single spot by the model of [1]. This is true for all tested values except for the concentration losses. The influence of this deviation is, however, minor.
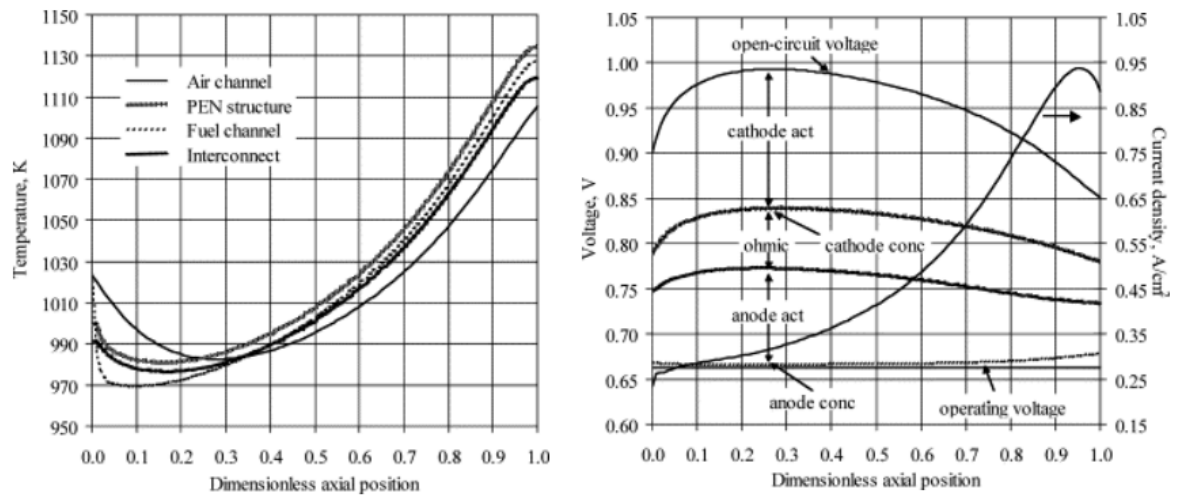
Figure 5.2: Shows the values for temperatures of the different components of the cell (left), and the constituents of the reversible voltage drop of the cell as along the cell length. These figures were taken from [1].
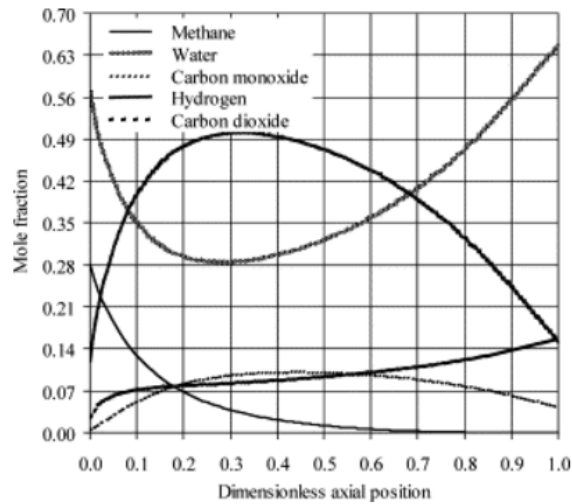

Figure 5.3: Partial pressures over the dimensionless length of the cell according to [1]

Input	Value [unit]		Output	[1]Value ($L^* = 0.3$) $[V]$	Value $[V]$
$i(0.3)$	$3200[A/m^2]$		E_{OCV}	0.99	0.99
$T_{PEN}(0.3)$	$985[K]$		$\Delta V_{act,a}$	0.155	0.155
$p_{H_2}(0.3)$	$50 \cdot 10^5 [Pa]$		$\Delta V_{act,c}$	0.105	0.105
$p_{H_2O}(0.3)$	$28 \cdot 10^5 [Pa]$		ΔV_{ohm}	0.70	0.68
$p_{CO}(0.3)$	$10 \cdot 10^5 [Pa]$		ΔV_{conc}	0.002	0.0005
$p_{CO_2}(0.3)$	$9.0 \cdot 10^5 [Pa]$				
$p_{CH_4}(0.3)$	$4.0 \cdot 10^5 [Pa]$				

Table 5.6: Caption

Cell model

Next, operation of the cell at given circumstances is tested.

The fact that [1] presents a 1-dimensional model demands a workaround if it is to be compared to the current model. It can be seen from figures 5.2 and 5.3 that values of temperatures, pressures voltages and current density vary wildly over the length of the anode. The here presented model is 0-dimensional, although it uses a compensation for the partial pressures in the flows. This model is less detailed, but at at a significantly smaller computational expense.

The model inputs that were used in the test by [1] are listed in table 5.7. The model outputs from these inputs will be called "MCdJ-1", and can be found in in table 5.8.

Parameter	Symbol [Unit of measure]	Value
Cathode flow inlet temperature	$T_{cf,in}$ [K]	1023
Anode flow inlet temperature	$T_{af,in}$ [K]	1023
Cathode flow pressure	p_{af} [Pa]	$1 \cdot 10^5$
Anode flow pressure	p_{af} [Pa]	$1 \cdot 10^5$
Current density	i $[A/m^2]$	5000
Fuel utilization factor	μ_{fuel} $[-]$	0.75
Oxygen utilization factor	μ_{ox} $[-]$	0.118
Molar fraction inlet Hydrogen	$y_{H_2,in}$ $[-]$	0.121
Molar fraction inlet steam	$y_{H_2O,in}$ $[-]$	0.566
Molar fraction inlet Carbon Mooxide	$y_{CO,in}$ $[-]$	0.004
Molar fraction inlet Carbon Dioxide	$y_{CO_2,in}$ $[-]$	0.027
Molar fraction inlet Methane	$y_{CH_4,in}$ $[-]$	0.282
Molar fraction inlet Oxygen	$y_{CH_4,in}$ $[-]$	0.210
Molar fraction inlet Nitrogen	$y_{CH_4,in}$ $[-]$	0.790

Table 5.7: The SOFC controlled parameters in the results as published by [1], and used as input for the validation of the current SOFC model.

The outputs of both models are compared in table 5.8. In the case of the model presented by [1], these would be mean values over the cell length.

In evaluating the result one has to be careful. The model by [1] features internal reforming, whereas the present model assumes a fully developed gas flow. Internal reforming varies the concentration differently from when only the electro-chemical combustion is taken into account. This means that the molar fraction at the inlet may not be representative for the molar fractions along the length of the cell. In fact, this is clearly shown in figure 5.3.

A way to account for the differences in the model was constructed: By reading figure 5.2 it seems that most of the reforming is done before the fluid reaches $L^* = 0.3$, as this is where H_2-, and H_2O- fractions experience a maximum and minimum, respectively. Therefore, the model is ran with the partial pressures there as input. The output from these inputs will be called "MCdJ-2" in table 5.8.

Thus, the outcomes of both cases is given in table 5.8.It is expected that the cell voltage and cell power generated in "MCdJ-1" will be close to the average outputs presented by [1]. This is because of the compensation measures are taken in the current model. These, are aimed to counter the voltage

overestimation that would otherwise occur, and should therefore produce a comparable result.

It is expected that the temperatures generated in ""MCdJ-2" are more to the higher end of the temperature range as given by [1], near $L^* = 1$ as internal reforming will no longer play a significant role on that end of the cell.

Parameter [unit]	Model output value MCdJ-1	Model output value MCdJ-2	Model output value Model by [1]
V_{cell} [V]	0.667	0.714	0.663
P_{cell} [W]	134.7	143.0	132.6
i $[A/m^2]$	5000	5000	5000
T_{PEN} [K]	1103	1118	982 - 1134
T_{int} [K]	1093	1106	978 - 1120
T_{af} [K]	1099	1114	970 - 1128
T_{cf} [K]	1090	1102	983 - 1104

Table 5.8: Model outputs for the current model with inputs as in table 5.7 (MCdJ-1), model outputs for the current model with fully developed fuel flow as in table 5.6 (MCdJ-2), and the outputs by the model by [1] for inputs as given in table 5.7.

From data presented in table 5.8,it is gathered that the model presented in the current document closely follows the behaviour of the the model presented by [1].

<div style="text-align: right">

6

</div>

<div style="text-align: right">

Results

</div>

This chapter is built up from the following sections:

- An overview of the methanol fuelled SOFC system

- Behaviour of the pre-reformer

- Behaviour of the SOFC

- Behaviour of the PHE

- Effects of AOGRC

- Effects of integrating PHE between the cathodic flows

- Behaviour of the cells at the stack extremes

- Control and behaviour of the methanol fuelled SOFC system in test circumstances

6.1. System overview

An overview of the methanol fuelled SOFC system under investigation is given in figure 6.1. It shows how the SOFC, pre-reformer and PHE are interconnected for this investigation.

Air is compressed to 20 Bar adiabatically and will thus reach the temperature of 710 K. The compressed air flows into the PHE, where it is heated using the heat of the cathode outflow. This air flows to the cathode where a share of the oxygen will provide the oxide ions that enable electro-chemical combustion of fuels.

Steam and methanol enter the pre-reformer at 485 K and 445 K respectively. At these temperatures both compounds are barely super heated at 20 Bar. These streams are joined by the AOGRC in the pre-reformer where the reforming process takes place. The resulting hydrogen-rich gas mix flows to the anode where it is partly electro-chemically combusted. The part of the fuel that is not used in this process may be either recaptured for later use (not within the scope of this investigation) or recycled directly through AOGRC.

6.2. Pre-reformer behaviour

The integration of the the pre-reformer in the SOFC system requires knowledge about behaviour of the pre-reformer in standalone operation. The questions that need to be answered are:
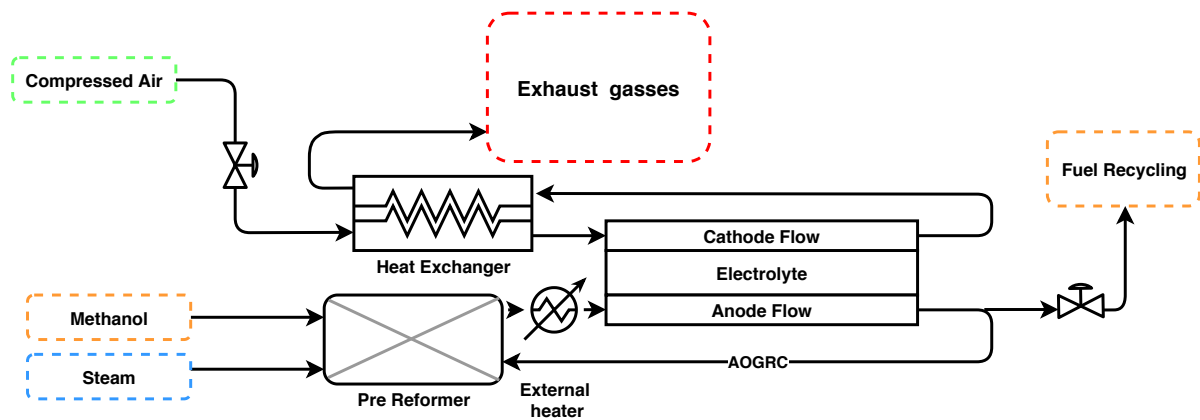
Figure 6.1: Shows the system that is investigated in this thesis, and its constituents

- *What should the dimensions of a pre-reformer be, and how do the dimensions influence the transient behaviour of the outflow?*

- *At what temperature and pressure should the pre-reformer be operated?*

- *What is the effect of the presence of methanation reactions on the process of MSR?*

These are an extension on the questions that were posed in section 1.3.

In order purposefully design a methanol fuelled SOFC system, the standalone behaviour of the pre-reformer is studied. Valuable information that was extracted is listed below:

- The rate at which an equilibrium is attained when it is disturbed

- The molar fractions of the gas species in the eventual equilibrium

- The heat that is produced or used in these reactions

To test the pre-reformer standalone behaviour, it is disconnected from the other components' models. The pre-reformer in the test setup has a volume of $2m^2$, contains $30.00 kg$ of catalyst and has a heat capacity $c_{pre-ref}$ of $276 \cdot 10^6 [J/K]$ *not considering the gasses*. It has a slender, tubular configuration and operates at an absolute pressure of around $20 Bar$. The inflow of *Methanol* and *Steam* occur at 445K and 485K respectively as these are the vaporizing temperatures for these compounds at 20 Bar.

In this configuration the pre-reformer practically behaves like a equilibrium reactor, as the in- and out-flows are small compared to the contents of the reactor[1]. Also, the system is regulated to maintain an internal pressure of 20 Bar, further increasing the number of moles inside the reactor compared to the number of moles that flow out.

6.2.1. Controlled parameters

For the pre-reformer, it was identified that the controllable parameters that can influence the reforming process are:

- **Heating**: This controls the temperature (partly). It is of influence as kinetics and equilibrium of all chemical reactions taking place are highly dependent on the environment temperature.

- **Inflow and outflow**: These largely determine the pressure. This is of infleunce as changes in pressure can shift the the equilibrium equation without altering the equilibrium constant.

- **Steam ratio** μ_{steam}, which has an effect on reaction kinetics and on equilibrium.

---

[1]This observation may not hold for higher through-flows and temperatures. In later stages of the investigation, it is determined that this observation remains true for all viable operation with the current pre-reformer configuration.
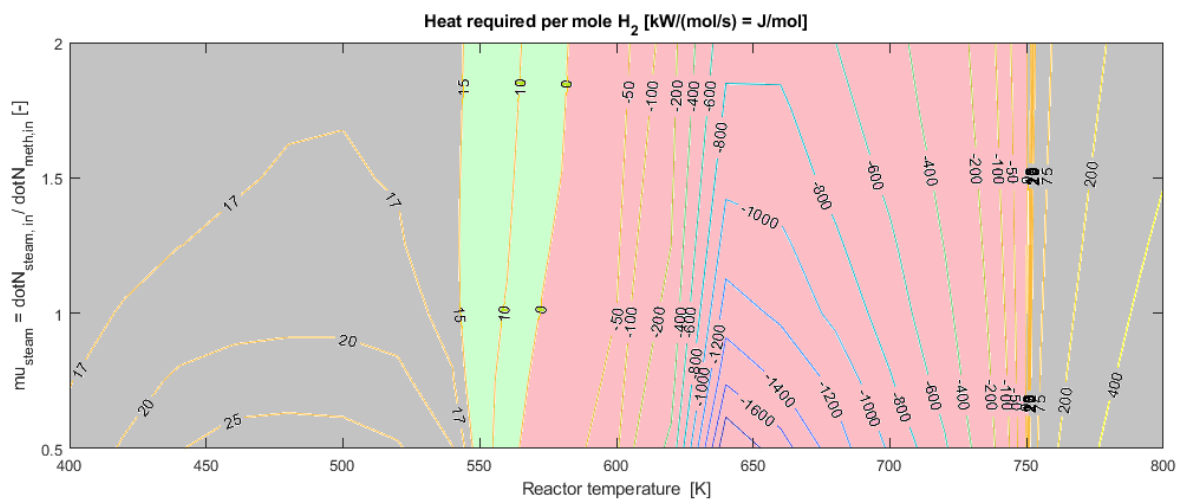
Figure 6.2: Shows the iso-lines for the required heat input per mole of hydrogen gas produced in [kW/(mol/s)] or [kJ/mol] from the chemical reactions in the pre-reformer. The reforming process demands energy addition for all shown values of the input parameters. The values are given for maintained temperature on the X-axis and for the introduced steam fraction on the Y-axis (for no AOGRC).

- **AOGRC ratio** μ_{AOGRC} , which is a measure for the inflow of AOGRC. This inflow is important for the heat recovery and steam recovery of the methanol fuelled SOFC system. In the tests of the pre-reformer in standalone operation however, AOGRC is not tested.

6.2.2. Stable operation

Stable operation of the pre-reformer is visualized in this section. The thermal behaviour of the subsystem is visualised first. The the outflow composition for varying input parameters is visualised. In appendix A.1 the methodology for studying the standalone behaviour of the pre-reformer is documented.

Thermal behaviour

The test results that show the thermal behaviour of the pre-reformer are compiled and shown in figure 6.2. This figure shows the required heat flow into the pre-reformer, per mole hydrogen produced. More precise: the heat that is required to maintain the indicated temperature (on the x-axis), for the indicated μ_{steam} (on the y-axis). The red area indicates unsafe operation due to (severely) exothermic chemical conversion. The green area indicates the area where the lowest amount of heat input is required, per mole hydrogen produced. It can be seen from figure 6.2, that the presence of a large share of steam in the reactor can mitigate this effect slightly. This finding means that the mitigating effects of the presence of a large share of steam in the gas mixture could provide a safety measure in the system (see section 7.2.7). *Note that the the preferable operating point may shift when reviewed in combination with the rest of the system (due to AOGRC).*

Outflow composition

In the pre-reformer model it is assumed that gasses are well mixed. The consequence is that the outflow composition is reflective of the the composition of the gas mixture in the pre-reformer. Figure 6.3 shows the compositions of the pre-reformer outflow as a function of the temperature of the pre-reformer for $\mu_{steam} = \{0.5\,,1.0\,,1.5\,,2.0\}$.

Figure 6.3 shows the following trends:

- Hydrogen yields of the reforming process are above 60% for temperatures below 550K.

- Carbon mono oxide production is cancelled out by other reactions as the steam ratio is increased [2]

---

[2]Note that, because the pre-reformer model includes kinetics, rather than only equilibrium, it verifies the assumption that all CO
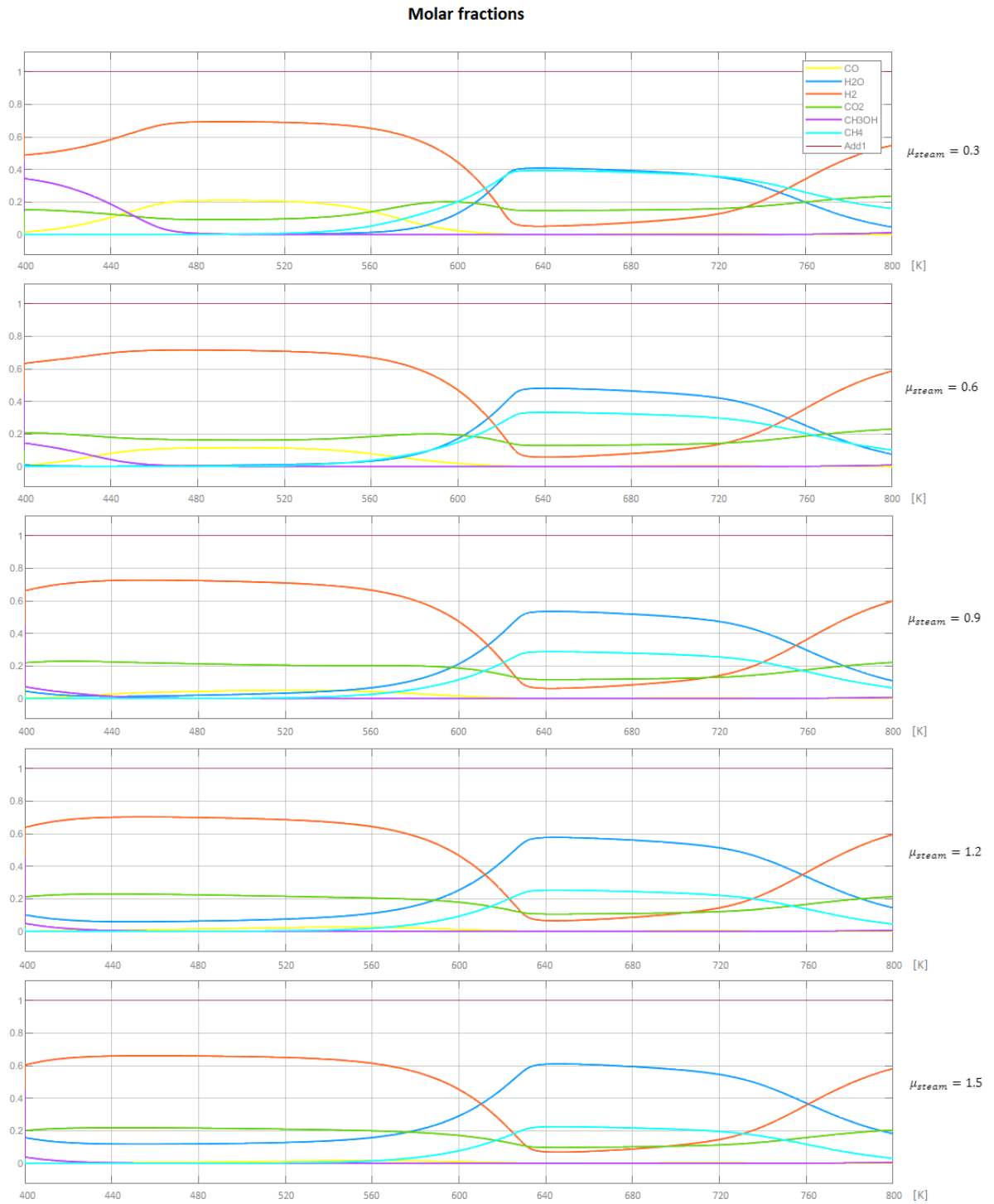
Molar fractions

Figure 6.3: Shows the fraction of outflow of species, as a function of temperature, for different steam ratios.

- The chemical reduction of methanol is total for temperatures over 470K. It is faster when the steam ratio is increased.

- From 520K and up, methane production becomes prominent. Increasing the steam ratio counters this effect slightly. Since both methanation reactions are very exothermic, this concurs with the findings in figure 6.2

Operation at 520K

As became clear in this section, the reactions present in the pre-reformer become exothermic over all when the reactor temperature becomes greater than 565K. This creates a safety issue and is best well avoided. therefore, re-circulation of anode off gasses is not preferred for operating temperatures of the pre-reformer greater than 540K due to the high temperature of these gasses.

This means that for safety reasons it is preferred to remain in the temperature range well below 570K, This way the heat from the AOG can be well used to reform methanol. The temperature is kept at 520K increase safety and create some slack for heat re-integration via AOGRC.

Using AOG to supply heat to the the reactor is a method that is responsive but bounded. And so, the behaviour of the pre-reformer is studied while using re cycling of AOG as a control variable, in section 6.5.

6.2.3. Transient behaviour

Figure 6.2 sheds light on the preferable and safe operating conditions of the pre-reformer, but leaves out the transient behaviour of the pre reformer. [3] The transient response of the outflow of the pre-reformer, to a change of the inflow, is two-fold. There are:

1. The actual amount of moles leaving the the pre-reformer

2. The composition of the gas mixture that is leaving the pre-reformer

The amount of moles that are leaving the pre-reformer is governed by a pressure valve. This pressure valve is simulated by a proportional controller. In any case, the immediate response by such a system will not be limiting for the behaviour of the system, observing the transient behaviour of other components of the SOFC system (see sections 6.3 and 6.4).

The composition of the outflow however, will have to be studied in more detail. The model allows only for evaluation of the reformer outflow composition which is a reflection of the total number of moles present of every species in the pre-reformer. That said, the model accurately describes the kinetics of all the reactions that are present, *so not* merely the equilibrium. This means that it *can* be assessed whether equilibrium will be reached within a certain amount of time, given a certain perturbation. This information can than be used to find the minimal volume of the reactor, for equilibrium to have been reached in the time between inflow and outflow of a certain particle.

Figure 6.4 shows the the molar fractions of the pre-reformer contents. The situation at $t = 0$ is such, that the only constituents at that point are methanol and steam. This situation is non-realistic, but it is constructed to show the model behaviour in the case of an extreme perturbation in the pre-reformer conditions. The the temperature is kept at 520k in this test, which is decided to be the optimal operational temperature for the pre reformer (see section 6.2.2). It can clearly be seen that the the equilibrium is reached within the span of a second, making the assumption that the mixture is well mixed at all times problematic. The mixing properties the gasses in the pre-reformer are *not* within the scope of this investigation. However, as will become clear from sections 6.3 and 6.4, it can be deduced that the transient behaviour of outflow composition or temperature are **not limiting** for the transient behaviour of the electrical output of the methanol fuelled SOFC system.

---

is, via WGS, converted to CO_2 before it is consumed at the anode.
[3]Again, the reader is referred to appendix A.1 for the details on the tests that have been run with the pre-reformer model.
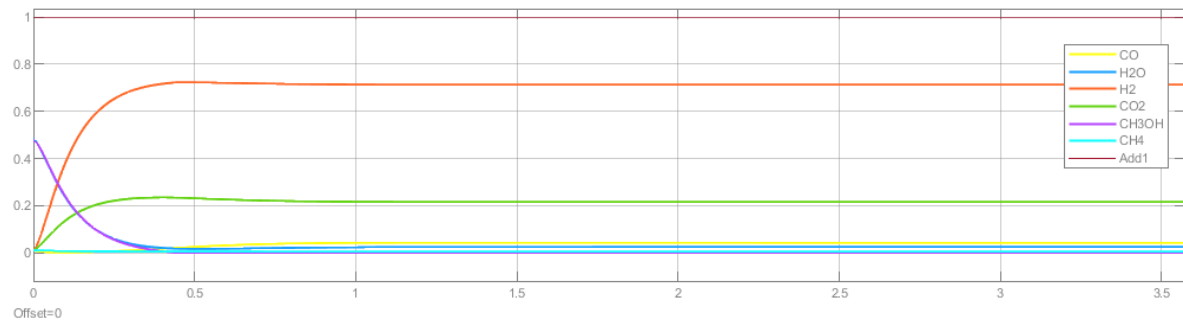
Figure 6.4: Shows the settling time of the chemical equilibrium within the pre-reformer at an operating temperature of 520K, assuming the contents are well mixed at all times.

6.3. SOFC behaviour

The integration of the SOFC in the methanol fuelled SOFC system requires knowledge about behaviour of the cell in standalone operation. The questions that need to be answered are:

- *What are the preferred operating conditions of the SOFC?*

- *What power outputs and efficiency can be expected in these conditions and in non-optimal conditions?*

- *What are the load-following characteristics of the reformed methanol fuelled SOFC?*

- *Does the position of a cell within the stack have an impact on its behaviour?*

These are an extension on the questions that were posed in section 1.3.

In order purposefully design a methanol fuelled SOFC system, the standalone behaviour of the SOFC is studied. Valuable information that was extracted is listed below:

- The efficiency, power and heat production in stable operation

- The preferred operating conditions

- The rate at which a equilibrium is attained when it is disturbed

6.3.1. Controlled parameters

The parameters that are likely to have the highest influence on the behaviour of the fuel cell stack are identified to be :

- **Temperatures and magnitudes of the inflows**; known to influence the activation losses, Ohmic losses and concentration losses in the cell, also affects the Nernst voltage.

- **Current density**; has such an extensive influence on the cells behaviour that in literature, it is used as the prime controlled parameter. Influence on Ohmic losses, activation losses, concentration losses[4].

- **(Partial) pressures**; have an influence on the Nernst voltage

---

[4]In realistic operation, current density is not simply a dail that can be adjusted. It is the product of the delivered voltage and electric impedance of the connected electric system. The way that this impedance is adjusted to suit the current demand of the electricakl system is not within the scope of this investigation.
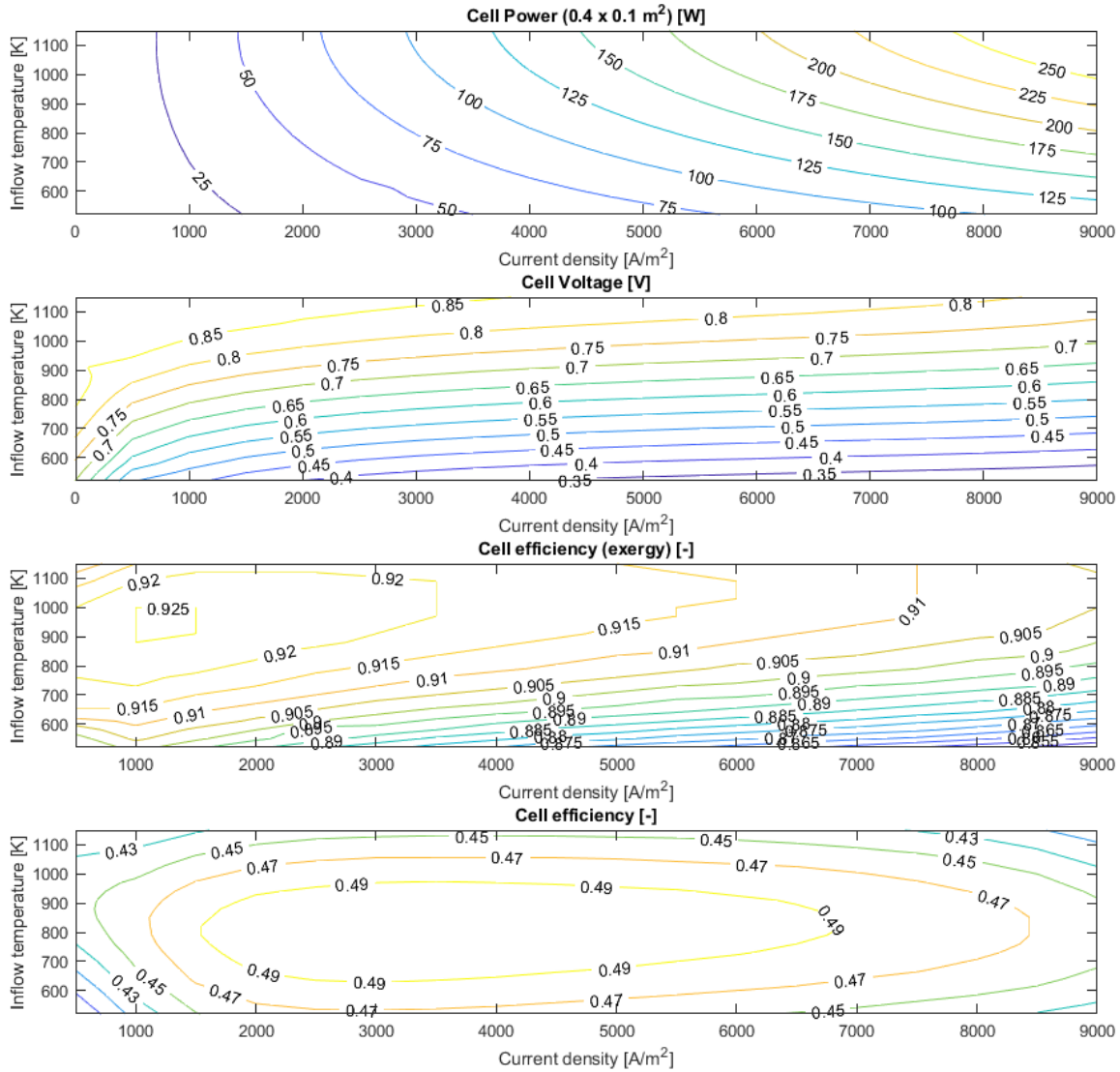
Figure 6.5: Shows the cell voltage, cell electrical power, heat production and efficiency, as functions of both current density $[A/m^2]$ (on the x-axis) and cell temperature [K] (on the y-axis).

6.3.2. Stable operation

The characteristics for stable operation of the standalone fuel cell as a function of both current density and cell temperature is shown in figure 6.5. These controlled parameters are far more influential than the (partial) pressures, as is shown in figure 6.6. With this knowledge it was decided to operate the *system* at the fuel- and air- inflow excess that was found to produce the highest cell efficiency. This means that the excess will not be a variable in the testing of the entire methanol fuelled SOFC system (see section 6.8). The efficiency and exergy efficiency of the cell are defined in equations 6.1 and 6.2 respectively.

$$\eta_{cell} = \frac{P_{cell}}{\sum_{in}(\dot{N}_i \cdot \bar{h}_i) - \sum_{out}(\dot{N}_i \cdot \bar{h}_i)} \qquad i \in \{N_2, O_2, H_2, H_2O, CO, CO_2, CH_3OH, CH_4\} \qquad (6.1)$$

$$\eta_{cell}^{EX} = \frac{P_{cell}}{\sum_{reacted}(\dot{N}_j \cdot \Delta\bar{g}_j)} \qquad j \in \{ox\ H_2, ox\ CO, ox\ CH_3OH, ox\ CH_4\} \qquad (6.2)$$
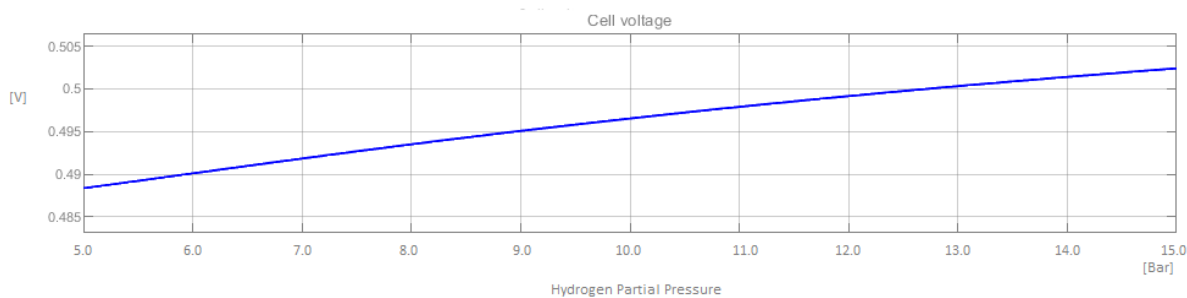
Figure 6.6: Shows the cell voltage [V], as a function of the partial hydrogen pressure [Bar].

concluding

The behaviours that should influence the implementation of the SOFC in the methanol fuelled SOFC system are noted:

- High cell voltages can be achieved at lower current densities at higher temperatures

- The cell will produce a maximal electrical output for higher current densities at higher temperatures.

- Efficiency experiences a maximum for inflow temperatures between 700 K and 900 K for the chosen inflow magnitudes

- As a decline in efficiency is caused by irreversible losses, one can remark that heat production is highest for high current densities and lower temperatures. This is important when the system needs to heat up.

6.3.3. Transient behaviour

The transient behaviour of the standalone fuel cell is of great importance to the question whether a methanol fuelled SOFC system would be able to power a naval vessel in a satisfying way. It is known from literature that SOFC systems are often ill suited to deal with rapid changes in power demand.

Standalone transient behaviour is tested as follows. First the most desirable inflow quantities and inflow temperatures for operation a certain current density are found. These inputs would enable stable operation at a certain power output. For a certain studied shift in current density, these values are changed instantaneously. This is done so the power output as a function of time can be studied, which is expected to be tied to the thermal inertia of the cell. An example of one such a test is given in 6.7, where the current density steps from 2000 $[A/m^2]$ to 6000 $[A/m^2]$. Mass flows and inlet temperatures change accordingly.

This process has been repeated for a range of possible steps in current density, in both positive and negative directions. The results are compiled in figure 6.8. The chart show the iso-lines for the settling time of the power output of the cell. The values on the X-axis represent the initial current density and the values on the Y-axis represent the magnitude of the step. The positive Y-direction of the chart shows the positive steps in current density, and vice versa. Since the cell is limited to operation up to 9000 $[A/m^2]$, the step- up or -down is limited. The grey area shows where a step is too large to be made.

Concluding

- The settle time for positive steps decreases as the terminal current density increases. This effect is due to the fact that the cell produces more heat at higher current densities, thereby heating the cell to its ideal temperature is a shorter time.

- The settle time for positive steps decreases as the initial current density increases. This effect is less distinct, but is has the same cause.
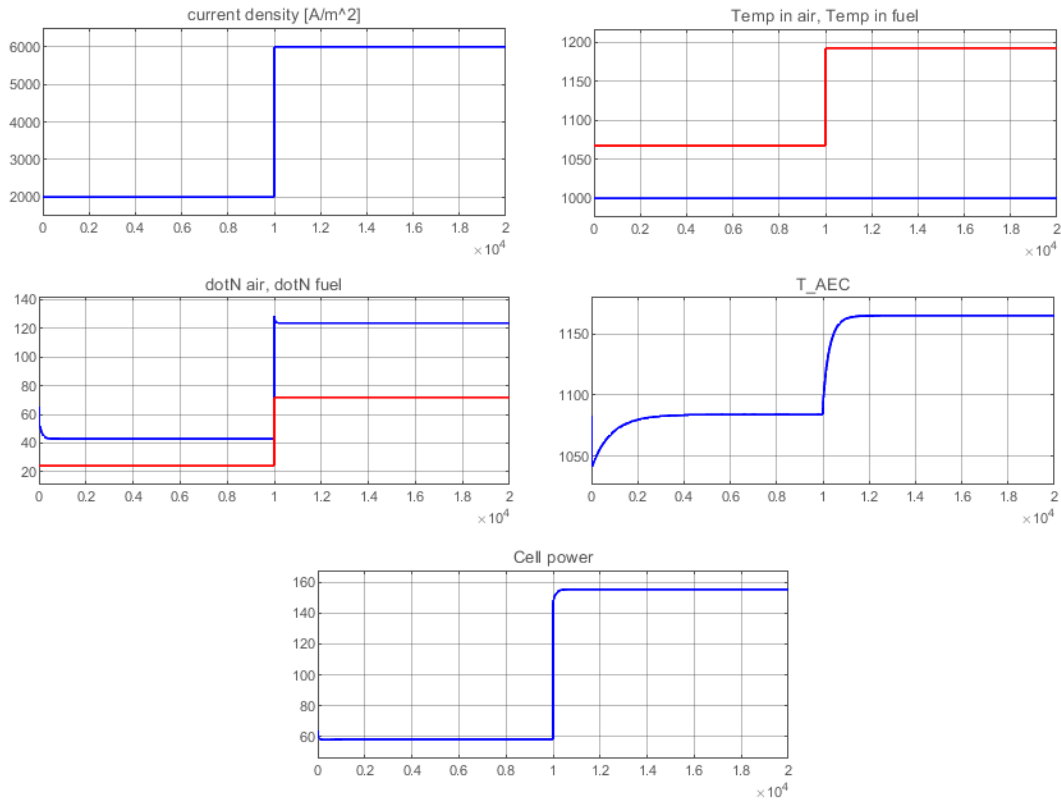
Figure 6.7: Shows the change in current density, inflow temperatures, inflow quantities for a step from 2000 $[A/m^2]$ to 6000 $[A/m^2]$ and the resulting temperature and electric power output of the cell.
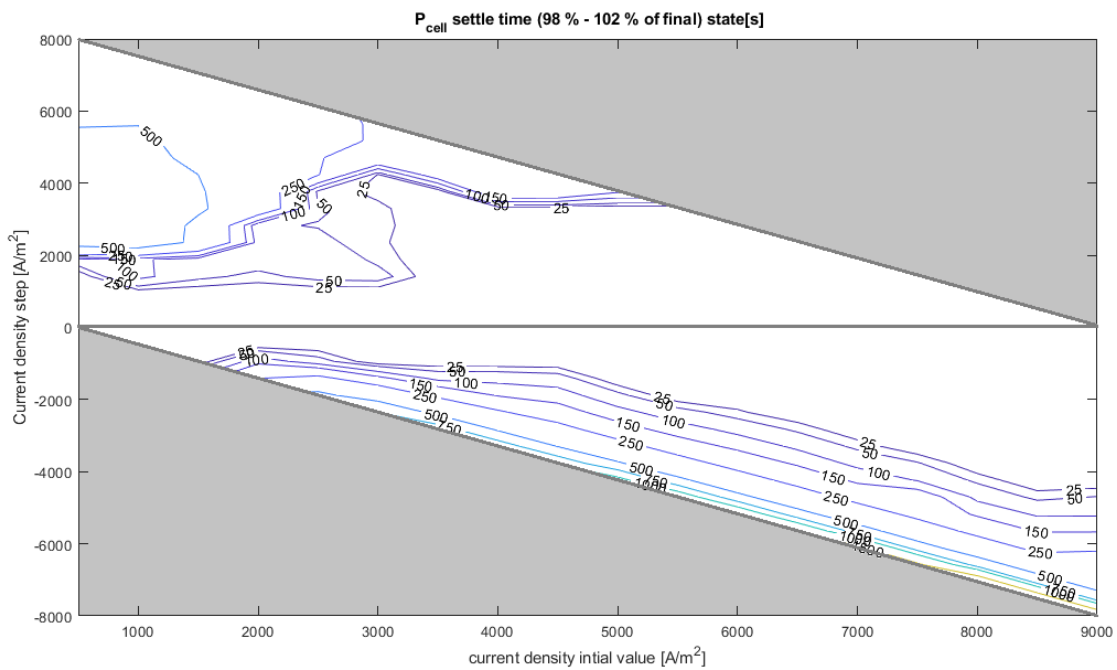

Figure 6.8: Shows the settling time of the power output of a fuel cell, plotted against initial operating point (X-axis) and step magnitude (Y-axis).

- The settle time for negative steps is far greater than that of positive steps. This indicates that it is harder to cool the cells down than it is to heat them up. However, in the cooling period, the cell will deliver more power than is demanded. This is less of an issue than producing too little power would be.

- The settle time for negative steps is mainly dependent on the terminal current density. This indicates that the cooling process is limiting for the cell power transient.

6.4. Plate Heat Exchanger performance

The integration of the PHE in the methanol fuelled SOFC system requires knowledge about behaviour of the heat exchanger in standalone operation. The questions that need to be answered are:

- What is the effectiveness ε_{PHE} of the PHE?

- What is the transient response behaviour of the PHE?

These are an extension on the questions that were posed in section 1.3. The focus on the transient response of the PHE was initiated by the statement by [2], that heat exchangers may be limiting for the (power output) response time of a Solid Oxide Fuel Cell and Gas Turbine Hybrid System (SOFC/GT-HS). The same may be the case for the current system, but a literature search delivered no answers.

Valuable information that was extracted from the current model is listed below:

- Stable operation effectiveness for different controlled parameters

- Optimal values for the controlled parameters

- The rate at which a equilibrium is attained when it is disturbed (transient behaviour)

6.4.1. Controlled parameters

The parameters that are likely to have the highest influence on the behaviour of the PHE are identified to be :

- Flow configuration: parallel- or counter- flow

- Geometry

    – Plate length

    – Combined plate width

    – Plate thickness

- Plate material

- Plate roughness

Some of these are determined by industry standards. E.g., plate material and thickness, which determine thermal conductivity, are often standardized. They have to be chosen with constructive limitations in mind. Some oteh such parameters are fluid channel space and plate roughness, which should ensure turbulent flow and an economic use of space. The counter flow configuration is chosen to enable more heat to be exchanged compared to parallel flow. Parallel flow is the exception in the industry.

This leaves plate length and combined plate width as the controlled parameters. They are varied in this investigation and the results are shared in the coming section.
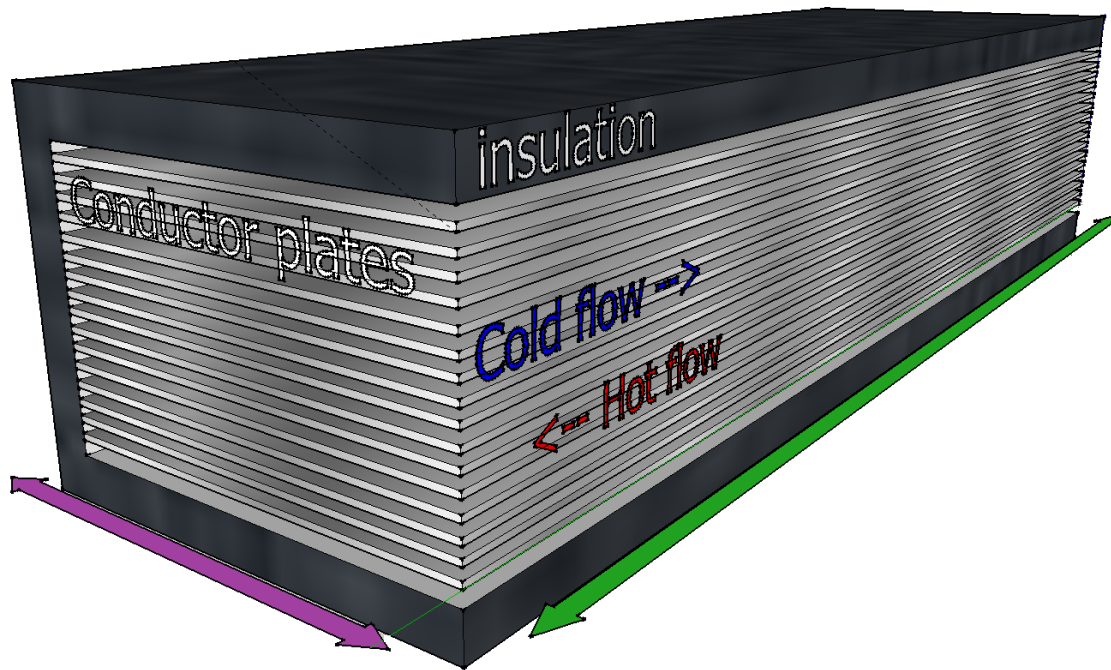
Figure 6.9: Visalisation of the Plate Heat Exchanger in a partially exposed insulation unit. Plate length 'L' is indicated by the green arrow. Plate width "b" is indicates by the purple arrow. The number of conduction plates is "n"

6.4.2. Stable operation

The dimensions of the PHE were integrated in the model and will therefore have an effect on the behaviour. Plate length along the flow direction "L" (green arrow in figure 6.9) is varied. Also the the number of plates times their width "$n \cdot b$" ("b" is the purple arrow in figure 6.9) is varied. This is done such that the the cross section normal to the plate length, of the PHE is more or less square, to prevent excessive heat losses to the environment. In current PHE technology, often a plate thickness of 0.4mm is used. This is often combined with a fluid channel of 0.8mm in order to ensure flow turbulent enough for optimal heat transfer to the separator plate .The plates are constructed in carbon steel for its constructive benefits. Furthermore, the significantly higher thermal conductivity of copper has little effect on the heat transfer between the two flows. The convective heat transfer between gas flow and separator wall is limiting for the heat transfer process.

The performance of the PHE in stable operation has been mapped. Conductor plate length L and combined conductor plate width $n \cdot b$ were varied. The influence in the PHE-effectiveness was logged. The effectiveness of PHE case is the effectiveness of the heater in counter flow operation. It shows how well the heat exchanger is able to pre heat the cathode flow. Effectiveness of the PHE in cathodic flow is defined in ε_{PHE}^{cf}, which is the effectiveness of the heater of the PHE in counterflow $\varepsilon_{heater}^{CF}$, is defined in equation 6.3

$$\varepsilon_{PHE}^{cf} = \varepsilon_{heater}^{CF} = \frac{\Delta T_c}{\Delta T_{max}} \tag{6.3}$$

The results are compiled in figure 6.10, where $n \cdot b$ is shown on the X-axis and L is shown on the Y-axis. the iso-lines show the value of the effectiveness of the PHE.

6.4.3. Transient behaviour

The transient behaviour of the PHE is of great interest for this thesis. The measure and time frame in which an input perturbation has an effect on the system output. In many cases such behaviour is evaluated by studying the response of the system to a step function.

In this case, 'the step' is the change in temperature and magnitude of the hot flow. This flow represents
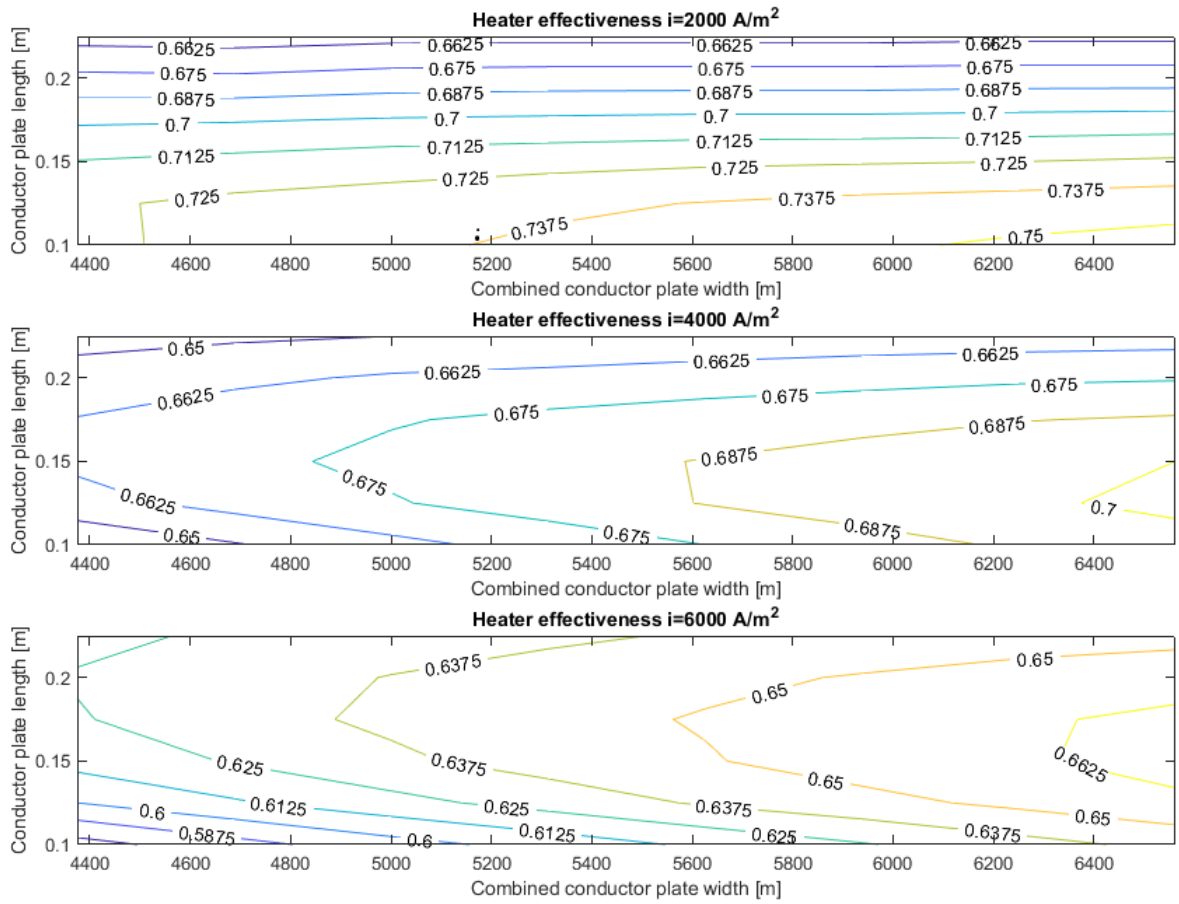
Figure 6.10: Shows the effectiveness of the heater of the PHE as a function of both the conductor plate length and the combined conductor plate width
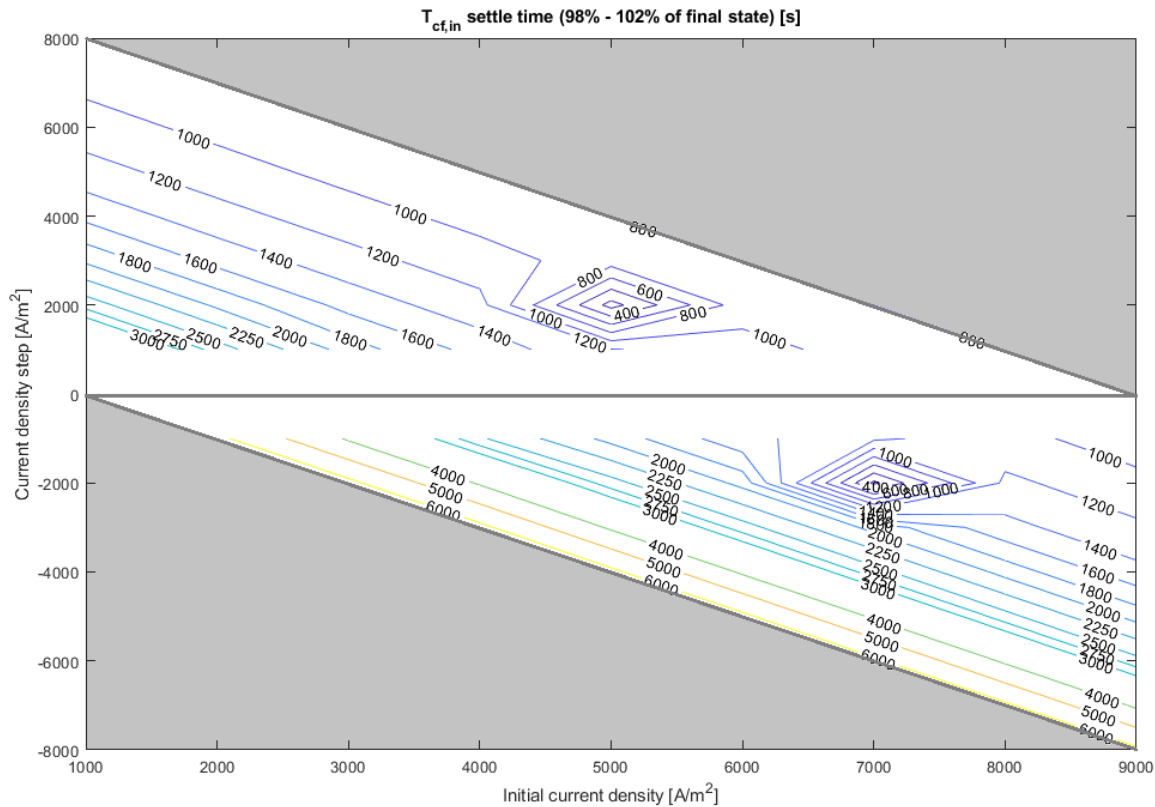
Figure 6.11: Shows the settling time for the outflow temperature of the cool flow in case of a step in inflow temperature and magnitude. In going flow magnitudes- and temperatures are changed to the preferred values for a certain current density. The initial current density is given on the X-axis. The step in current density is given on the Y-axis.

the outflow of the cathode. For the tests, the temperature and flow magnitude change according to the preferred operating values of the SOFC for a certain current density. This is done for varying $n \cdot b$. The results are compiled in figure 6.11. Two anomalies are present in the this figure. They are real values, however. As can be seen in section 6.3.2, ideal inflow and outflow temperatures of the SOFC are not monotonically rising. The outflow temperature for SOFC operation at $5000 A/m^2$ and $7000 A/m^2$ are nearly equal. The two anomalies represent a step from $5000 A/m^2$ to $7000 A/m^2$ and vice versa.

concluding

- Increasing the combined conductor plate width increases the effectiveness of the heater of the PHE for all flow rates of the fluids, but the effect is less strong for lower flow rates.

- Heater effectiveness as a function of conductor plate length experiences a maximum for values between 0.1m and 0.2m. The ideal plate length increases as temperature difference and fluid strength F increase, which happens at higher higher flow rates[5].

- Increasing temperature difference and fluid strength F, as would happen when the SOFC current density is increased, decreases the overall heater effectiveness.

- The transient behaviour of the acPHE is significantly slower than that of the SOFC.

- The dynamic response of the PHE is especially slow when the fluid magnitudes and temperatures are stepped down. This poses less of a problem than it would the other way around.

---

[5]Increasing plate length indefinitely does not increase the heater effectiveness to a certain maximum. This may seems counter intuitive, but it is explained by the fact that the (position dependent) temperature difference between the hot and cool flows "$\Delta T(x)$" decreases over the entire length of the plate as the plate is elongated. This limits the specific heat flow through the conductor plate.

- The terminal flows and temperatures are far more important to the dynamic response of the PHE than that of the initial flow magnitude and temperature.

6.5. Anode Off Gas Re-Cycling

As can be seen in section 6.2.2, the temperature of the pre-reformer cannot remain stable if the reactor is not provided with an external heat flow, either positive or negative. To enable the desired outflow of the pre-reformer, its temperature should remain around 520K (see section 6.2.2). The exothermic reactions at higher temperatures, and the endothermic reactions at lower temperatures, make for an unstable system. A too low temperature results in slow reactions and a high required heat. A too high temperature results in an unwanted production of methane and high internal heat production of the subsystem, resulting in dangerous situations.

6.5.1. Pre-reformer temperature control

In the current setup, of which the test results are shown in this section, temperature is controlled exclusively by the the ratio $\dot{m}_{AOGRC}/\dot{m}_{AOG}$ via a PID-controller.

Using the AOG to control heat, offers a way that controls the temperature of the pre-reformer in a responsive manner. Operation should be kept at 520 K, to limit the required heat flow to or from the reactor[6].

Transient pre-reformer temperature response to the introduction of AOGRC is tested. Parameters are changed as one could expect them to change as a result of a step in current density:

- The fuel flow is a ratio to the set current density:
  $\sum_{i,af} \dot{N} = \frac{i}{2 \cdot F} \cdot \sum_{sys} A_{cell} \cdot C_{fuel}$ where $C_{fuel} = 1.75[mol/C]$

- The air flow is a ratio to the set current density:
  $\dot{N}_{O_2} = 1.15 \cdot \left(\dot{N}_{H_2} + \dot{N}_{CO} + 3 \cdot \dot{N}_{CH_3OH} + 4 \cdot \dot{N}_{CH_4} \right)$

- The introduced steam is a function of the current density:
  $\mu_{steam} = 700/(\frac{i}{1000})^{0.9}$ see section 6.5.2

Therefore, in this test, the current density behaves as a step function, and the quantities listed above, are adjusted accordingly. Figure 6.12 shows the response in current density step is from 1000 A/m^2 to 9000 A/m^2 to demonstrate the most severe step. The resulting

- Reactor temperature $T_{pre-ref}$

- AOGRC ratio μ_{AOGRC}

- Molar hydrogen outflow $\dot{N}_{H_2,af,in}$

of the pre reformer are shown in time as a result of this step. It can be seen that the settle time of the response is well within 100s. This is significantly faster than other subsystems presented in this work.

6.5.2. Steam ratio

In order for the methanol to be converted to hydrogen it is desirable to introduce steam to the gas mixture in the pre-reformer. The steam ratio is defined as

$$\frac{\dot{N}_{H_2O}}{\dot{N}_{CH_3OH}} = \mu_{steam}$$

at the inflow of the pre-reformer (not counting the AOGRC).

---

[6]This remains true for all modes of operation, save operation at $i = 500A/m^2$ and below. Then the gas mixture stays in the reformer for too long. This enables methane forming to take place to a limited extent
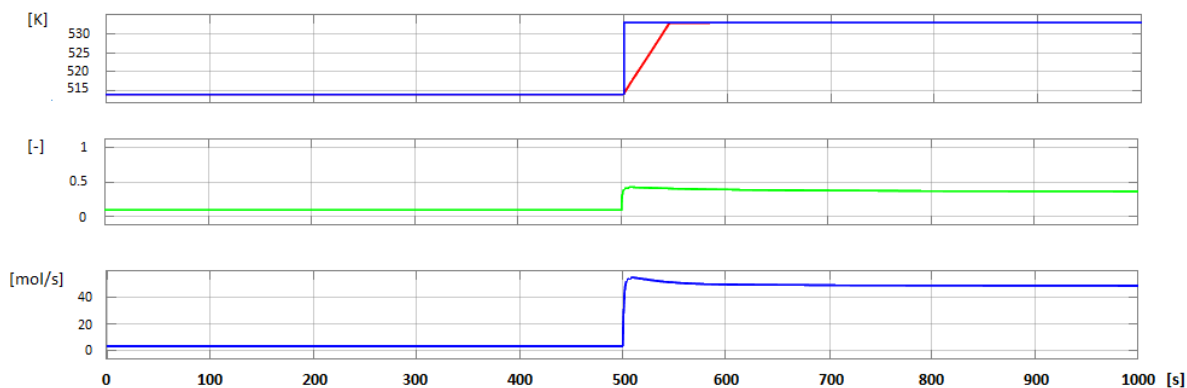
Figure 6.12: Shows the variation in time of the pre-reformer temperature, the AOGRC ratio, and the molar hydrogen outflow, as a result of the

From figure 6.2 it is known that a high steam presence, enables operating the pre-reformer at slightly higher temperatures. Steam also limits the amount of CH_4 that is created in the reactor. It shows how heat production from the reactions is slightly less for higher steam ratios.

It was found that $\mu_{steam} = 700/(\frac{i}{1000})^{0.9}$ ensures that there will always be (barely) enough steam available in the pre-reformer, when AOGRC is accounted for. This relation is emperical and has been found by trial and error.

Concluding

- It **is** possible to maintain constant reactor temperatures by using only AOGRC regulation, up to a certain temperature. In fact, in stable operation the temperature of the of the AOG is so high, that a AOGRC ratio of $\mu_{AOGRC} = 0.4$ is sufficient to heat up the pre-reformer to the desired temperature.

- Due to the high AOG temperature, there is a maximum amount ($\mu_{AOGRC} \approx 0.4$) of AOG that can be safly recycled to the pre-reformer. This creates losses of chemical energy and heat energy to the environment. Furthermore, steam needs to be added tot the pre-reformer. Possibilities for improvements are named in the recommendations (section 7.2.4).

6.6. Integrated PHE for air

The PHE is positioned between the gas flows that go into and out of the cathode. It is intended to heat up the the gas to the cathode to enable operation of the fuel cell at optimal temperature. The position of the PHE is depicted in figure 6.1.

The amount of air that is compressed is dependent on the current density of the cell. It is calculated directly from the the set current density. Determining the ideal airflow to the cathode channel is done with the following dilemma in mind

- It is desirable to decrease the air into the fuel channel as much as possible. Excessive cooling of the cell may be prevented by decreasing the airflow to the cathode.

- It is desirable to have the highest possible partial pressure for oxygen at the cathode. This increases reactivity and therefore the Nernst-voltage.
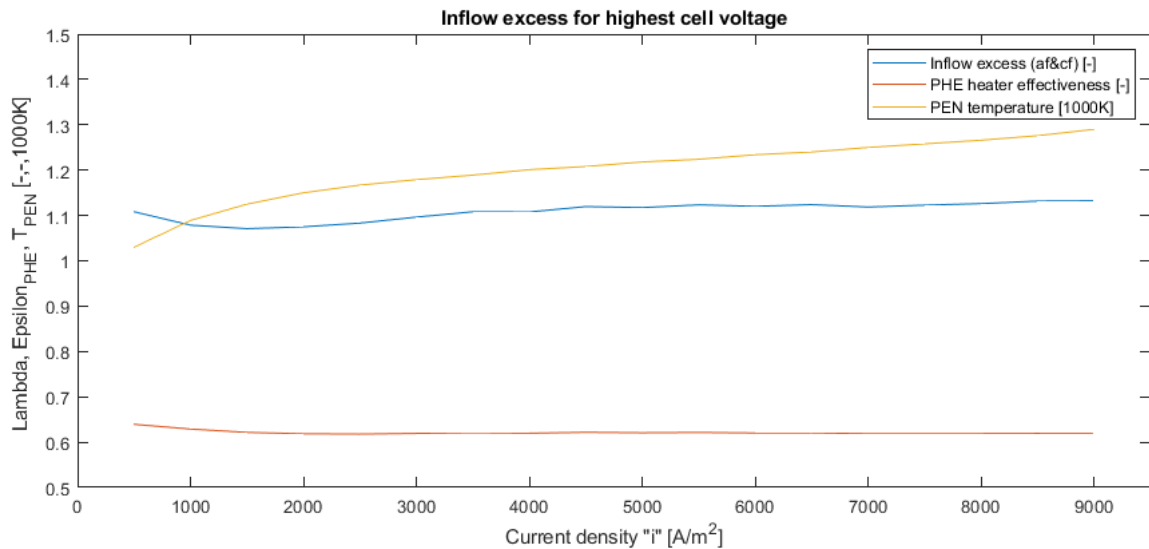
Figure 6.13: Top shows the effectiveness PHE for steam ratios 0, 0.2, 0.5, as a function of the current density. Bottom shows the optimal operating temperature for the SOFC, and the actual cell temperatures for steam ratios 0, 0.2, 0.5, as function of current density.

A sufficiently pre-heated air flow may offer the solution to this dilemma, as the oxygen supply may be increased without the excessive cooling of the cell.

6.6.1. Stable operation

The effects of integrating the PHE in the methanol fuelled SOFC system are studied. For every value of i the optimal operating temperature of the cell is known from section 6.3.2. The magnitude of the cathode flow is varied, and the effect on the fuel cell temperature is studied.

The temperature in the PEN-structure is, for a large part, a product of the in- and out- flow temperatures of the cathode flow. This means that the temperature of the PEN-structure is indicative of the effectiveness of implementing a heat exchange between the inflow and the outflow of the cathode.

The performance of the PHE is studied as a function of the current density and the correlated airflow. The inflow excess:

$$\lambda_{ox} = \frac{2 \cdot \dot{N}_{O_2}}{i/(2 \cdot F)} \tag{6.4}$$

$$\lambda_{fuel} = \frac{\left(\dot{N}_{H_2} + \dot{N}_{CO} + 3 \cdot \dot{N}_{CH_3OH} + 4 \cdot \dot{N}_{CH_4}\right)}{i/(2 \cdot F)} \tag{6.5}$$

In the testing case : $\lambda_{ox} = \lambda_{fuel} = \lambda$. The results are gathered in figure 6.13. It shows the values of λ, for which the heater effectiveness ε_{PHE}^{cf} is highest (indicated in blue). It also shows the achieved ε_{PHE}^{cf} (indicated in red) for these values of λ , as well as the PEN-temperature that has been achieved in 1000K (indicated in yellow).

concluding

- The effectiveness of the heater of the PHE experiences a maximum at around $\lambda \approx 1.1$ because further lowering of λ enhance the effect of the decrease in Nernst voltage

- PEN temperatures of 1015 K to 1290 K can be achieved using the PHE

- The heater effectiveness remains relatively low due to the fact that the fluid strength of the ingoing cathodic flow is significantly greater than that of the outgoing cathodic flow
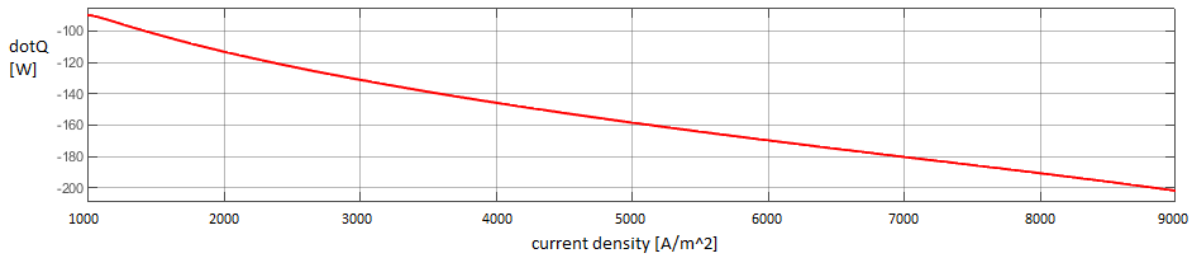
Figure 6.14: Shows the the heat flow through 1 end plate of a fuel cell stack ($0.04 m^2$)as a function of the current density of that stack.

It was felt that the description of standalone transient behaviour of the PHE, and the description of the methanol fueled SOFC system transient behaviour, sufficiently describes the transient behaviour of the integrated PHE for air. It was therefore decided to omit a section on transient response, specifically for a PHE between the ingoing and out going cathodic flows.

6.7. Stack extremes

The stacking of the cells, and the consequent varying proximity to the end-plate of the various cells, have a profound effect of the behaviour of the system. Whereas heat flux between two neighbouring cells in the middle of the stack will be in near equilibrium, the cells near the stack extremes will experience a heat flux to the environment. The cooling effect on these cells will influence the power- and heat- of production of these cells.

6.7.1. Heat losses trough endplates

The heat flow through one endplate (0.04 m^2) is shown in figure 6.14 for operation at current densities, ranging from $1000 A/m^2$ to $9000 A/m^2$.

It can be seen from figure 6.15, that the behaviour of the cells at the extremes of the stacks is severely impacted by the difference in temperature compared to center cells. It is remarkable to see that the position of the cell has a severe impact on the ultimate temperature, not so much on the settle time.

6.7.2. Stack geometry

A cell endplate has a surface area of $A_{cell} = 0.04 m^2$. Excluding the combined endplate surface, the system has a maximal total surface area of 36.84 m^2 and a absolute minimal total surface area of 5.17 m^2, dependent on the stacking of the cells. Table 6.1 shows non-endplate surface area for different stacking options.

# stacks	$A_{edge}[m^2]$	# stacks	$A_{edge}[m^2]$
1	36.92	24	10.516
6	12.76	32	10.649
12	10.784	48	11.822
18	10.45	64	12.969

Table 6.1: Lists the total boundary area for the number of stacks in the configuration

concluding

- The heat flux through one endplate and the module insulation is in the range $\dot{Q}_{leak} = \langle 100W, 200W \rangle$. For a configuration of 36 stacks, with 334 cells each, the heat flux through the endplates is $72 \cdot \langle 100W, 200W \rangle = \langle 7.20kW, 14.40kW \rangle$.

- It is assumed that the heat flux through the non-endplate, non-inflow, non-outflow surfaces is in the same order; comparatively small for this system.
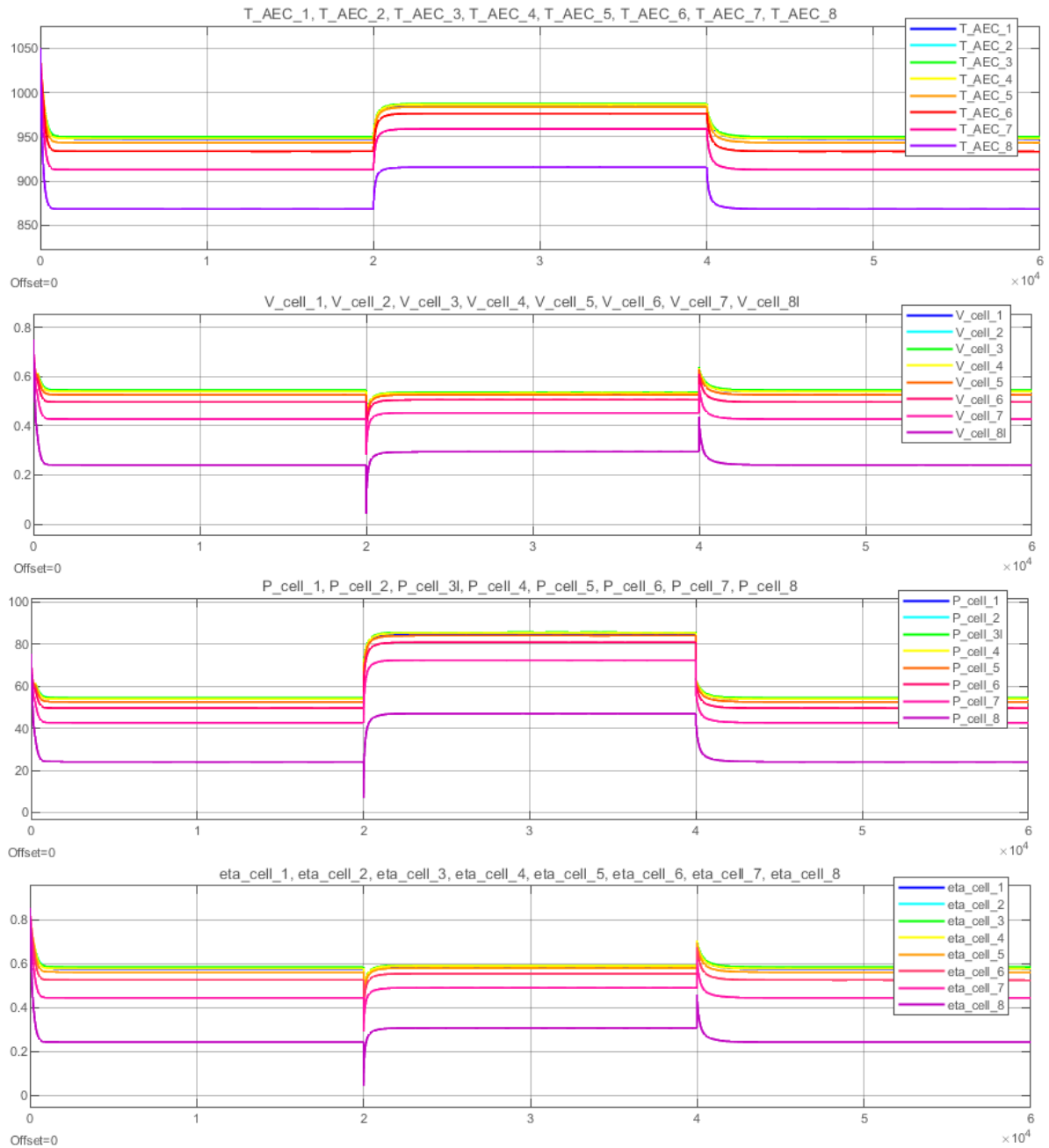
Figure 6.15: Shows the behaviour of the cells at the extremes of the stack. Current density changes from $i = 2500A/m^2$ to $i = 4000A/m^2$ and back to $i = 2500A/m^2$ at $t = 2000s$ and $t = 4000s$ respectively. Other system parameters change accordingly. This figure shows, from top to bottom, the PEN-structures Temperature, cell Voltage, cell power and cell efficiency.
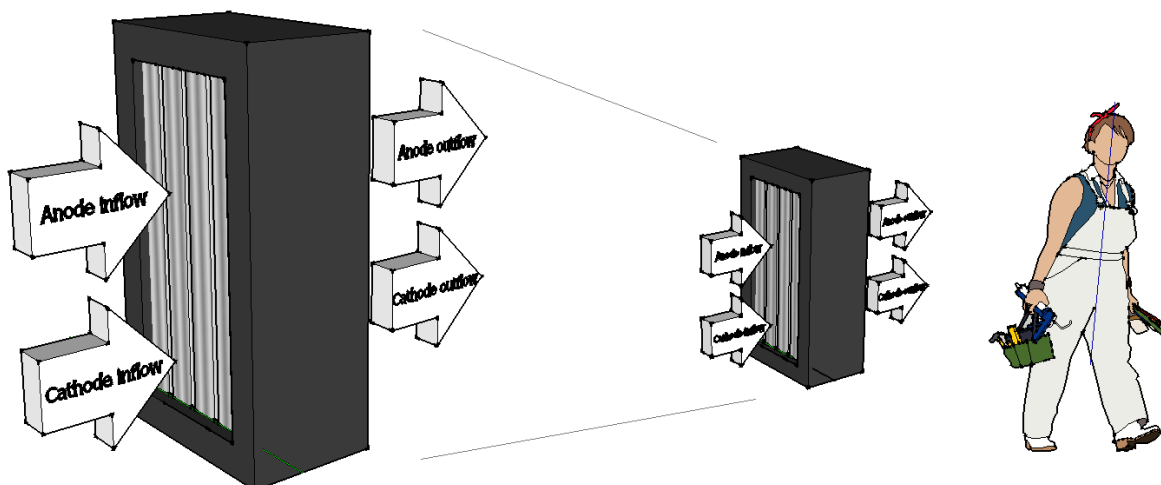
Figure 6.16: Shows one insulated module which contains 4 stacks of which each contains 334 cells. Th righ shof such a module in perspective to a human figure

- The magnitude of the total heat flow to the environment are not very significant to the total losses in the methanol fuelled SOFC system.

- The detrimental effect on the individual cells' performance at the extremes of the stack is significant.

- The detrimental effect of the cooling of the cells near the extremes is significant up to 4 cells from the endplate.

A consequence is that the the difference in behaviour within single cells may also be severely impacted. to truly explore the extent of these effects it is advised that a 1-dimensional, or even 2-dimensional model is constructed and studied.

6.8. Methanol Fueled SOFC system

The knowledge from the previous sections is used to further define the configuration of the the methanol fuelled SOFC system. This concerns the configuration of the stacks. The entire methanol fuelled SOFC system is connected as described in figure 6.1. It was decided that calculations would be a fuel cell configuration of 36 stacks. Four stacks are installed parallel within a module, of which there will be nine. One such module is shown in figure 6.16. This configuration features $2.88m^2$ of insulated endplate surface area[7]

It also concerns some controllable parameters: controllable parameters have been set to certain values. They are listed below:

- The air flow is a ratio to the fuel flow which is a function of the current density:
$\dot{N}_{O_2} = \dot{N}_{H_2} + \dot{N}_{CO} + 3 \cdot \dot{N}_{CH_3OH} + 4 \cdot \dot{N}_{CH_4} = \lambda_{ox} \frac{i}{4 \cdot F} = \lambda_{fuel} \frac{i}{2 \cdot F}$

- The introduced steam is a function of the current density:
$\mu_{steam} = 700/(\frac{i}{1000})^{0.9}$

---

[7]There will also be $7.38m^2$ of non- endplate, non-inflow, non-outflow surface area, of which some portion will be exposed to the (insulated) environment boundary. Based on the figures gathered in figure 6.14 however, the max heat loss of $18.45kW$ at operation at $1000A/m^2$ is not included in the calculations.

6.8.1. controlled parameters

Other controllable parameters are chosen to control the system. These will be varied to find optimal operational points and describe system behaviour. These are:

- Current density

- Fuel- and air inflow: Higher fuel rates will increase stack power but also increase discarded fuel. Furthermore, more compression power is required for higher flow rates.

- Fuel inflow temperature: Higher inflow temperature decreases electrical resistance in the cell, which is especially significant at higher current densities

When the effect of varying the fuel- and air-flow excess is studied, the inflow temperature will be kept stable at $T_{af,in} = 520K$. When the effect of the of varying the anode inflow temperature is studied, the fuel- and air-flow excess is kept at $\lambda_{ox} = \lambda_{fuel} = \lambda = 1.1$.

6.8.2. Stable operation

Influence of external heating and of the implemented fuel flow excess are shown in figures 6.17 and 6.18. The system net power is calculated in equation 6.6 .The system efficiency is calculated using equation 6.7.

$$P_{sys} = P_{stack} - P_{compr,H_2O} - P_{compr,CH_3OH} - P_{compr,air} - \dot{Q}_{heater} \tag{6.6}$$

$$\eta_{sys} = \frac{P_{stack} - P_{compr,H_2O} - P_{compr,CH_3OH} - P_{compr,air} - \dot{Q}_{eh}}{\dot{N}_{CH_OH,in} \cdot LHV_{CH_3OH}} \tag{6.7}$$

This calculation assumes that all the fuel (CH_3OH, H_2, CO, CH_4) in the AOG that is not re cycled into the pre-reformer is discarded.

Concluding

The following is concluded from these figures:

- Whereas cell efficiency decreases as the current density increases, system efficiency experiences a maximum at $3000 A/m^2$. Decreasing efficiency for lower current densities is due to balance-of-plant effects, as can be seen from contributions of the compressor to the net power output.

- The effect of external heating of the anode inflow on the cell output is marginal. Implementation of external heating of the anode inflow therefor amounts to a net loss for all current densities. However, External heating could well be instrumental in preventing extreme thermal stresses at the inflow of the cells due to the temperature difference in ingoing anodic- and cathodic- flows.

- The net power loss of the system due to external anode inflow heating means that the efficiency goes down as well.

- Positive effects of larger flow excess on voltage is marginal. Implementation of a large excess for both flows therefor amounts net loss (due to higher compression power) for all current densities. However, the way that the partial pressures at the electrodes are calculated means that there there is possible overstating of the partial pressures of the reactants for excess ratios very close to 1 (see equation 4.47). Therefore it is stated that the excess ratios for both flows should be kept at $\lambda = 1.1$

- Whereas power output of a cell slightly increases, system experiences a decrease in efficiency due to increase of flow excess, for all current densities.
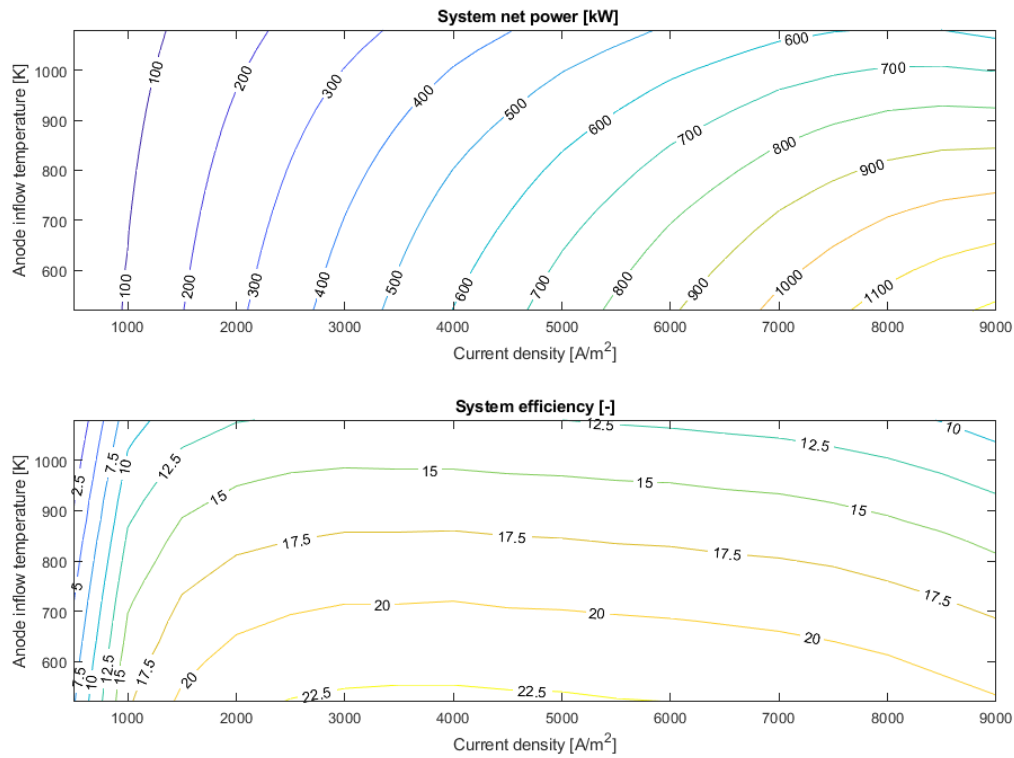
Figure 6.17: Shows the system net power and the system efficiency, as calculated in equations 6.6 and 6.7 respectively, as a function of current density(X-axis) and anode inflow temperature(Y-axis).
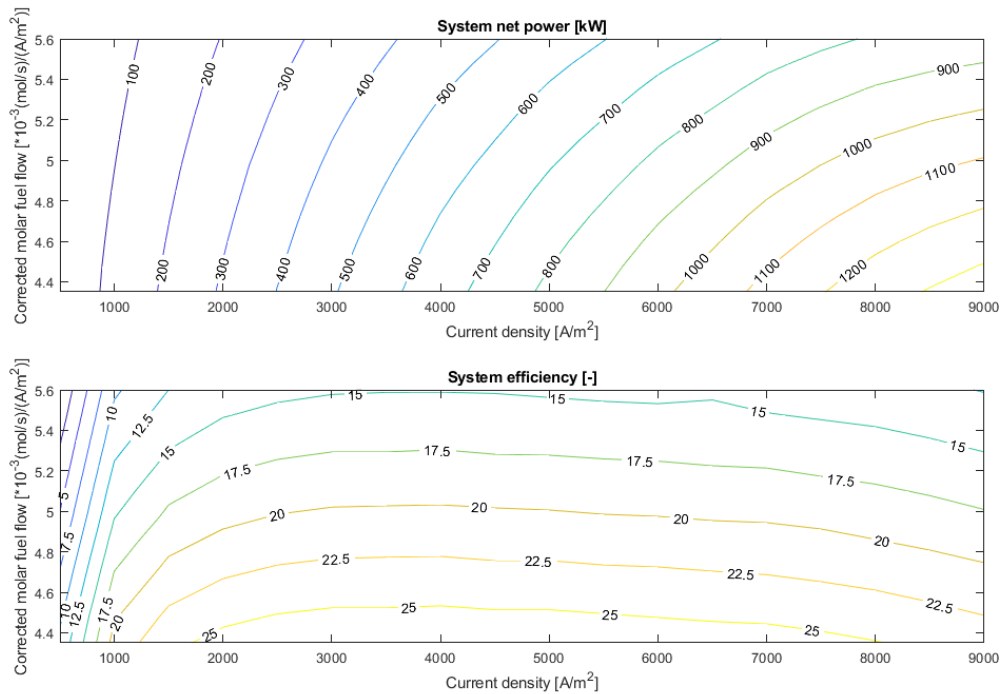

Figure 6.18: Shows the system net power and the system efficiency, as calculated in equations 6.6 and 6.7 respectively, as a function of current density(X-axis) and fuel- and oxygen- flow excess $\lambda_{ox} = \lambda_{fuel} = \lambda$(Y-axis).
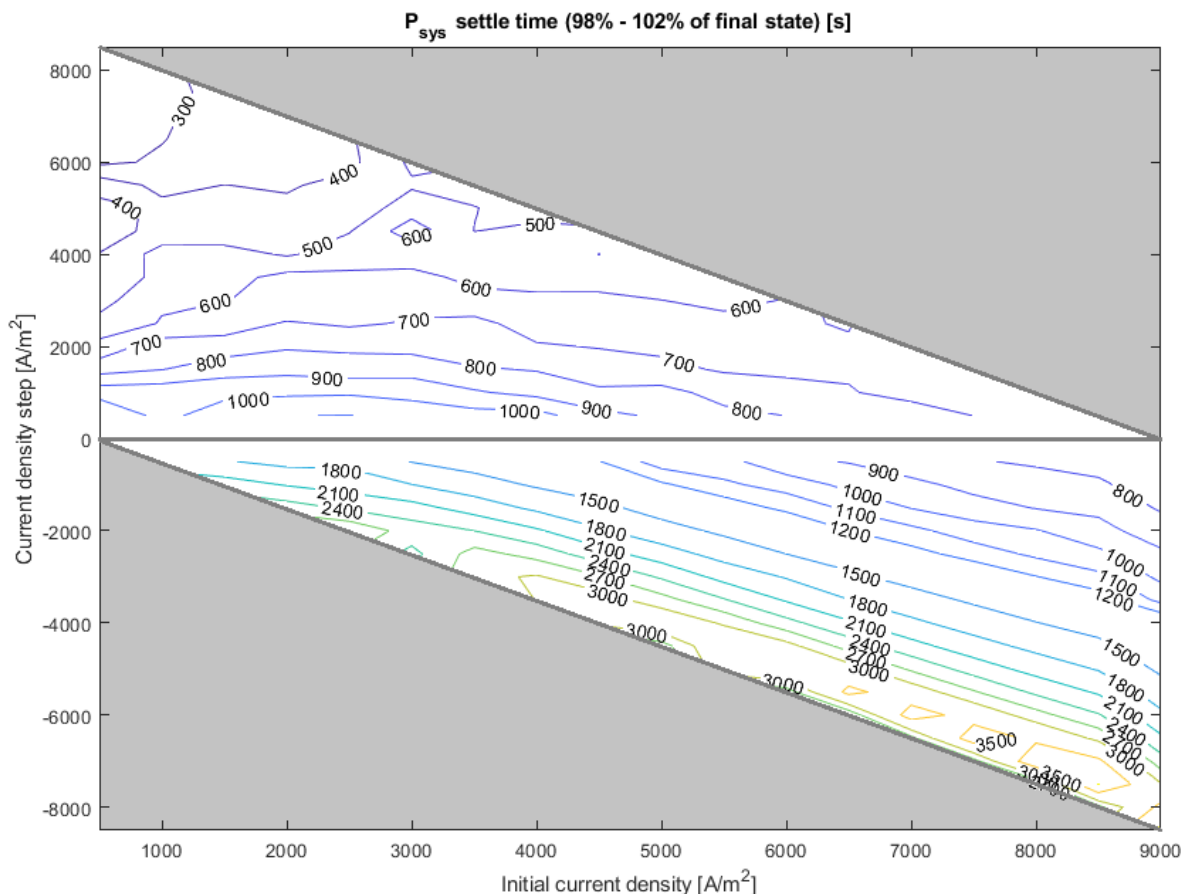
Figure 6.19: Shows the settling time of the methanol fuelled SOFC system as a function of the magnitude of the step (in both positive and negative directions) and the initial value of the current density. Airflow, fuel flow, steam ratio and AOGRC ratio change accordingly.

6.8.3. Transient behaviour

Transient behaviour of the entire connected methanol fuelled SOFC system is tested and the results are gathered in figure 6.19. It shows the settle time for the electric power of a cell. The current density undergoes a step function, in either positive or negative direction. This is done for varying step magnitudes and from varying initial values. The position on the X-axis indicates the initial value of the current density. The position on the Y-axis indicates the magnitude of the step in either positive or negative direction. The inflow, fuel flow, steam ratio and AOGRC ratio change to the values given in section 6.8. The time it takes for the electric cell output to approach the final cell output up to 2% is called the settle time.

concluding

It can be seen from figure 6.19 that the settle times are significant,and they show the following trends:

- The settle time for the entire system is significantly longer than the settle time for the isolated SOFC (see section 6.3.3). This indicates that the PHE has a negative effect on the overall transient behaviour of the system, despite its necessity.

- Settle time for a step in positive direction is much shorter than for steps in negative direction. This indicates that the cooling process of the cell is slower than the heating up of the cell.

- The terminal value of the step is significantly more influential on the settle time than the initial value, or the magnitude of the step.

- In all step up cases, the immediate system output is lower than the eventual system output. This could pose a problem when a large step in power is required.

- In all step down cases, the immediate system output is higher than the eventual system output. Therefore, the long settle time for the step down is less problematic than similar settle time would be for step up.

7

Conclusions & Recommendations

7.1. Conclusions

This thesis has provided a number valuable insights on the operation of a methanol fuelled SOFC system onboard a naval vessel. Furthermore, it has created valuable content to be used in further research. The models that have been created are modular in nature and could be used to find better suited configurations of this system. Some of these improved configurations are suggested in the recommendations.

7.1.1. Fuel reforming

- Methanol is a suitable candidate as the marine fuel in SOFCs.

  – Storage is relatively safe

  – Energy density is high compared hydrogen, methane and ammonia

  – Large scale production has been proven feasible and efficient compared to other fuels

- If methanol is used as a fuel, the implementation of a pre-reformer is desirable to counter the cooling effect of MSR and MDR at the anode, which could lead to harmful thermal stresses.

- This research is inconclusive about what the chemical behaviour of the fuel gas mixture is above 800 K. The kinetics based pre-reformer model uses parameters which are highly dependent on temperature, which are defined only for a certain temperature range in literature. Since the anode temperature is higher than 800K, the actual magnitude of the cooling effect on the anode remains unknown.

- This work shows that the dynamic response of the methanol fuelled SOFC system *is not* significantly impaired by the use of the a pre-reformer when:

  – It is operated in the pressure range $19 \cdot 10^5 \leq p \leq 21 \cdot 10^5$

  – A reforming reactor with a volume of 2.0 m^2 is used, where 30.0 kg nickel based catalyst is present

  – For a fractional steam input $\mu_{steam} = 700/(\frac{i}{1000})^{0.9}$ (this excludes the steam present in AOGRC)

- This responsveness argubly increases the load folowing capabilities of the entire methanol fuelled SOFC system

Influence of methanation

Methanation can occur in a hydrogen rich gas mixture containing carbon oxides

- The kinetics of the methanation reactions are slow compared to the other reactions present in these gas mixtures when the reactor temperature is under 520K. They do not play a significant role in this temperature range, provided that the trough flow of the pre-reformer is higher than 2.1 mol/s flow to the anode.

- The methanation reactions play a more prominent role at higher temperatures.

- The strong exothermic nature of the methanation reactions can create a runaway effect that could jeopardize the safety and operability of the system.

- An injection of water or steam into the pre-reformer may be an adequate safety mechanism in case a methanation-driven runaway is at risk of occurring (see section 7.2.7).

7.1.2. SOFC operation

The Solid Oxide Fuel Cell is a fuel cell that is capable to convert chemical energy in fuels to electric energy through electrochemical processes. Contrary to some other types of fuel cell, it is able to electrochemically combust non-hydrogen fuels. This is due to their high operating temperatures and the presence of oxygen atoms at the anode. The heat production SOFC due to various effects were modelled. It was found that the ideal operation temperature for the cell the highest temperature that can be achieved, although of course, this has structural limitations.

7.1.3. Methanol fuelled SOFC system heat integration.

Heat re-integration in the current methanol fuelled SOFC system is done in two ways.

- A Plate Heat Exchanger is installed between the incoming and outgoing flows of the cathode. This PHE uses the heat from the outgoing cathode flow to raise the temperature of the incoming cathode flow.

- Anode Off Gas Re-Cycling is used to heat the pre-reformer to provide steam for the reforming reactions in there.

Influence of the PHE

As seen from the temperature data of the PEN after implementation of the PHE (figure 6.13), the inflow temperature of the cathodic is such that the PEN structure in the fuel cells reach temperatures ranging from 1162K for $i = 500 A/m^2$ to 1349K for $i = 9000 A/m^2$

- The main factor that limits the responsiveness of the heat exchanger is convective heat transfer coefficient α. Increasing the value of the α could drastically improve the **transient** performance of the heat exchanger. The stable system efficiency could be marginally improved increasing the α value. Finding methods to improve this value however, is not within the scope of this investigation.

- Appendix A.4 gives an estimate of the extent to which the "constant α assumption" could have had an effect on the power calculation. The effect of this assumption is not severe.

- Implementing a PHE in between the anode in and outflow might be a solution See section 7.2.4. However, with the results of the current thesis, there is no way of knowing how the reactive anode gas mixture will react to further heating than 800 K(see section 7.2.1). This temperature is the upper limit for the accuracy of the pre- reformer model.
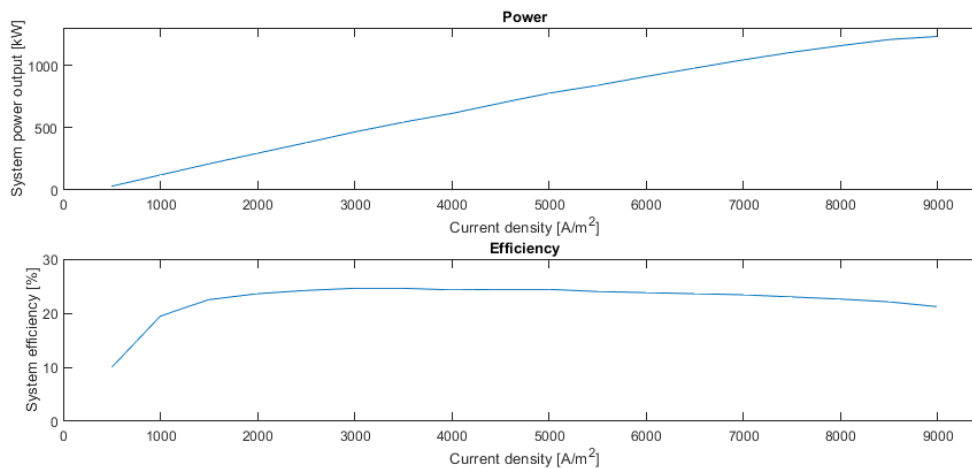
Figure 7.1: shows the maximum power and maximum efficiency of the methanlol fuelled SOFC system as a function of cell current density, for the current system configuration.

influence of AOGRC

- AOGRC is an adequate way to heat up the pre-reformer to the desired temperature of 520 K

- AOGRC is an adequate way to provide enough heat to the pre-reformer to keep the reforming reactions in the pre-reformer going.

- Controlled AOGRC can heat the pre-reformer quickly enough to assume that the pre-reformer has *no* detrimental effect on the transient behaviour of the methanol fuelled SOFC system. By including the positive effect this component potentially has on the thermal stresses in the fuel cell, one could argue that this component improves the transient behaviour of the system substantially.

- In the current confiruration, $\mu_{AOGRC} \leq 0.4$ for all operation. This severely limits the amount of steam, fuel and heat that could otherwise be reused.

7.1.4. Methanol fuelled SOFC system performance

- A methanol fuelled SOFC system as described in the current document can reach a power output and efficiency as shown in figure 7.1.

- In the current configuration, unsatisfactory use is made of waste heat and the fuel in AOG, which means that there is much room for improvement.

- Thermal inertia is the main limiting factor for the load following capabilities of SOFC based power unit.

- The response time of the PHE is the slowest in the system, and limits the usability in naval vessels

- The reactive nature of the anode flow gas mixture could jeopardize the operability and safety of the power unit if methanation reactions are allowed to to occur freely.

- Without external heating of the anode inflow, the temperature difference between the anodic- and cathodic- inflows would almost certainly produce unallowable thermal stresses on the PEN structure of the cell.

- A system of SOFC, PHE and pre-reformer exclusively will produce transient behaviour too slow for naval applicability.

7.2. Recommendations

7.2.1. Anode flow composition I.

A knowledge gap exists where the gas mixture from the pre-reformer flows to the anode. As studies into the use of methanol in high temperature SOFCs are scarce, there remains a lack of knowledge of what happens at a chemical level. The pre-reformer model in this work shows that the gas mixture is highly reactive at the high end of its temperature range (800K). Since pre-reformer model may generate inacurate results above 800K, one can only assume that the gas mixture will be even more reactive at higher temperatures. The situation at the anode is one that needs to be understood if one wants to predict the systems behaviour. The situation at the anode is currently not understood well. There is a presence of a highly reactive gas mixture in combination with catalytic materials. On top of that, electro-chemical reactions constantly alter the state of the system. In this area, there are opportunities to improve on this work.

7.2.2. Anode flow composition II.

Extended from the previous paragraph, it would be worth looking into the possibility of reforming at higher temperatures. When the pre-reformer is operated at temperatures above 550K the exothermic methanation reactions gain dominance in the reactor. In a carefully designed system, the heat that is produced in those reactions could be put to good use.

For lower temperatures, hydrogen yields from methanol reforming are favourable, provided the trough flow of gasses is high enough. Above 52OK the kinetics of the methanation reactions become faster, so methanation becomes dominant. At even higher temperatures, the equilibrium of these reaction shifts towards Hydrogen production.

From literature on methane fuelled SOFC systems, it is known that methane steam reforming takes place at higher temperatures (above 900K) where hydrogen yields are highest. It would be sensible to look into the possibility of fuel reforming at temperatures over 900K.

A system such as here proposed would combine the the convenience of methanol as a fuel with the possibility to apply knowledge from decades of methane fuelled SOFC research.

7.2.3. Anode flow heating

Though accuracy the pre-reformer model might be impaired above 800 K, its behaviour in the temperature range up to 800 K suggests that heating above that temperature may require an extremely high heat flow to the anode flow. Figure 7.2 shows the required heat flow to the anode flow in order to heat it up to 1000 K *if the pre-reformer model were to be trusted in this temperature range*. This observation, of course proves little, but it *does* suggest that a large steam ratio would help decrease the required heat flow thereby increasing system efficiency.
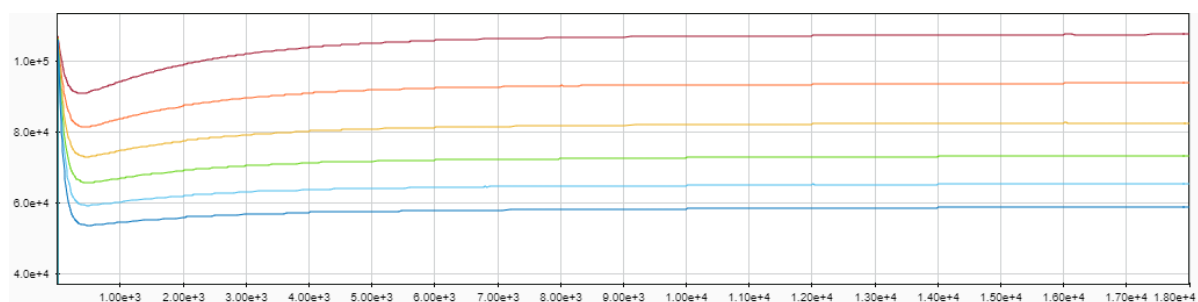

Figure 7.2: Shows the required heat flow to the anode flow in order to heat it up to 1000 K *if the pre-reformer model were to be trusted in this temperature range*. The steam fractions in this test were set at 0.0, 0.2, 0.4, 0.6, 0.8 and 1.0

Therefore it is highly recommended that an investigation is conducted into the behaviour of the gasses at the anode to obtain a clear view of the systems effectiveness and safety.
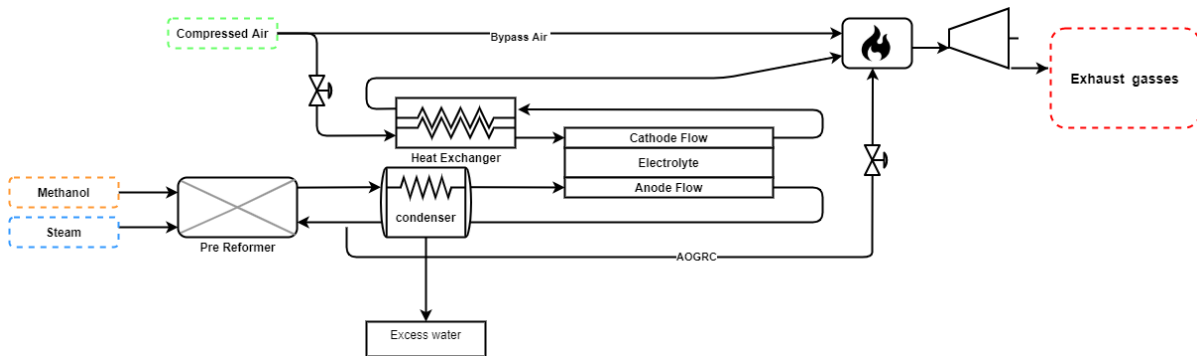
Figure 7.3: An overview of a proposed system with a Plate Heat Exchanger, after burner and a turbine to be investigated in further research.

7.2.4. System configurations

Since it is clear that in the current configuration, a substantial amount of potential energy (pressurized gas), heat and chemical energy is simply discarded, multiple other configurations are proposed. Two main alterations to the current system are suggested. Conducting an investigation in to these proposals would be highly recommended (see figure 7.3).

1. A condenser should be installed to condense some of the moisture in the AOG. This could potentially:

   • Extract some of the steam in the AOG potentially maximizing the amount of AOG that can be recycled. Which could in turn lower the fuel utilization ratio which could increase the Nernst voltage and the power density of the cells.

   • The heat that would be extracted from the condensation process could be used to heat the anode flow, even to temperatures at which methane reforming would take place (see recommendation 7.2.2)

2. The addition of a burner and a turbine would solve the issue of the discarded potential energy and chemical energy. It would solve create possibly even more waste heat to be uses for re integration in to the system. This would:

   • System responsiveness could be severely increased if provisions were made for extra burning of methanol in the combustion chamber.

   • Increase the overall system efficiency by increasing electric output (from a generator attached to the turbine), and making more high temperature heat flows available for the sub-systems and auxiliary users.

In attaching a turbine, the methanol fuelled SOFC system would be transformed into a hybrid system of gas turbine and high temperature fuel cell. These types of systems have shown a lot of merit when fuelled with methane. The outlook is very promising for future innovations concerning methanol fuelled hybrid systems.

7.2.5. Changing partial pressures along the anode

In the fuel cell the change in flow, especially for the higher fuel utilisation ratios, is significant. The effect of this change on the chemical processes along the electrodes is fully not captured in this model presented in this thesis. In this thesis there was settled for an approximation: $P_x = (p_{x,in} + 2 \cdot p_{x,out})/3$. For very high fuel utilisation ratios, this approximation is expected to become less accurate.

To study these effects more indepth, a model should be used that incorporates the length of the electrodes along the flow directions; a so called 1-dimensional model. A model like this remained out of reach for this thesis.

### 7.2.6. Modelled pre-reformer chemistry

Even though great care has been taken to make the pre-reformer model as precise as possible, the chemical processes that occur there are too complex to be captured exactly in the pre-reformer model. Hence this model will still be a gross simplification of reality.

for example, it skips over the fact that certain catalysts promote a certain reactions in one direction and demote the opposite reaction. This would alter the equilibrium.

Experimental testing would have to be carried out to study the influence of such deficiencies in the model on its accuracy.

7.2.7. Steam injection as mitigating tool for pre-reformer

The danger of the pre-reformer overheating should be looked into. One of the options that came to mind to increase the safety of the pre-reformer, was a system that could inject a large quantity of water vapor into the reactor. The idea is to make the reaction shift to the more endothermic side of the equilibrium, whilst at the same time lowering the temperature of the system, which also shifts the reactions in the pre-reformer to the endothermic side. This obviously has to be tested rigorously before being made practice.

A
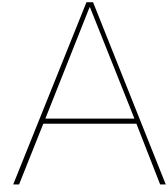
Testing methodology & Assumptions

A.1. Pre-reformer Testing methodology

The strategy for showing the reactors behaviour under changing parameters is visualized in the following manner:

1. The pre-reformer model is equipped with an imaginary heat exchanger that is capable of meeting the inflow of heat required to retain constant temperature.

2. The pre-reformer is fitted with an outlet valve which is perfectly equipped to keep the contents of the reactor under a constant pressure

3. Input parameters are are changed in time, so a plot of the reactors contents in time will show the behavioural trends of the reactor.

   (a) the ratio of either AOGRC- or steam- inflow to methanol inflow is changed every 200s

   (b) the operating temperature is changed every 1000s

   These periods enable the system to regain equilibrium.

4. The results for stable operation can be collected (Required heat flow, hydrogen production, temperature) for all valueas of μ_{steam} and $T_{pre-ref}$. Together these can be put in a surface plot.

5. Qualitative conclusions about the behaviour of the pre-reformer can be drawn from interpretation of the surface plots.

This process is illustrated in figures A.1, A.2, A.3 and A.4.

$$\frac{\dot{N}_{H_2O}}{\dot{N}_{CH_3OH}} = [0.5, 0.75, 1, 1.25, 1.5]$$

The temperature is changed every 1000 seconds, from 400K to 800K in incremental steps of 20 K.(see figure A.2)

Note that for this case the volume of the reformer reactor is chosen to be $2.00m^3$. The inflow of methanol is chosen to be 11 mol/s, as this reflects the fuel flow that would be required for a methanol fuelled SOFC system with a power demand of 4000kW at an efficiency of 0.5. It is assumed that the contents of the pre-reformer are well mixed at all times. Increasing the volume of the reactor vessel would result in a longer presence of a certain particle inside the pre-reformer, therefore giving it more time in the reactor and for the gas mixture to reach equilibrium. Hence, an increase in the reactor volume or a change in its configuration will result in a faster reaction time.
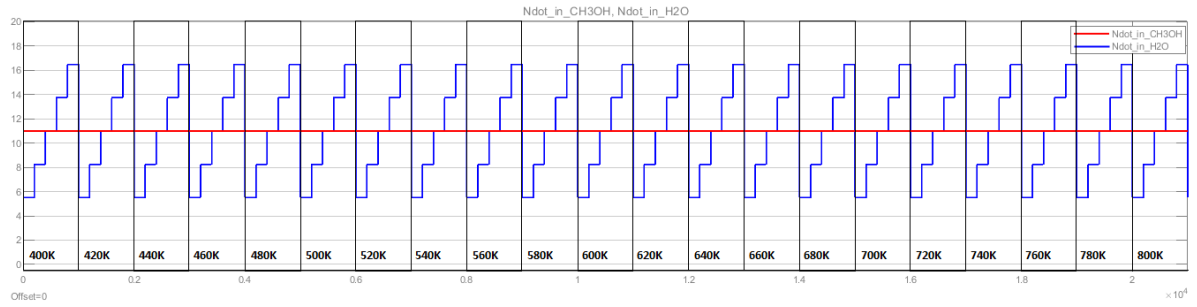
Figure A.1: Molar inflow of methanol and steam through time.The inflow of methanol remains constant at 11 mol/s. The ratio (steam/methanol) varies from 0.5 1.5. The ratio changes every 200 s.
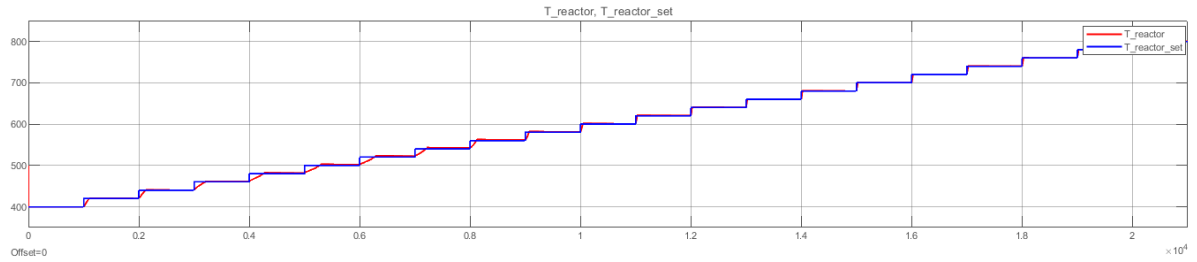
Figure A.2: Shows the set reactor temperature and the actual reactor temperature through time. The set temperature level increases every 1000s. The temperature is stabilized by an imaginary heat exchanger, in order to study the required external heat flows required to maintain constant temperature levels
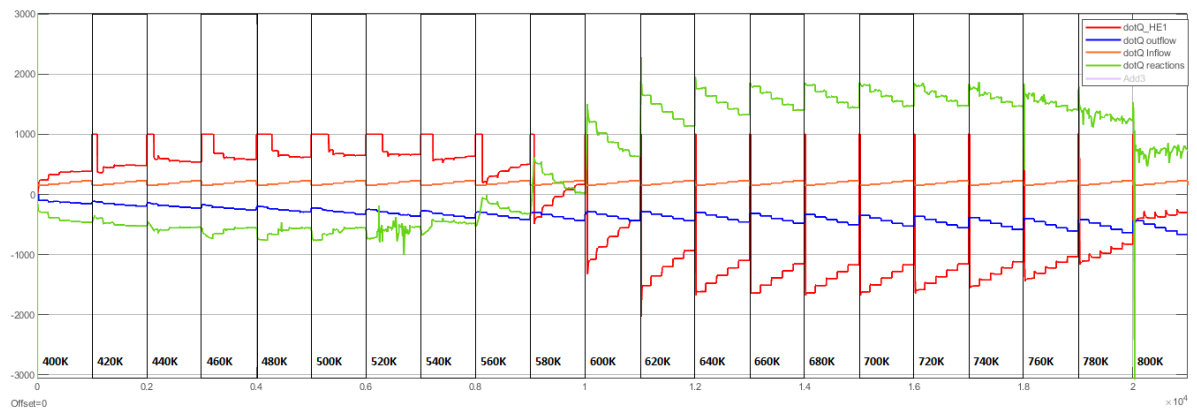

Figure A.3: Shows heat flows to or from the reformer system. The green line represents the heat flows associated the sum of enthalpy change of the reactions inside the reformer. The the yellow line represents an imaginary heat -source or -sink in the system that should maintain the set temperature level.
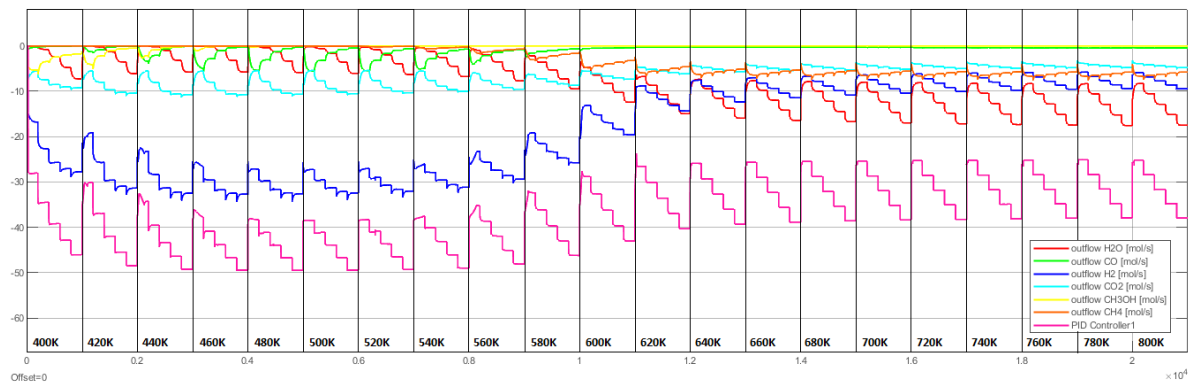
Figure A.4: Shows the molar outflows of the pre-reformer per species.
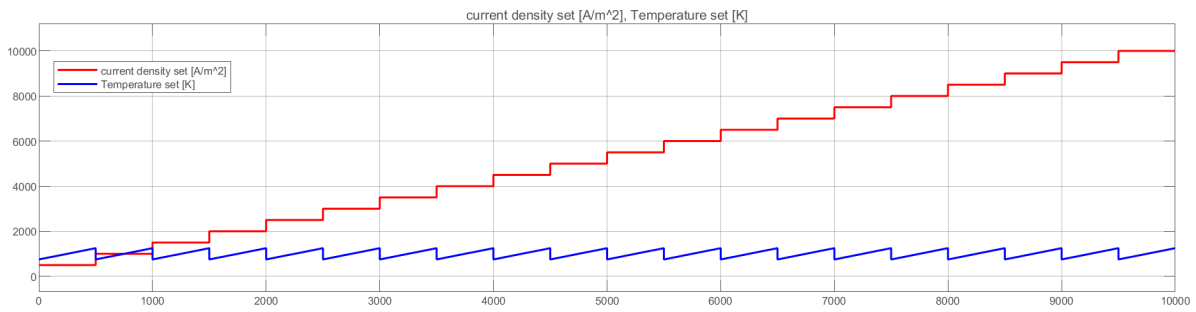
Figure A.5: Cell temperature and current density as they are varied to obtain an understanding of the behaviour of the SOFC at different temperatures and current densities
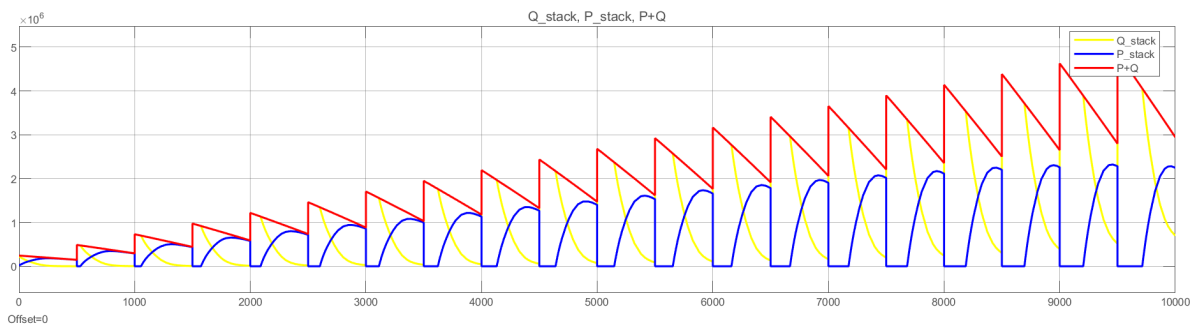
Figure A.6: Stack (12000 cells) electrical power output, heat output and combined output for the prescribed cell temperatures and current densities

A.2. SOFC testing methodology

A.2.1. stable behaviour

The strategy to map the behaviour of the cell is to artificially control the temperature of the cell in the model and vary the current density. The method is much the same as the method used in section A.1, but with varied current density in stead of steam inflow ratio.

A.2.2. Transient behaviour

To capture the transient behaviour of the SOFC in a singe figure, settle time was used. Settle time, for this thesis, is defined as the time it takes the system to produce 98% of the output at $t = \infty$ for the same inputs, after a perturbation in inputs. See figure A.9

Gathering of the settle times for all the possible step functions that could be undergone by the system,
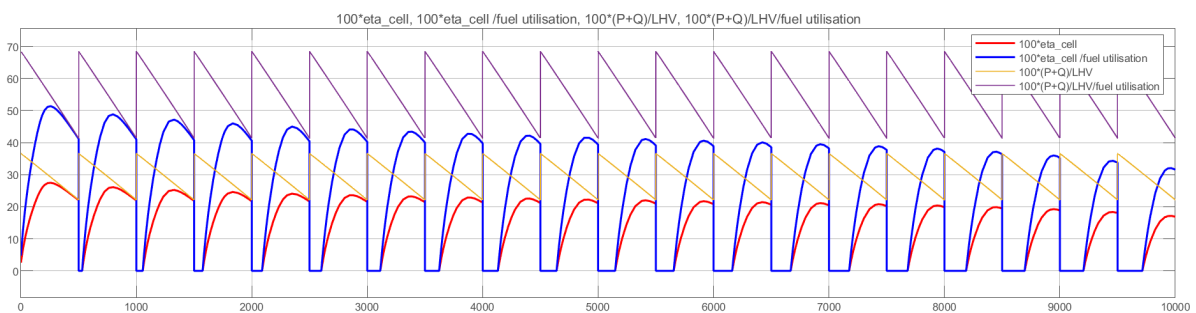
Figure A.7: Cell efficiency and cell efficiency when corrected for the fuel utilisation factor, for the prescribed cell temperatures and current densities in
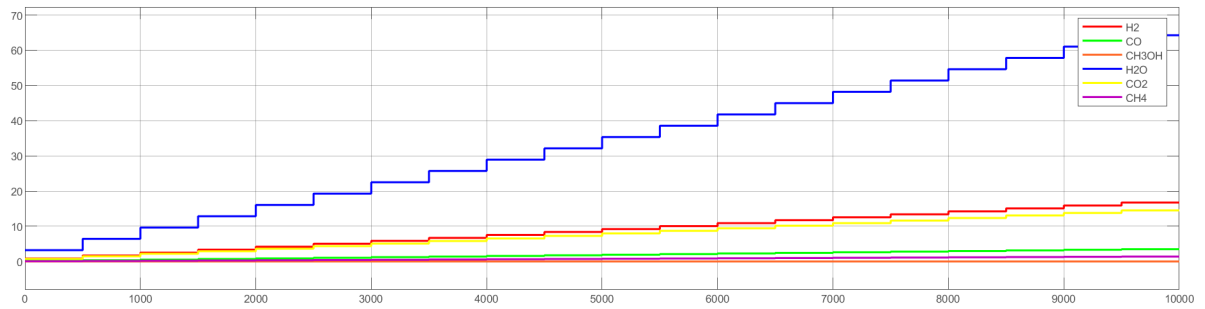
Figure A.8: The magnitude and composition of the anode gas outflow for the prescribed temperature and current density of the stack.
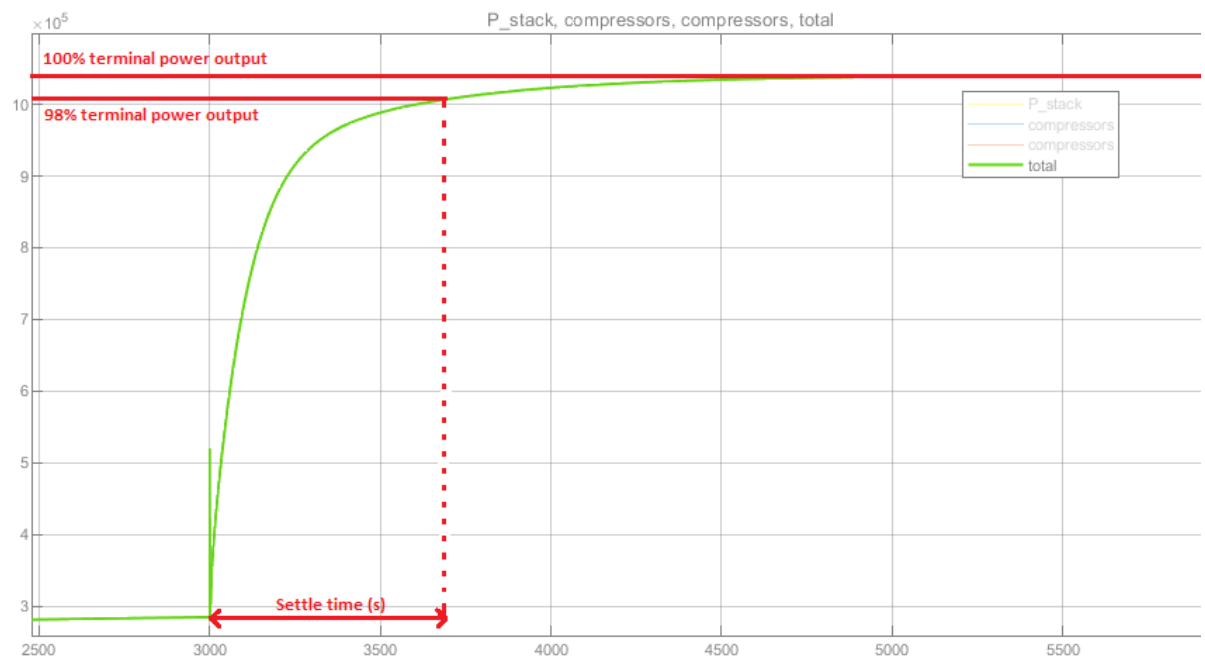
Figure A.9: Shows how, for this thesis, the settle time is defined.

happened much in the same way that data for the figures for stable operation were gathered: an list of step functions were prescribed to the system model, and the settling times were manually collected to create a single figure (see figures 6.8, 6.11 and 6.19)

A.3. Testing assumptions

A.3.1. constant pressure in channels

For the methanol fuelled SOFC system, operating at 9000 A/m^2 with efficiency of 23% this assumption seems to be a sound one: 12000 cells with a combined fuel channel cross section of $A_{af} = 12000 \cdot 0.001m \cdot 0.1m = 1.2m^2$ need to pass $41.1mol/s$ at the outlet of the anode channel.

$$\dot{V} = \frac{R \cdot T \cdot \sum \dot{N}}{p} = 0.23m^3/s$$

The dynamic pressure is

$$\Delta p_{dyn} = \frac{1}{2}\rho \cdot u^2 << 2 \cdot 10^6 [Pa]$$

A.3.2. Use of the ideal gas law

The use of the ideal gas law in the the SOFC- and pre-reformer model is convenient. It simplifies the the calculations in the model significantly. The validity of the assumption that the ideal gas law holds, under the circumstances defined in SOFC and the pre-reformer has to be tested.

	T_c [K]	P_c [MPa]	T_r [−]	P_r [−]	
CH_3OH	512.6	8.104	0.975	4.052	0.52
H_2	33.2	1.300	15.06	0.650	1.13 [28]
H_2O	647.1	22.06	0.772	11.03	0.91
CO	132.9	3.498	3.762	1.746	1.01
CO_2	304.2	7.380	1.643	3.690	1.02
CH_4	190.8	4.640	2.621	2.320	1.00
O_2	154.6	5.050	3.234	2.525	1.03
N_2	126.2	3.39	3.962	1.695	1.02

Table A.1: Reduced temperatures and pressures for gas species present in the reformer and the SOFC for T=500 K and P= 20 Bar

Following the trend that higher reduced temperatures and lower reduced pressures lead to a compressibility factor that tends more towards one, the lower temperature in the pre-reformer was chosen to illustrate the severity of the influence nonlinear behaviour of gasses under pressure.

It can be seen from the values obtained from table A.1 that for CO, CO_2, CH_4, O_2, and N_2, the Z-factor remains well in between 0.95 and 1.05 ($Z_{steam} = 0.92$ in these conditions). This would indicate that deviation of the model from reality will be limited. However, the Z-values of hydrogen($Z_{hydrogen} = 1.13$, from [28]) and methanol($Z_{methanol} = 0.52$) are far from close to 1. Questions were raised if the models for the pre-reformer, the SOFC and the gas turbine can be trusted to be accurate. After all, all three of these models seem to be, to a certain extent, dependent on the pressure.

Nonetheless, it is expected that the influence of the compressibity of these species will be limited. This outcome is expected for the following reasons:

1. in the pre-reformer

    • in the current configuration, the reactions happen so fast that the consistency of the gasses is determined by the equilibrium constants. These are a function of temperature, and not of pressure.

- Although partial pressures are a convenient way to describe the kinetics of reactions, the actual reaction rates are governed by the probability of reactants interacting in the right way. This is a function of *concentration* and temperature.

2. in the SOFC

- Methanol will have all reacted at the temperature in the anode flow
- Nernst voltage will be affected when pressure changes, but only very marginally. In the very severe case (90% H_2, 10% H_2O at the anode, 20% O_2 at the cathode) the difference between the Nernst voltage for ideal gas-pressure and actual gas-pressure will be no more than $5 \cdot 10^{-3}V$

3. In the PHE

- The air compressor will compress air. Air has a compressibility factor of 1.003 in the temperature and pressure range.
- Hydrogen and methanol will be combusted at such a rate that no significant amount of these substances will enter the turbine

Concluding, the overall impact of the accuracy of the model is suspected to not be severe.

A.4. Assumption constant convection coefficient

In the model of the PHE, the assumption is made that the convection coefficient α is constant. α proportional to the convection between the gas flows in and the separator walls of the PHE.

$$\dot{q} = \alpha \cdot (T_h - T_c)$$

In reality however, the value of α varies with temperature, flow speed, turbulence, gas composition, material properties of the separator plate, plate geometry and numerous other factors. Finding a close approximation for the value of α for every state of the system is not within the scope of this investigation. However, an estimation can be made with regards to the magnitude of the influence of the fault in α value.

[6] Lists the convection coefficient of moving gasses on plates to be between 20 and 100 $W/(m^2 \cdot K)$. In figure A.10 the difference in system output and system efficiency is shown between calculation for $\alpha = 25W/(m^2 \cdot K)$ (as in the reported calculations) and calculation for $\alpha = 100W/(m^2 \cdot K)$

The difference is marginal. Therefore, it is gathered that the assumption that α remains constant at $25W/(m^2 \cdot K)$, does not have a severe detrimental effect on the accuracy of the model in stable operation.

Figure A.11 shows the transient behaviour of the PHE, calculated for $\alpha = 100W/(m^2 \cdot K)$. When compared to figure 6.11, it can be seen that the response time of this subsystem is sensitive to change in convection coefficient. It should be noted that the value chosen for α in the simulations, is conservative ($25W/(m^2 \cdot K)$).
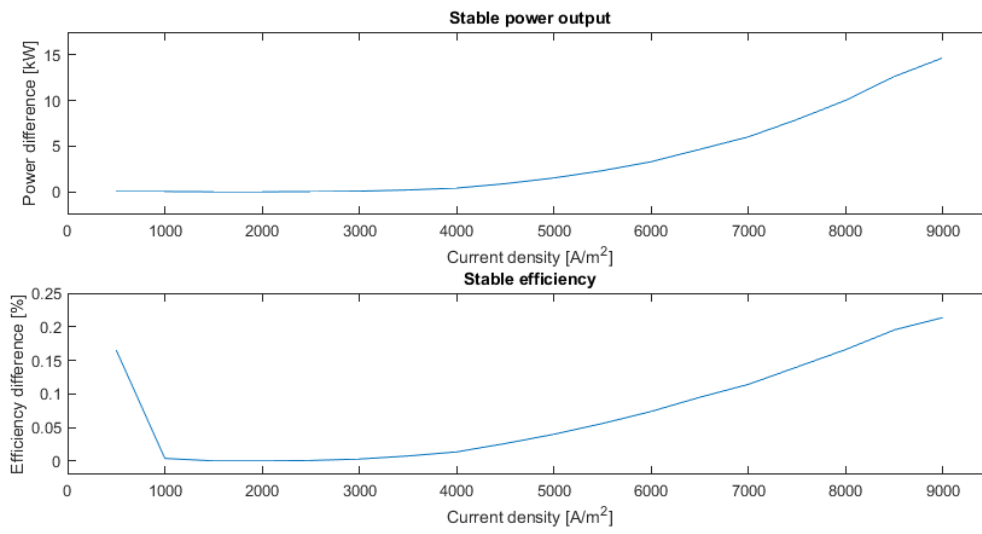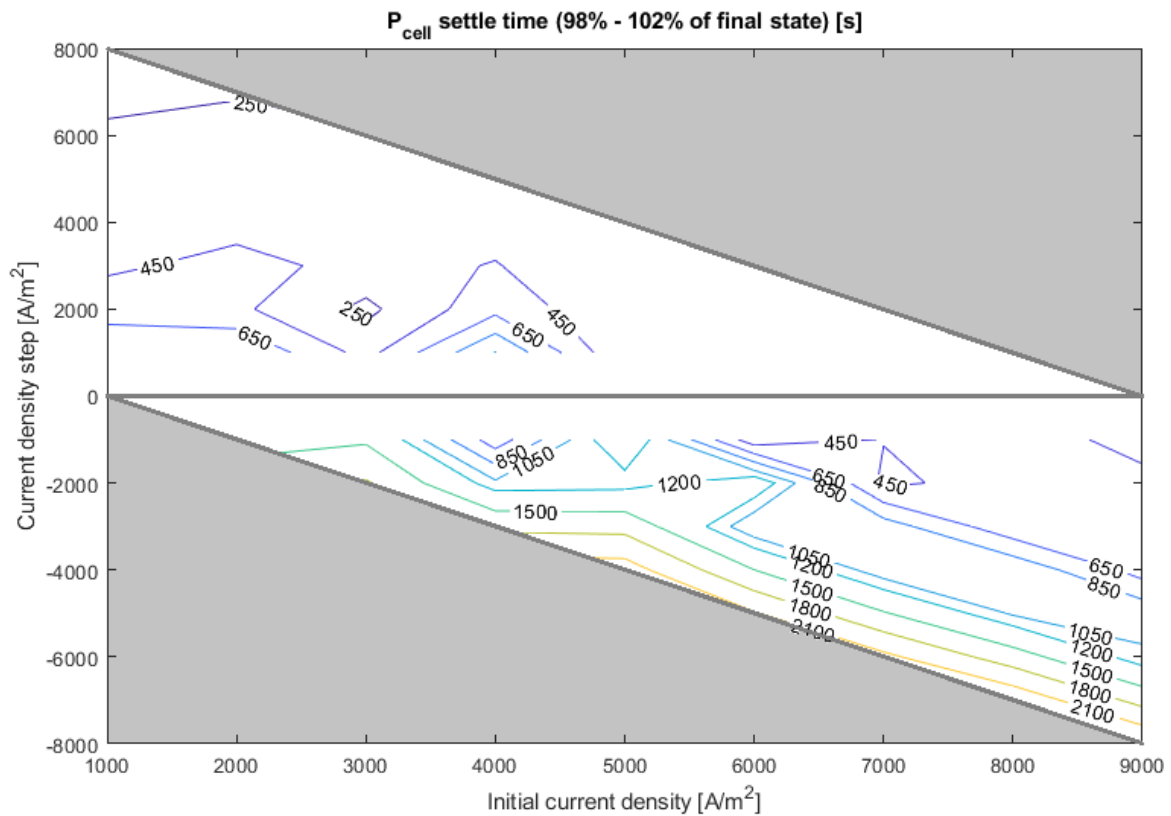
Figure A.10: Caption

Figure A.11: Shows the settle time of the PHE, for a convection coefficient $\alpha = 100W/(m^2 \cdot K)$. The rest of the parameters are equal to the parameters used to generate figure 6.11(which was generated for $\alpha = 25W/(m^2 \cdot K)$).

Fuel Cell equations

B.1. Governing equations

In this section an overview of several important equations that describe the behaviour of fuel cells will be given. These will be valid for most fuel cells and in particular to SOFCs. Listing these these equations and implementing them in the Simulink®will be instrumental in producing a working model. A distinction will be made between the factors that influence the the cell voltage trough reversible processes (see sub section **Reversible cell**) and factors that influence the cell trough irreversible processes, divided into activation losses (see sub section **Activation losses**), Ohmic losses (see sub section **Ohmic losses**) and mass transport- and concentration losses (see sub section **Mass transport & concentration losses**).

B.1.1. Reversible cell

For fuel cells, most important are the enthalpy H and Gibbs Free energy G within the system. It denotes the amount of energy that system that is available to do external work [7].The rest of the enthalpy is released as heat (entropy S) to the system. The relation between enthalpy and Gibbs free energy is given in equation B.1.

$$G = H - T * S \tag{B.1}$$

We can make the equation B.1 into a molar specific expression and obtain equation B.2

$$\Delta \bar{g}_f = \Delta \bar{h}_f - T \Delta \bar{s} \tag{B.2}$$

The subscript f in equation B.2 mean that het values for $\Delta \bar{g}$ and $\Delta \bar{h}$ are of formation meaning that they are measured relative to the point of STP $(25°C, 100KPa)$. These energy levels are therefore not dependent on the temperature and the pressure at which the substances react. Thus, it can be seen from equations B.1 and B.2 that at higher temperatures, the max obtainable work from a reaction will be lower at higher temperatures. It is obvious that the maximal obtainable efficiency of the system will be the amount of energy in the system available for external work divided by the total amount of energy in the system (enthalpy).

$$\eta_{max} = \frac{\Delta \bar{g}_f}{\Delta \bar{h}_f} \tag{B.3}$$

$$P = E * I \quad \rightarrow \quad E = \frac{P}{I} \tag{B.4}$$
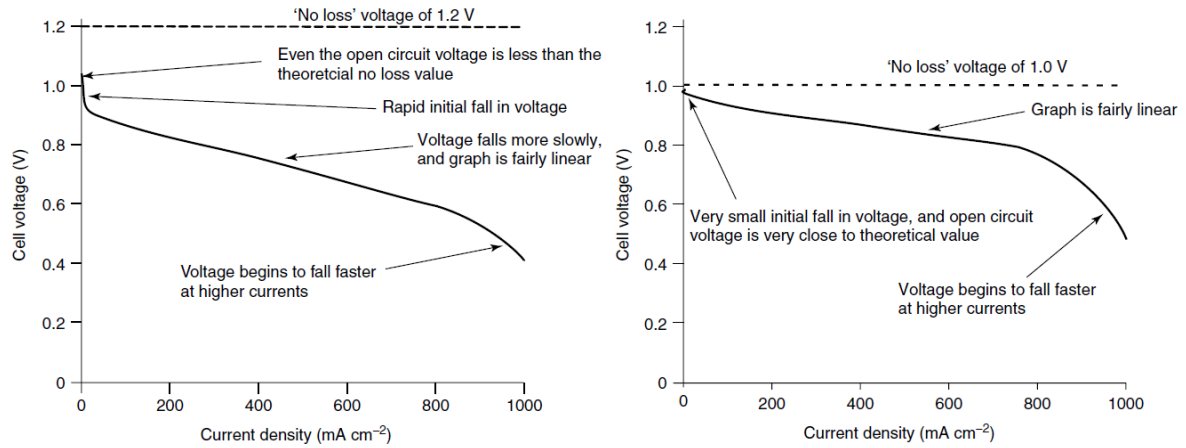
$$E_{max} = \frac{\Delta \bar{g}_f}{zF} \tag{B.5}$$

Figure B.1: a qualitative indication of what irreversibilities (voltage drops) occur where, as a function of the cell's current density.These images were taken from Fuel Cell Systems Explained by A. Dicks & J. Larminie. [7] The left image relates to low temperature fuel cells like PEMFCs. The right image relates to high temperature fuel cells like SOFCs.

$$E_{OCV} = E_0 + \frac{RT}{zF} \ln Q \tag{B.6}$$

Where Q represents the reaction quotient:

	reactant 1	reactant 2	product 1
name	J	K	M
Nr of moles	j	k	m
"activity"	a_j	a_k	a_m

$$Q = \frac{a_J^j * a_K^k}{a_M^m} \tag{B.7}$$

The term "activity" will, for the high temperatures at which the SOFC operates be the partial pressure of the gas species. Note that this particular example shows 2 reactant species and 1 product species, as is the case for the reaction $H_2 + \frac{1}{2} O_2 \rightarrow H_2 O$. This is by no means the case for all possible reactions. For example, in the case of the combustion of methanol the number reactant species are 2, $2\,CH_3OH + 3\,O_2$, and the number of product species are 2, $2\,CO_2 + 4\,H_2O$.

B.1.2. Irreversible losses

The irreversibilities show as a drop in the reversible cell voltage and have the form as shown in figures B.1 . The initial fast drop in reversible cell voltage is a product the activation losses of which the constituents are twofold. The shall be addressed in the subsection **"Activation losses"** of this section. The nearly linear drop of cell voltage in the mid-range of the current density is caused by the Ohmic losses that occur inside the fuel cell which will be briefly addressed in the subsection **"Ohmic losses"** of this section. The steepening drop in cell voltage is accounted to irreversibilies due to mass transport and concentration losses. This will be explained in the subsection **"Mass transport & concentration losses"** of this section.

Activation losses

Activation losses are the losses that occur due to the slowness of the electro-chemical reaction. The relation between the irreversible voltage drop and the current density in the fuel cell was found by Julius Tafel to be

$$\Delta V_{act} = a \cdot log_{10}(\frac{i}{i_0}) \quad \Rightarrow \quad \Delta V_{act} = A \cdot ln(\frac{i}{i_0}) \tag{B.8}$$
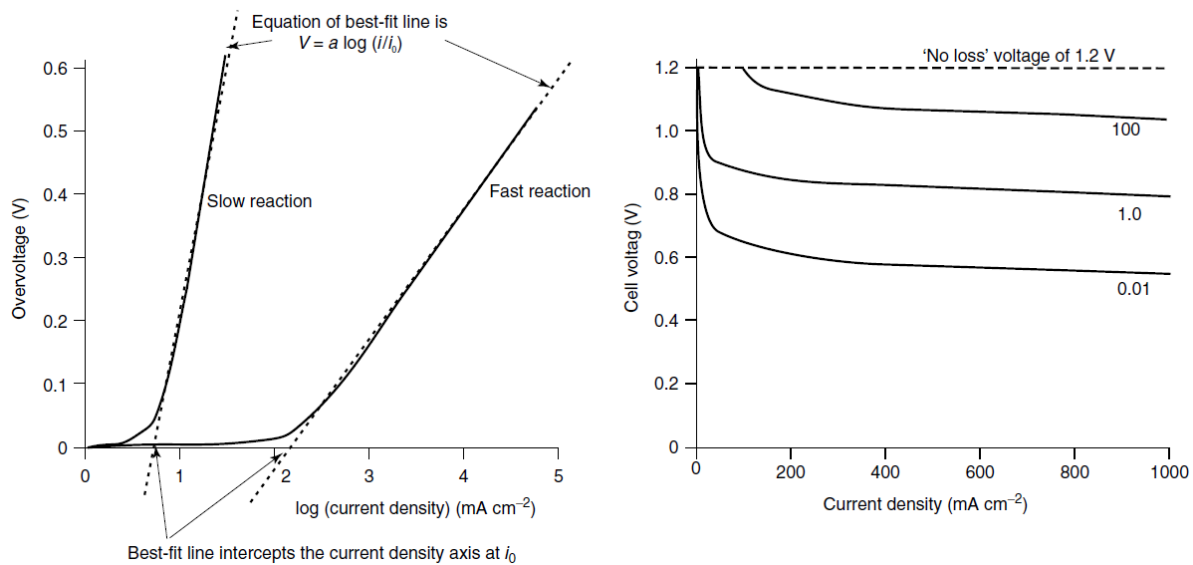
Figure B.2: This graph shows the relation between the irreversible activation losses and the the current densities for a reaction that is naturally slow (left graph in left figure) and a reaction that is naturally faster (right graph in left figure). . the image on the right show the influence of increasing i_0, for example by interesting the operating temperature.This image was taken from [7]

This relation was discovered experimentally and was only later rewritten as the equation on the right side. This is done because the natural logarithm is preferred, as the Nernst equation is written in the same syntax, and it was discovered that the coefficient A could be written as

$$A = \frac{RT}{\beta zF}$$

thereby giving physical meaning to the term.

β is called the *charge transfer coefficient*$(0 \leq \beta \leq 1)$ and is a property of the electrode. The coefficient A is therefore calculated for both electrodes separately. The value of β is commonly around0.5 for the anode and 0.1 to 0.5 for the cathode.

i_0 is called the *exchange current density*. It can be seen as the the current density at which the irreversibilities move away from zero. The physical meaning of I_0 is more related to the name. Even when there is no current through the electrical circuit, The reaction rate of the reactions at the electrodes is not zero. There is an equilibrium, which merely means that the reactions occurring at the electrode have the same rate but opposite reactions, and do not cause a net change in the species present. The reaction rates at which the reactions in both directions take place are tied to the excange current density by $i_0 = r \cdot z \cdot F = r_f \cdot z \cdot F = r_r \cdot z \cdot F$

The relation between current density i and the activation losses is visualized in figure B.2. It shows what are called Tafel plots, for fast and slow reactions.

It would seem that an increase in the temperature T would increase irreversible losses, but this is rarely so. Increased temperature increases i_0 dramatically, of which the influence far outweighs the the influence of the temperature on the coefficient A. The result of raising the temperature is thus that the activation losses tend to decrease.

Rearranging the Tafel equation (eq B.8) produces a more commonly used equation called the Butler-Vollmer equation, which is given in equation B.9. It can be seen that in this equation, the exchange rate current, which can vary several orders, is of paramount importance to the actual current density. Increasing i_0 can be done by

- increasing the operating temperature (this is why there are less activation losses in high temperature fuel cells)

- finding better catalysts (mainly at the cathode)

- increasing surface area by making finer granulated electrodes

- increasing reactant concentration and increasing pressure

$$i = i_0 EXP\left(\frac{z \cdot \beta \cdot F \cdot \Delta V_{act}}{R \cdot T}\right) \tag{B.9}$$

$$\Delta V_{act} = A \, ln\left(\frac{i}{b}\right) \tag{B.10}$$

where

$$A = A_a + A_c \quad \text{and} \quad b = i_{0,a}^{(A_a/A)} + i_{0,c}^{(A_c/A)}$$

Fuel crossover & Internal currents

For a fuel cell to work properly is is important that the only electrons travel through the electrical circuit (this demand is obviously always met), and that there is no crossover of electrons through the electrolyte. Similar to this, it is important that the fuel does not crossover trough the electrolyte. All these occurrences would direct energy away from the power circuit as intended.

Total elimination of fuel crossover and, to a lesser extend, electron crossover, however, is impossible to obtain. The negative effect on the the efficiency of the machine however, is small. The crossover does not have a a magnitude that significantly impedes high efficiencies.

A problem *does* occur at very low current densities. The crossover through the electrolyte, be it electrons or non oxidised fuels can be seen as an internal current, and the fuel cell behaves in the same manner as it would with any other internal current. The steep initial fall in voltage due to activation losses will will be incurred by the internal current. Fortunately, this effect is only profound at very low current densities. Moreover, since i_0 is so much higher for high temperature fuel cells, the influence of the crossover current is far less in these machines.

The way to describe the crossover in a mathematical sense is by adding the equivalent crossover current to the current density in the equation for the activation voltage drop

$$\Delta V_{act,cross} = A \cdot ln\left(\frac{i + i_{cross}}{i_0}\right) \quad \text{where} \quad A = \frac{RT}{\beta zF} \tag{B.11}$$

Ohmic losses

Ohmic losses are incurred by the electric resistance of all the components; connector plates, electrodes and electrolyte. Of these, the resistance of the electrolyte will have the most influence. Internal current by means of transportation of ions will always have a higher resistance than free movement of electrons through a metallic matrix. Therefore the brunt of the internal electrical resistance will occur in the electrolyte.

The losses that are connected to Ohmic resistance are described by equation B.12 (area specific on the right):

$$V = R \cdot I \quad \Rightarrow \quad \Delta V_{Ohm} = r \cdot i \quad \text{where} \quad r = r_{\text{electrolyte}} + r_{\text{electrode}} + r_{\text{connector}} \tag{B.12}$$

the power that is converted in the process is (equationB.13)

$$P = I \cdot V = I^2 \cdot R \tag{B.13}$$

Mass transport & concentration losses

When further increasing the density, the cell voltage begins to drop faster than it did in the region of ohmic voltage drop. This is where the effect of lower concentrations of reactants at the electrodes starts to take hold. The flow to the electrodes can no longer provide enough reactants to the electrodes

to create a favourable composition of species to enable the desired reaction speed. These losses in voltage are called the transportation losses. It is important to note that this phenomenon comes forth from the diffusion limit of the reactants and cannot be countered by increasing the pressure or providing more reactants at the anode.

In order to describe the behaviour of the cell in the current density region where the fall in voltage is dominated by the transport losses, the relation between change in pressure and change in voltage is used (equation B.14, to find an expression for the drop in voltage due to the limits associated with mass transport.

$$\Delta V_{p_1, p_2} = \frac{R \cdot T}{z \cdot F} ln \left(\frac{p_2}{p_1} \right) \tag{B.14}$$

The term i_l is introduced to be the current density in the cell at the point that the geometry of the electrodes no longer allows for a higher mass flow. In this case the concentration of a certain reactant at the "far" end of the electrode is zero. The pressure in the new situation, p_2, can be defined in terms of p_1, i_l and i.

$$p_2 = p_1 \left(1 - \frac{i}{i_l} \right)$$

Then the voltage drop due to the limits of mass transportation becomes.

$$\Delta V_{\text{trans}} = \frac{R \cdot T}{z \cdot F} ln \left(1 - \frac{i}{i_l} \right) \quad \Rightarrow \quad \Delta V_{\text{trans}} = B \cdot ln \left(1 - \frac{i}{i_l} \right) \tag{B.15}$$

Note that here, z can take a different value because the mass transportation can be limited at both electrodes. therefore the the coefficient A has been replaced by the coefficient B.

Another way of modelling the transportation losses is by fitting an empirical formula to the the measured decline in voltage. One such empirical formula, which is widely used these days is given in equation B.16. A very good fit can be gained, when the coefficients m and n are chosen carefully. Typically the values for m and n are chosen to be: $m \approx 3 \cdot 10^{-5} [V]$ and $n \approx 8 \cdot 10^{-3} [(mA)^{-1}]$. This description of the transportation losses will be used in further writing, as it has been proven to be most accurate[7].

$$\Delta V_{\text{trans}} = m \cdot ln \left(n \cdot i \right) \tag{B.16}$$

Compiling irreversibilities

Adding all the irreversibilities together will form the voltage characteristic as show in figure B.1 for low temperature and high temperature fuel cells respectively. Because the equations for the voltage drops due to their respective causes were all expressed in the same terms, the cell voltage as a function of the current density can now be expressed as in equation B.17

$$\begin{aligned} E &= E_{OCV} - (\Delta V_{\text{act}} + \Delta V_{\text{cross}}) - \Delta V_{\text{ohm}} - \Delta V_{\text{trans}} \\ &= E_0 + \frac{RT}{z \cdot F} - A \cdot ln \left(\frac{i + i_{\text{cross}}}{i_0} \right) - r \cdot i - m \cdot ln \left(n \cdot i \right) \end{aligned} \tag{B.17}$$

In equation B.17 the main differences between low- and high- temperature cells can be identified as

- For low temperature Fuel Cell (FC)s, the Open Circuit Voltage (OCV) is higher.

- For low temperature FCs, the impact of crossover currents is more severe, because i_0 is so much lower.

- For low temperature FCs, the impact of activation losses is more severe, because i_0 is so much lower.

B.1.3. Anode poisoning

The electrodes of a fuel cell consist out of fine, porous materials, in order to create as much surface area of the TPB as possible. The finer the structure of the electrode, the larger the TPB area. One of the effects of such refined structures is that they easily contaminate. This contamination can originate from multiple sources and can take different forms. Contamination of electrodes is undesirable as it decreases the surface area of the TPB ant thus of the maximal current density. Most contamination occurs at the anode because that is where the fuels are presented, and the fuel is often where the undesirable compounds reside.

B.1.4. CO oxidation

In SOFC's the phenomenon of carbon poisoning is less of a problem. The high operating temperatures of these machines enable omittance of the use of a catalyst. CO is not considered poisonous to the anodes of SOFC's, contrarily, it is considered a fuel by [7](page 239). This is due to the fact that O^{2-} is presented at the anode. This means that the reaction:

$$CO + O^{2-} \leftrightharpoons CO_2 + 2e^- \tag{B.18}$$

Though in reality the speed of the WGS ($CO + H_2O \leftrightharpoons CO_2 + H_2$ mildly exothermic) at these temperatures prevents nearly all CO from ever reaching the surface of the anode (from [35]). [16] even suggests that carbon formed on the electrode of a SOFC can be oxidised when pure argon is presented at the anode and pure oxygen is presented at the cathode. This process would remove the Carbon from the electrode and deliver power in doing so.

B.1.5. Sulphur

Sulphur poisoning is a very real problem for all fuel cells that are exposed to sulphur. This exposure can happen in the form of Hydrogen sulfide (H_2S) or Carbonyl Sulfide (COS) with which the fuel is contaminated.

C
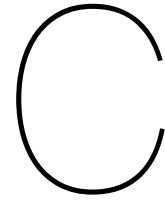
Appendix: Simulink visualisation

This appendix shows how calculations were made in Simulink. Print screens of mathematical operations are shown with a brief explanation
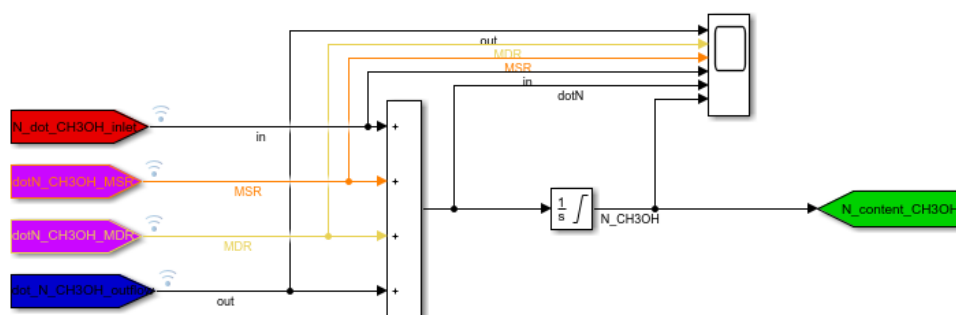
Figure C.1: Implementation in Simulink of the calculations the quantity of moles present in the pre-reformer. In this case the calculation of the quantity of moles of methanol is calculated. The reactions WGS, MDMO and MCMO do not have influence on the presence of methanol and are therefore omitted in this calculation.
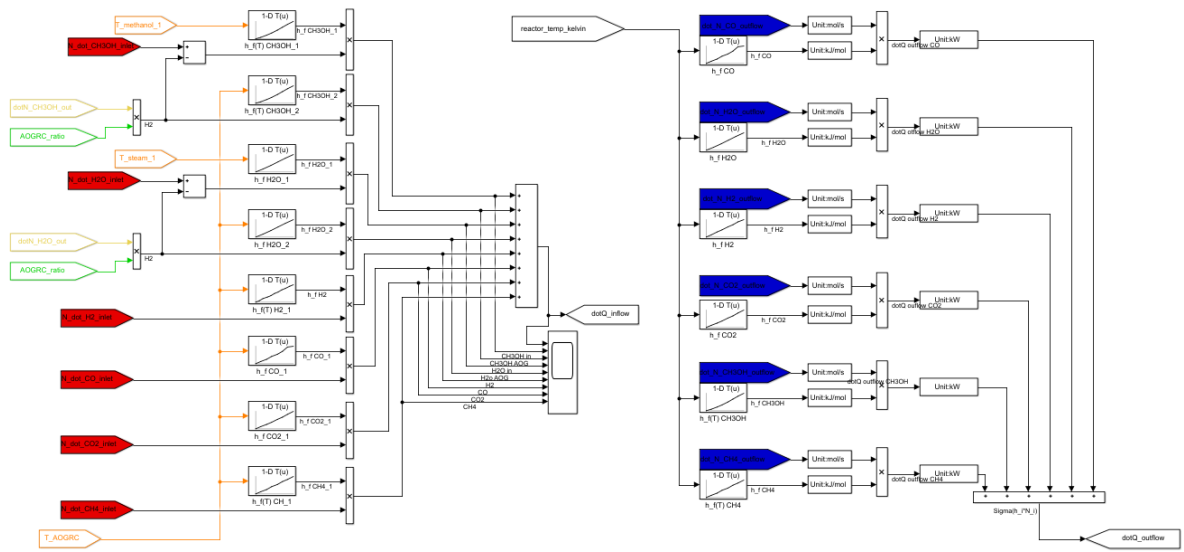
Figure C.2: Implementation in Simulink of the calculations of the heat fluxes into and out of the pre-reformer due to the inflow and outflow of gasses.
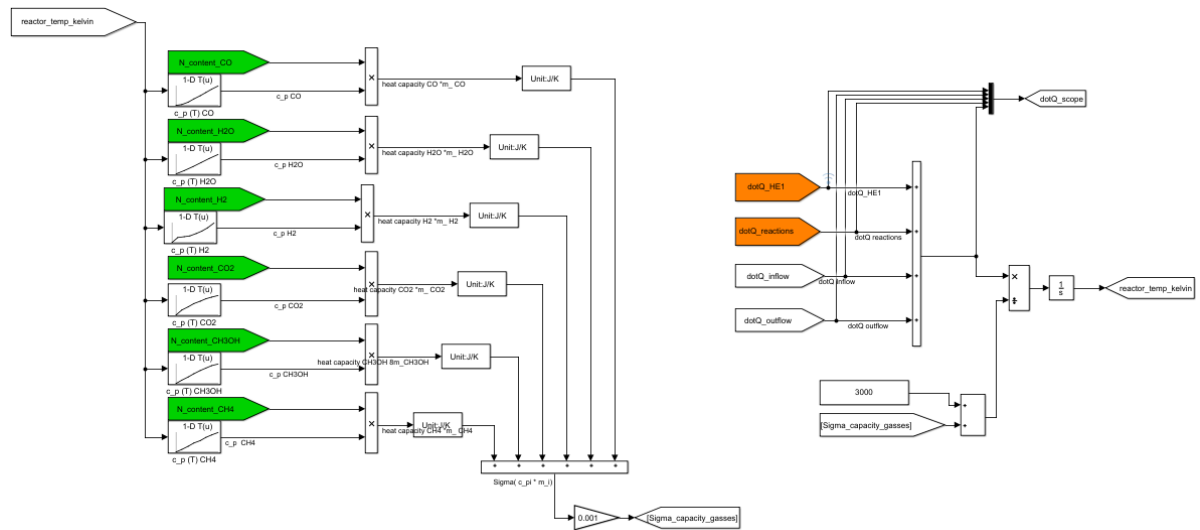
Figure C.3: Implementation in Simulink of the calculation of the heat capacity and temperature of the pre-reformer.
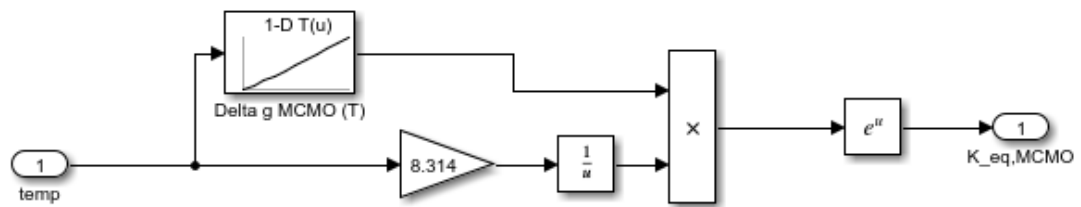
Figure C.4: Implementation of the van 't Hoff equation to find the equilibrium constant of MCMO as a function of the temperature.
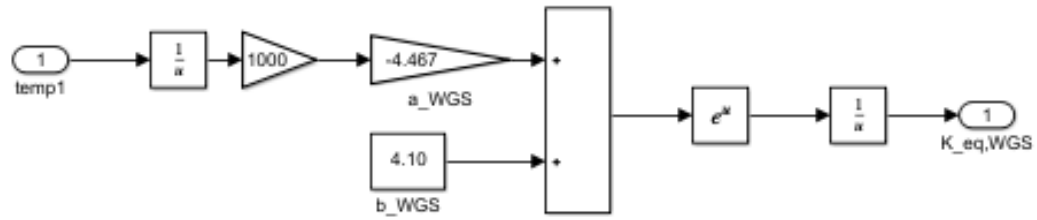
Figure C.5: Implementation of the relation between temperature and K_{eq} in Simulink for the Water Gas Shift reaction (WGS). The same circuit is used to obtain the equilibrium constants for Methanol Decomposition Reaction (MDR) and Methanol Steam reforming reaction MSR. Parameters for thes reactions can be found in table 4.5 in section 4.2
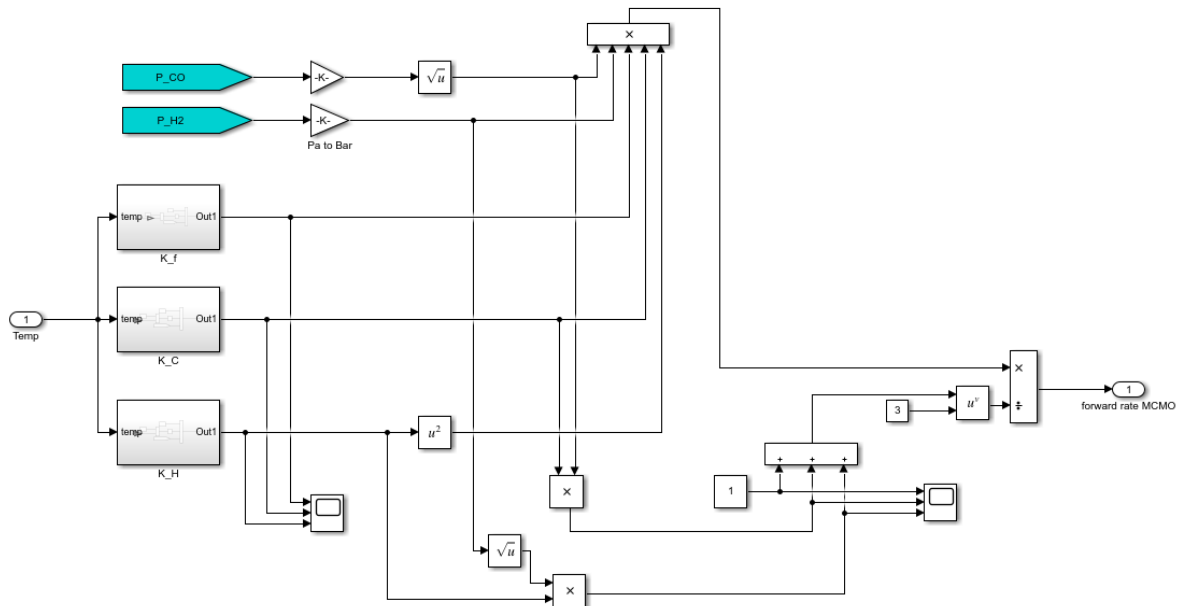
Figure C.6: Implementation of the calculation of the forward rate of the MCMO reaction.
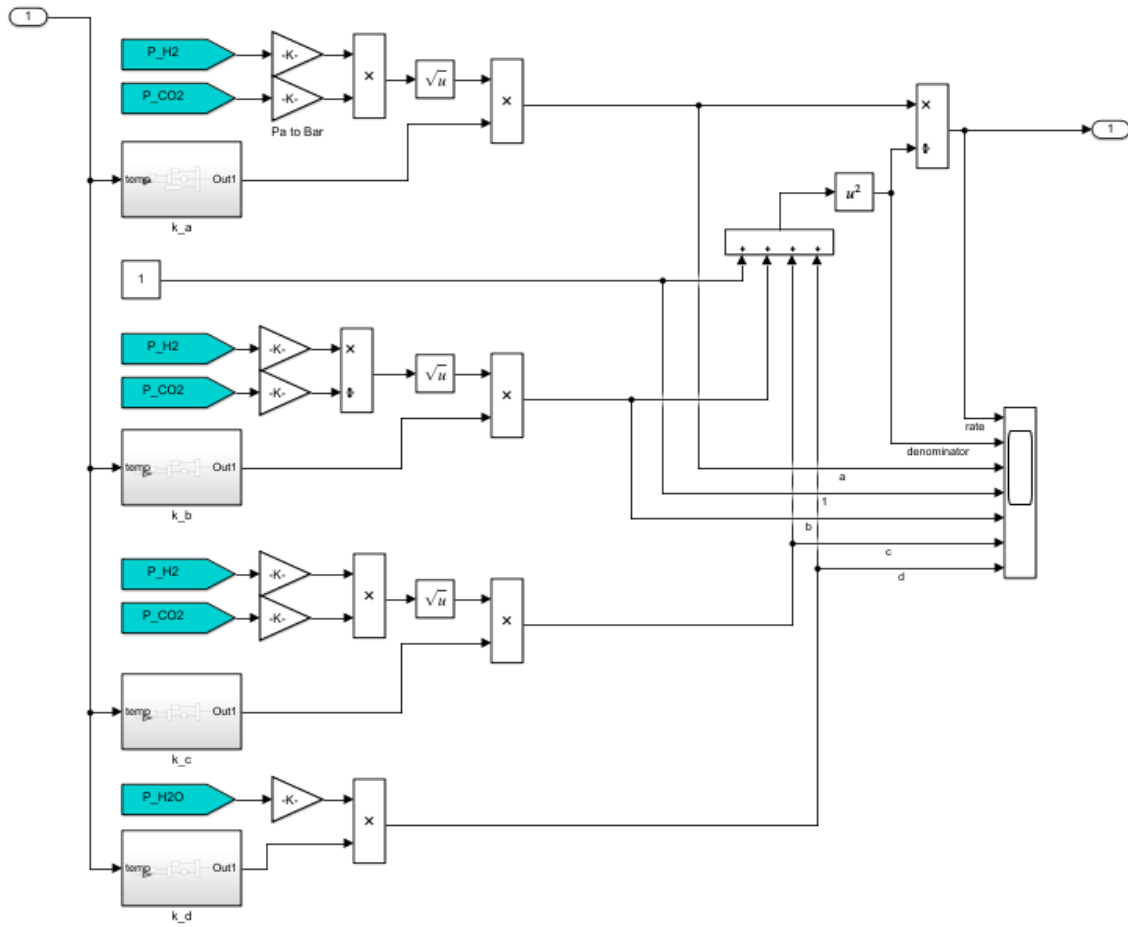
Figure C.7: Implementation of the calculation of the forward rate of Methanation reaction of Carbon Dioxide in Simulink
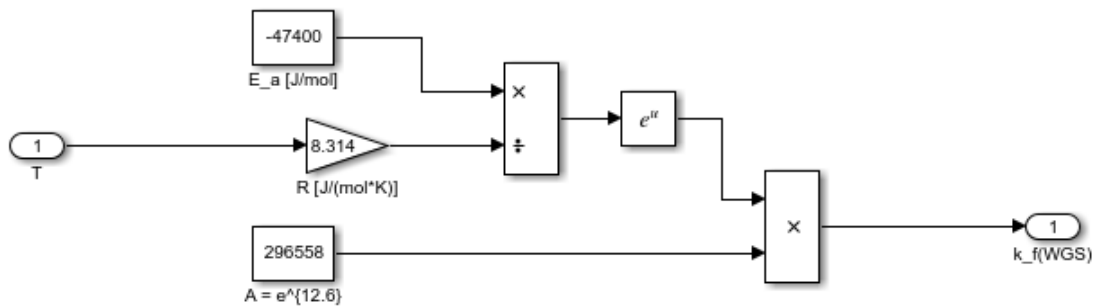
Figure C.8: Implementation of the forward rate of the Water Gas Shift reaction
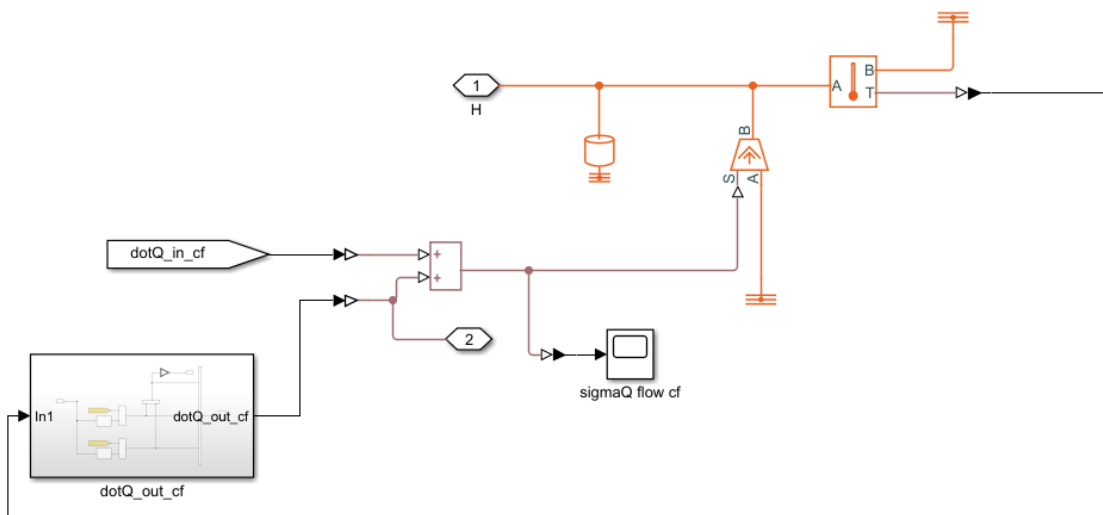
Figure C.9: The heat and temperature of a single component of a single cell of the SOFC. In this case, the "component" is the cathode flow. It features a thermal mass, heatflow in and heatflow out as a function of the cell temperature.
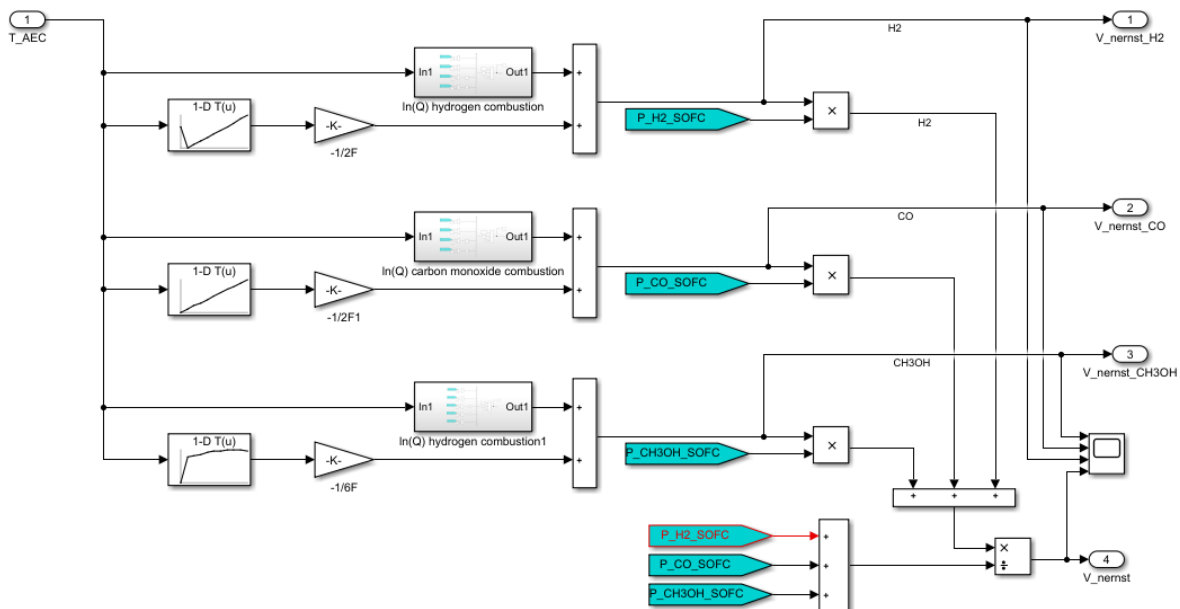
Figure C.10: Simulink implementation of the calculation of the Nernst voltage of the SOFC
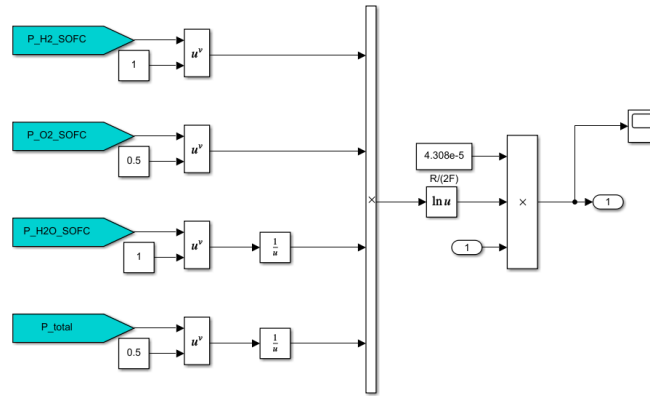
Figure C.11: Simulink implementation of the calculation of the reaction quotient Q, for the oxidation of Hydrogen
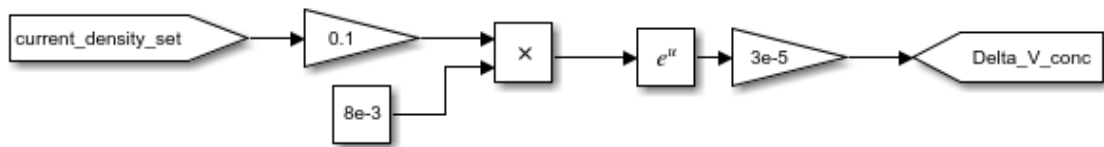
Figure C.12: Voltage drop of a single cell due to concentration losses, implemented in the Simulink model
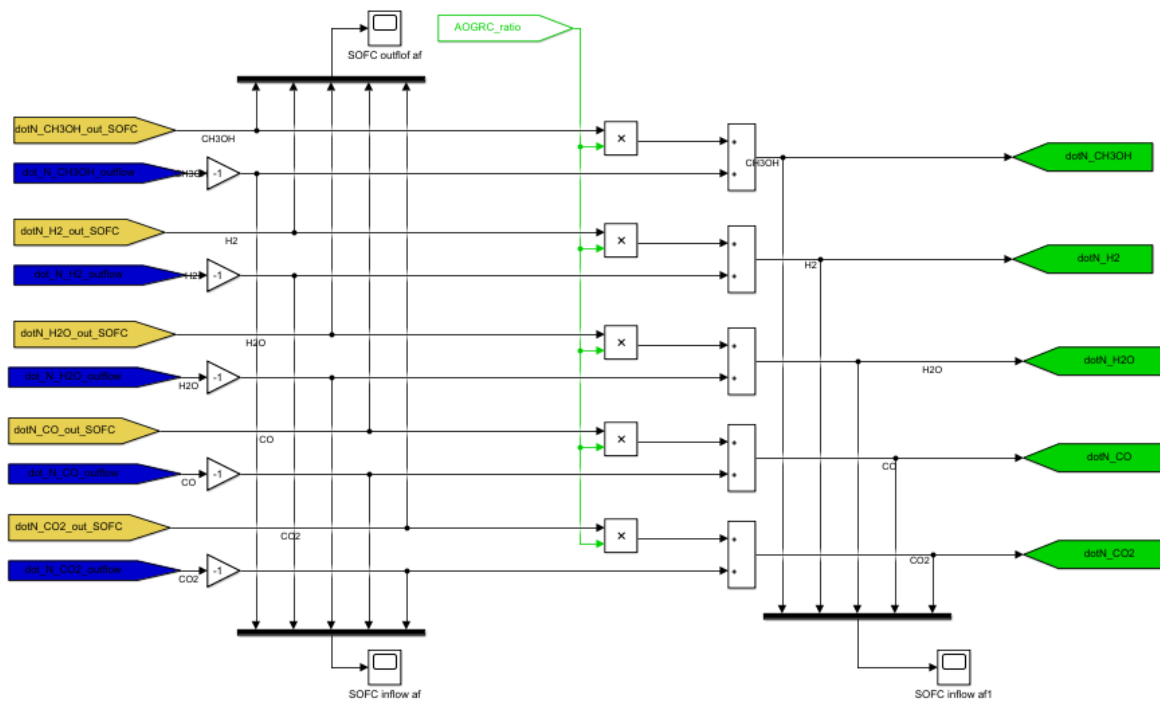
Figure C.13: The total molar inflow of gasses is calculated by adding the the AOG that is recycled (AOGRC = AOGRC_ratio $\cdot \dot{N}_{o}ut$) the molar flow from the reformer, for all species in the anode flow. The factor -1 is used to because outflow is from the pre-reformer model and is defined to be negative in that model.
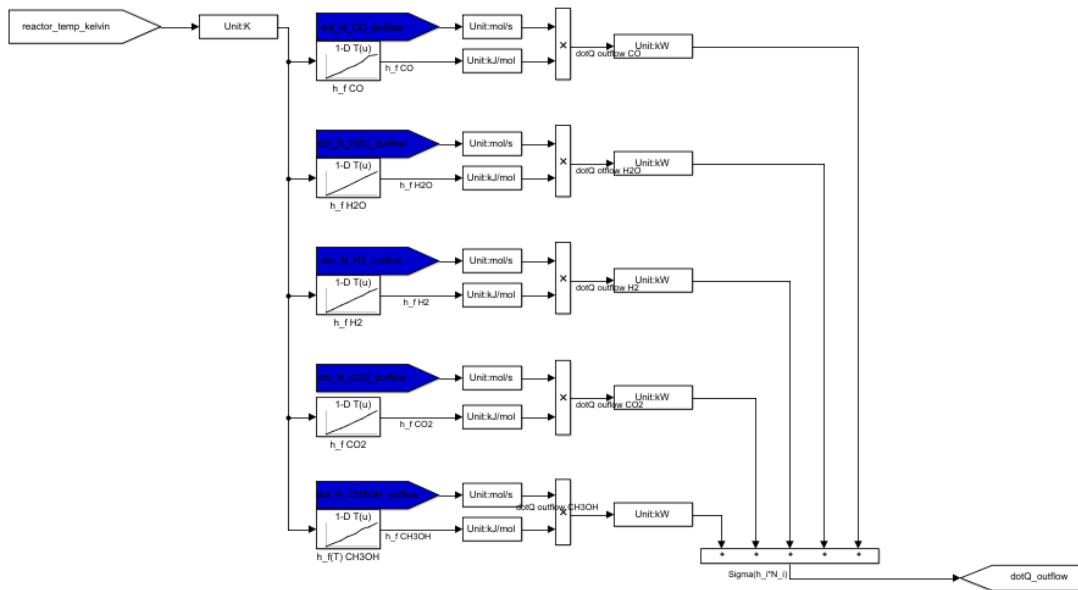
Figure C.14: Calculation of the heat flow from the pre-reformer to the SOFC by multiplying the molar flows of all species to their temperature dependent molar enthalpies. Not that this does not cover the heat flow from the recycle AOG, as this is covered in figure C.15
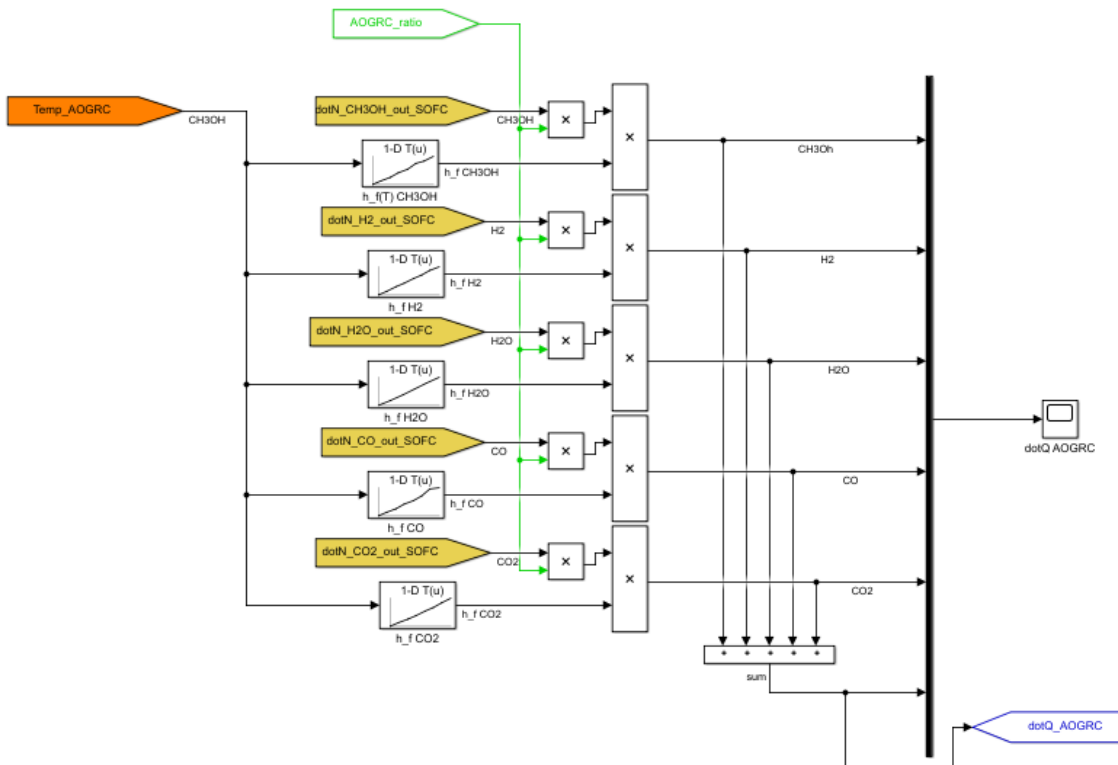

Figure C.15: Heat flow from the recycled Anode Off Gas is calculated by multiplying the molar flows of the AOGRC by the molar entropy for all species in the AOG. Enthalpy is gathered from a temperature dependent lookup table.
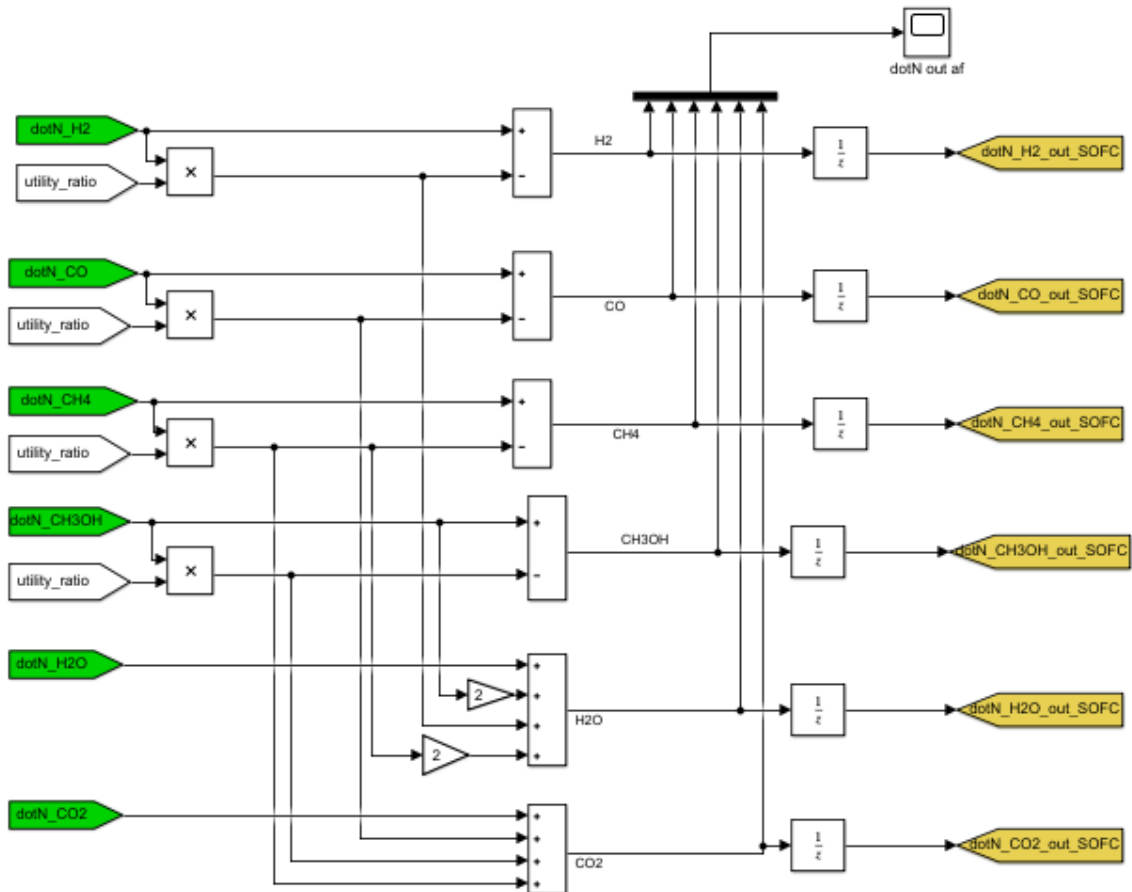
Figure C.16: The molar outflow of the anode channel is calculated by subtracting the quantity that is oxidized ($\dot{N}\cdot$ utility ratio) from the quantity that flows in to the anode channel for every species present in the anode flow. The unit delay is used to prevent an algebraic loop in the calculation.
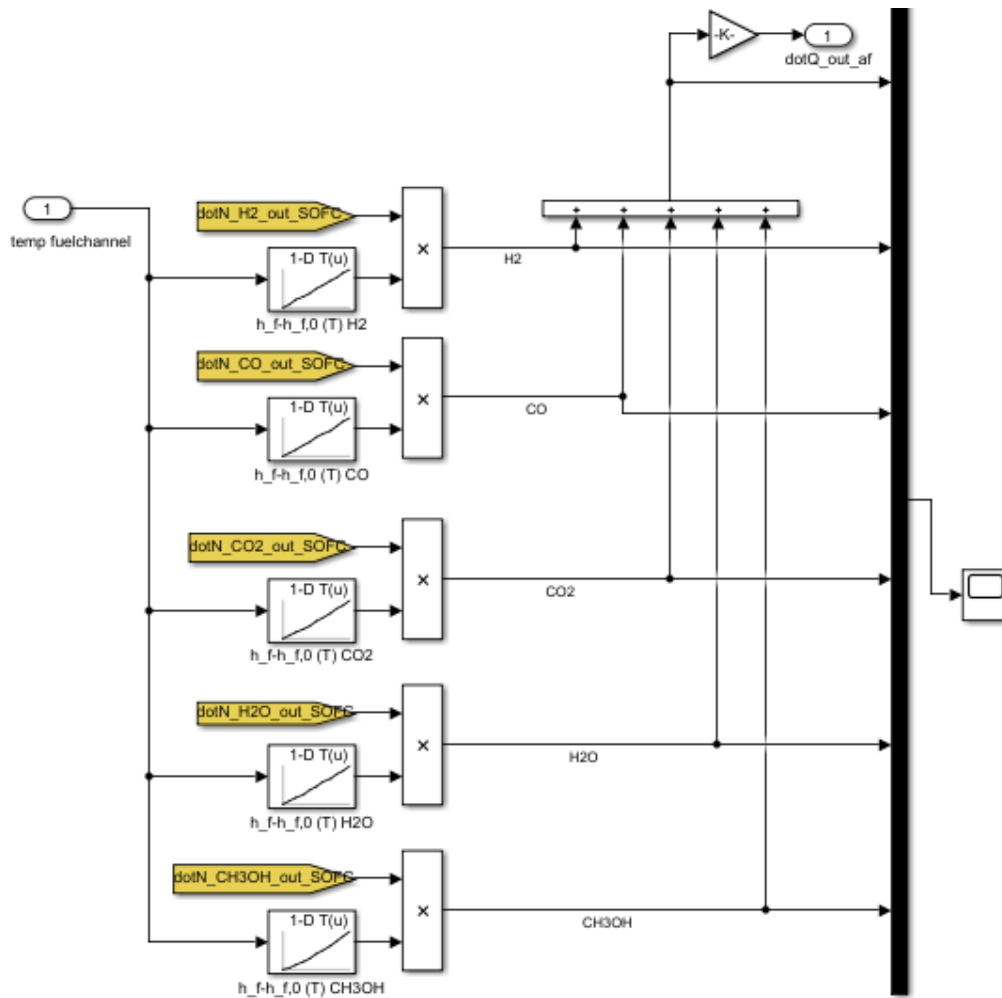
Figure C.17: Heatflow out of the anode channel is calculated by multiplying the molar flows of the outflow of the anode channel by the molar entropy for all species in said outflow
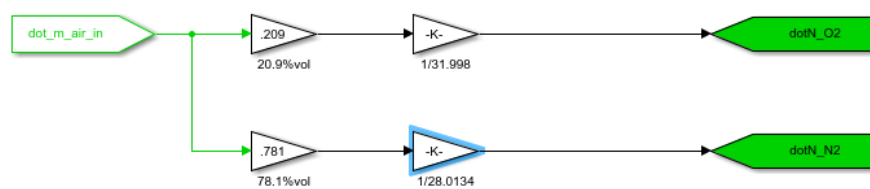

Figure C.18: The molar inflows at the cathode are calculated from the mass flow that Simscape calculates will enter the SOFC from the air compressor.
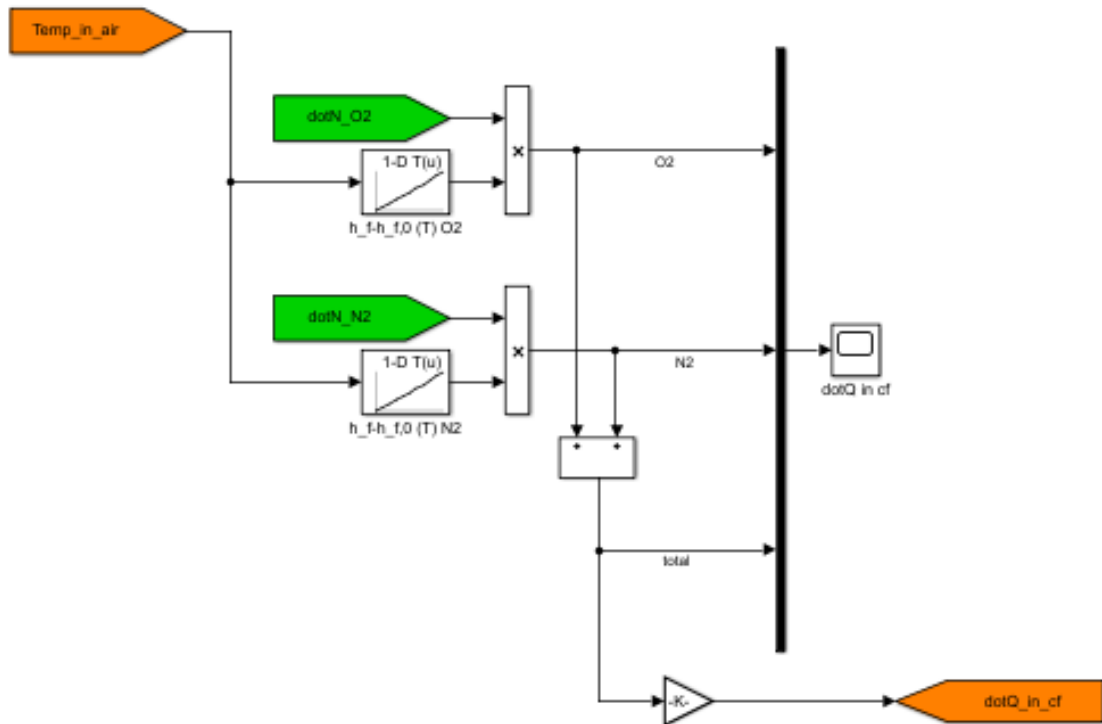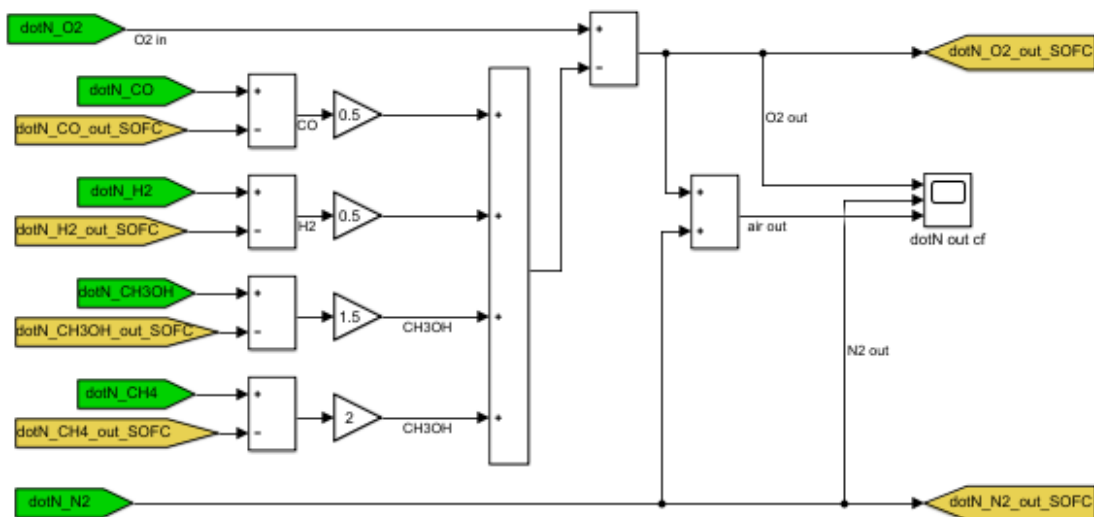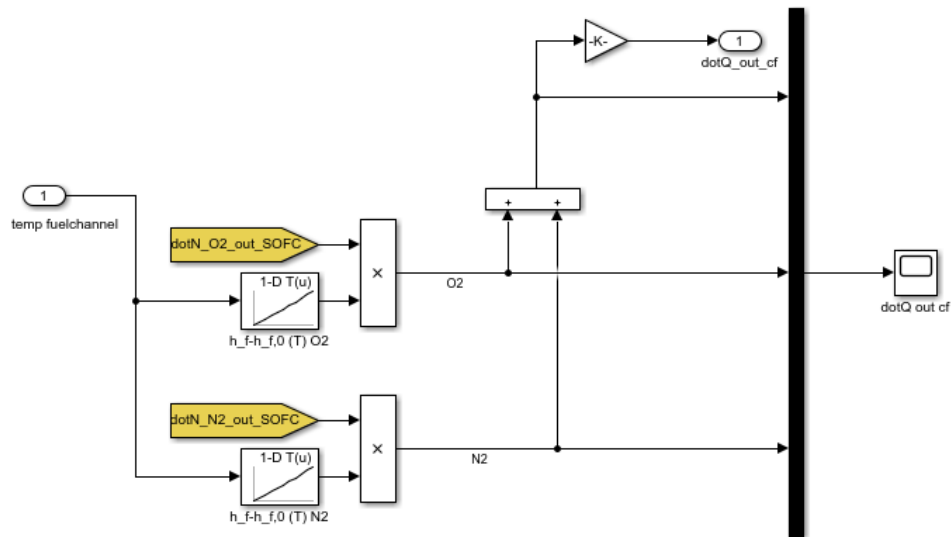
Figure C.19: Caption

Figure C.20: Caption

Figure C.21: Caption

Bibliography

[1] P. Aguiar, C.S. Adjiman, and N.P. Brandon. Anode-supported intermediate temperature direct internal reforming solid oxide fuel cell. i: model-based steady-state performance. *Journal of Power Sources*, 138(1):120 – 136, 2004. ISSN 0378-7753. doi: https://doi.org/10.1016/j.jpowsour.2004.06.040. URL http://www.sciencedirect.com/science/article/pii/S0378775304006950.

[2] L.Barelli G.Bidini A.Ottaviano. Part load operation of a sofc/gt hybrid system: Dynamic analysis. *Applied Energy vol 110*, 2013.

[3] S. A. Barnett. *Direct hydrocarbon SOFCs, Fuel Cell Technology and Applications Solid oxide fuel cells and systems (SOFC), New concepts*. wiley & sons, 2010. doi: https://doi.org/10.1002/9780470974001.f308089.

[4] Daniel J.L. Brett, Alan Atkinson, Denis Cumming, Elvia Ramírez-Cabrera, Robert Rudkin, and Nigel P. Brandon. Methanol as a direct fuel in intermediate temperature (500–600□c) solid oxide fuel cells with copper based anodes. *Chemical Engineering Science*, 60(21):5649 – 5662, 2005. ISSN 0009-2509. doi: https://doi.org/10.1016/j.ces.2005.05.030. URL http://www.sciencedirect.com/science/article/pii/S0009250905004641.

[5] Peter de Vos Phd. *On early-stage design of vital distribution systems on board ships*. PhD thesis, TU Delft, 2018.

[6] THEODORE L. BERGMAN ADRIENNE S. LAVINE FRANK P. INCROPERA DAVID P. DEWITT. *Fundamentals of Heat and Mass Transfer*. Jonh Wiley & sons, 2011. ISBN 978-0470-50197-9.

[7] James Larminie & Andrew Dicks. *fuel cell systems explained*. john Wiley & sons, 2003.

[8] directie wapensystemen en bedrijven. weekbrief directie wapensystemen en bedrijven. Technical report, Defensie Materieel Organisatie, wk17-2019.

[9] Hans Klein Woud en Douwe Stapersma. *Design of auxilliary systems, shafting,and flexible mounting*. Technische Universiteit Delft, 2016.

[10] Xiongwen Zhang; Jun Li; Guojun Li; Zhenping Feng. Dynamic modeling of a hybrid system of the solid oxide fuel cell and recuperative gas turbine. *journal of power sources vol. 163*, 2006.

[11] C.J.M. Fletcher. The thermal decomposition of methyl alcohol. *The royal society publishing*, 0209:119–128, 1934. URL https://royalsocietypublishing.org/doi/pdf/10.1098/rspa.1934.0209.

[12] Jiajian Gao, Yingli Wang, Yuan Ping, Dacheng Hu, Guangwen Xu, Fangna Gu, and Fabing Su. A thermodynamic analysis of methanation reactions of carbon oxides for the production of synthetic natural gas. *RSC Adv.*, 2:2358–2368, 2012. doi: 10.1039/C2RA00632D. URL http://dx.doi.org/10.1039/C2RA00632D.

[13] Victor Gold. *Compendium of Chemical Terminology*. International Union of Pure and Applied Chemistry, 1997. ISBN 0-86542-684-8.

[14] Jan Hendrik Annema (GasTerra); Friso Postma (Microbial Analysis) Harm Vlap; ; Robert Mellema; Nynke Verhaegh; Daniël Aalfs; Remco Zeijlmaker (DNV GL); Bert van Halen ; Martijn Theelen (Gasunie New Energy). Methanation technical fundamentals and market overview. In *report OAG.19.R.10157194*, pages 1–54, Groningen Nederland, 2019.

[15] R. A. Hubble, J. Y. Lim, and J. S. Dennis. Kinetic studies of co2 methanation over a ni/γ-al2o3 catalyst. *Faraday Discuss.*, 192:529–544, 2016. doi: 10.1039/C6FD00043F. URL http://dx.doi.org/10.1039/C6FD00043F.

[16] Manabu Ihara, Keisuke Matsuda, Hikaru Sato, and Chiaki Yokoyama. Solid state fuel storage and utilization through reversible carbon deposition on an sofc anode. *Solid State Ionics*, 175 (1):51 – 54, 2004. ISSN 0167-2738. doi: https://doi.org/10.1016/j.ssi.2004.09.020. URL http://www.sciencedirect.com/science/article/pii/S0167273804005533. Fourteenth International Conference on Solid State Ionics.

[17] Ing AJ Blokland Ing. CJCM Poshumus, Ir. IP Barendregt. The adaptable energy platform. Technical report, DMO,WPSN,ASM, bureau Marine Engineering, 2019.

[18] Mohammad Ommian Jamasb Pirkandi, Mostafa Mahmoodi. An optimal configuration for a solid oxide fuel cell-gas turbine (sofc-gt) hybrid system based on thermo-economic modelling. *journal of cleaner production vol.144*, 2017.

[19] Zhang Jiaying. Kinetic study of carbon monoxide methanation over mesoporous ni-mo catalyst prepared by a hydrothermal method. *Progress in Reaction Kinetics and Mechanism*, 44 (1):3–17, 2019. doi: 10.1177/1468678319825692. URL https://doi.org/10.1177/1468678319825692.

[20] Moritz Krijgsman KLTZ dr. ir. Rinze Geersma. haalbaarheidsstudie emissieloze hulpvaartuigen. Technical report, MARIN, DMO, 2019.

[21] Moritz Krijgsman. ships power and energy concept. report of conceptual design tanks and engine room. klein boven water. Technical report, MARIN, 2019.

[22] A Ottaviano L. barelli, G. Bidini. Integration of sofc/gt hybrid systems in micro-grids. *Energy vol.118*, 2016.

[23] Dipl.-Ing. Jonathan Lefebvre. *Three-phase CO2 methanation, Methanation reaction kinetics and transient behavior of a slurry bubble column reactor*. PhD thesis, der Fakult¨at fu¨r Chemieingenieurwesen und Verfahrenstechnik des Karlsruher Instituts fu¨r Technologie (KIT), 2019.

[24] Fabio Ruggeri Letizia Romanoa. Methane from syngas – status of amec foster wheeler vesta. *Energy Procedia*, 81:249 – 254, 2015.

[25] Hongjiao Li, Ye Tian, Zhiming Wang, Fuchang Qie, and Yongdan Li. An all perovskite direct methanol solid oxide fuel cell with high resistance to carbon formation at the anode. *RSC Adv.*, 2:3857–3863, 2012. doi: 10.1039/C2RA01256A. URL http://dx.doi.org/10.1039/C2RA01256A.

[26] Mingfei Liu, Ranran Peng, Dehua Dong, Jianfeng Gao, Xingqin Liu, and Guangyao Meng. Direct liquid methanol-fueled solid oxide fuel cell. *Journal of Power Sources*, 185(1):188 – 192, 2008. ISSN 0378-7753. doi: https://doi.org/10.1016/j.jpowsour.2008.06.076. URL http://www.sciencedirect.com/science/article/pii/S0378775308013529.

[27] Brant A. Peppley; John C. Amphlett; Lyn M. Kearns; Ronald F. Mann. Methanol–steam reforming on cu/zno/al2o3. part 1: the reaction network. *Applied Catalysis A: General*, 179(1):21 – 29, 1999. ISSN 0926-860X. doi: https://doi.org/10.1016/S0926-860X(98)00298-1. URL http://www.sciencedirect.com/science/article/pii/S0926860X98002981.

[28] Frank D. Maslan and Theodore M. Littman. Compressibility chart for hydrogen and inert gases. *Industrial & Engineering Chemistry*, 45(7):1566–1568, 1953. doi: 10.1021/ie50523a054. URL https://doi.org/10.1021/ie50523a054.

[29] Mahmut D. Mat, Xiangrong Liu, Zhigang Zhu, and Bin Zhu. Development of cathodes for methanol and ethanol fuelled low temperature (300–600°c) solid oxide fuel cells. *International Journal of Hydrogen Energy*, 32(7):796 – 801, 2007. ISSN 0360-3199. doi: https://doi.org/10.1016/j.ijhydene.2006.12.012. URL http://www.sciencedirect.com/science/article/pii/S0360319906006227. Fuel Cells.

[30] Peter Mizsey, Esmond Newson, Than binh Truong, and Peter Hottinger. The kinetics of methanol decomposition: a part of autothermal partial oxidation to produce hydrogen for fuel cells. *Applied Catalysis A: General*, 213(2):233 – 237, 2001. ISSN 0926-860X. doi: https://doi.org/10.1016/S0926-860X(00)00907-8. URL http://www.sciencedirect.com/science/article/pii/S0926860X00009078.

[31] Shiang-Wuu Perng, Rong-Fang Horng, and Hui-Wen Ku. Numerical predictions of design and operating parameters of reformer on the fuel conversion and co production for the steam reforming of methanol. *International Journal of Hydrogen Energy*, 38(2):840 – 852, 2013. ISSN 0360-3199. doi: https://doi.org/10.1016/j.ijhydene.2012.10.070. URL http://www.sciencedirect.com/science/article/pii/S0360319912023944.

[32] J.W. Reurings. A modeling study to investigate performance sofc-ice hybrid systems for marine applications. Master's thesis, TU Delft, 2019.

[33] Stefan Rönsch, Jakob Köchermann, Jens Schneider, and Steffi Matthischke. Global reaction kinetics of co and co2 methanation for dynamic process modeling. *Chemical Engineering & Technology*, 39(2):208–218, 2015. doi: 10.1002/ceat.201500327. URL https://onlinelibrary.wiley.com/doi/abs/10.1002/ceat.201500327.

[34] Kuliyev S.A., Aksongur S., İbrahimoğlu B., and Sevgi Fettah. Direct methanol solid oxide fuel cell. In *DIRECT METHANOL SOLID OXIDE FUEL CELL*, 08 2009.

[35] L. van Biert, M. Godjevac, K. Visser, and P.V. Aravind. A review of fuel cell systems for maritime applications. *Journal of Power Sources*, 327:345 – 364, 2016. ISSN 0378-7753. doi: https://doi.org/10.1016/j.jpowsour.2016.07.007. URL http://www.sciencedirect.com/science/article/pii/S0378775316308631.

[36] L. van Biert, T. Woudstra, M. Godjevac, K. Visser, and P.V. Aravind. A thermodynamic comparison of solid oxide fuel cell-combined cycles. *Journal of Power Sources*, 397:382 – 396, 2018. ISSN 0378-7753. doi: https://doi.org/10.1016/j.jpowsour.2018.07.035. URL http://www.sciencedirect.com/science/article/pii/S0378775318307432.

[37] Production van Biert, L. (TU Delft Ship Design and Operations). *Solid oxide fuel cells for ships: System integration concepts with reforming and thermal cycles*. PhD thesis, Delft University of Technology, 2020-02-14.

[38] Minister van Defensie. Operationele energie strategie. Technical report, Ministerie van Defensie, 2015.

[39] Geert H. Graaf & Jozef G.M. Winkelman. Chemical equilibria in methanol synthesis including the water–gas shift reaction: A critical reassessment. *industrial & engineering chemistry research*, 55 (20):5854–5864, 2016. doi: 10.1021/acs.iecr.6b00815. URL https://doi.org/10.1021/acs.iecr.6b00815.

[40] Byung Chan Yang, Junmo Koo, Jeong Woo Shin, Dohyun Go, Joon Hyung Shim, and Jihwan An. Direct alcohol-fueled low-temperature solid oxide fuel cells: A review. *Energy Technology*, 7(1): 5–19, 2017. doi: 10.1002/ente.201700777. URL https://onlinelibrary.wiley.com/doi/abs/10.1002/ente.201700777.